MAGNETIC RESONANCE IMAGING ARTIFACTS: MECHANISM AND CLINICAL SIGNIFICANCE

Elizabeth Pusey, M. D.(1), Robert B. Lufkin, M.D.(1), Richard K.J. Brown, M.D.(1), Murray A. Solomon, M.D. (2), David D. Stark, M.D. (3), William N. Hanafee, M.D. (1)

Dept of Radiologic Sciences, University of California, Los Angeles (1), San Jose Imaging Center (2), Massachusetts General Hospital (3)

A thorough understanding of artifacts is important to avoid errors in clinical interpretation and to improve image quality. We will present some of the more reproducible artifacts that occur on both superconducting and permanent magnet systems. The mechanisms, clinical significance, and strategies to reduce artifacts will be discussed. Examples will include artifacts due to extrinsic factors such as patient motion and metallic artifacts (Figure 1). Artifacts specific to the MR imaging system such as zero line artifacts and chemical shift will be presented. Additionally, artifacts due to general image processing techniques such as truncation artifact and aliasing will be discussed.

Figure 1: Distortion of right eye caused by cobalt based eye makeup. A normal MR scan was obtained following removal of the make up.

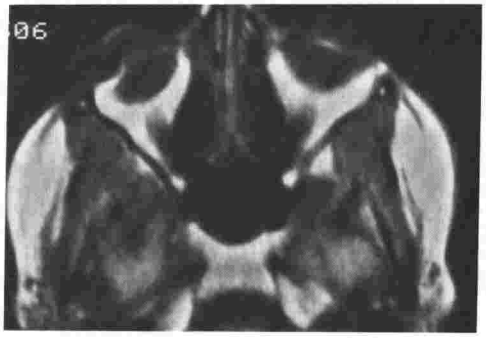

Figure 2: Asymmetric brightness artifact causing decrease in signal on the right side of the pelvis. The artifact was caused by filter bands that were too tight about the signal band. Asymmetric brightness may cause difficulty in the evaluation of the femoral head for aseptic necrosis.

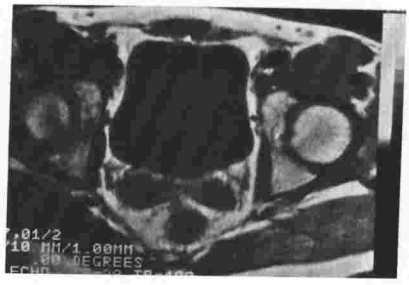

SHORTENING THE GRADIENT RISE TIME ON A 33CM 2T NMR IMAGING SPECTROMETER

D.J. Jensen, W.W. Brey, P.A. Narayana, V.P. Tong, J.L. Delayre

The University of Texas Health Science Center Houston
Department of Radiology, 6431 Fannin Street, Houston, TX 77030

When a magnetic field gradient is rapidly switched in an MR system, eddy currents form in the cryostat which decay in a multiexponential fashion characterized by the geometry and the material properties of the metal. The magnetic field produced by these induced currents is superimposed upon the field generated by the gradient coils, and thus degrades the overall gradient rise time. Even more than in standard MR imaging, the problem becomes important in spectroscopic imaging and localized spectroscopy experiments. Here, magnetic field gradients are used for selective excitation or phase encoding while no residual gradient can be allowed during the data acquisition in order to preserve the spectroscopic information. Since the spectral width is shorter in these experiments, the acquisition time increases, and the magnetic field changes can not be neglected within this time window.

The magnetic field due to eddy currents in the cryostat can be compensated at any given point in the magnet to within a few milliseconds by using an electronic current compensation. In order to achieve a short gradient rise time over a larger volume, however, the magnet structure and the gradient coil system have to be perfectly symmetrical and concentric. This condition is not easily met by horizontal bore magnets. We describe a method to reduce the gradient rise time over a larger volume for the case of slight asymmetry.

Since our magnet is equipped with a fiberglass bore tube, eddy currents are mainly generated in the low temperature shield. Fig.1 shows a plot of gradient rise curves for one of the transverse gradient coils in our 33cm 2T horizontal bore magnet. For these measurements, the induced voltage in a pickup coil was integrated by an analog integrator and displayed as a function of time. Individual curves in the plot correspond to different positions of measurement along the vertical axis. At the geometric center of the gradient coil system (position 0"), a decaying eddy current field remains. This component of the eddy current field vanishes approximately 3/16" upwards. The finding indicates that the axis of the gradient coil system and the axis of the low temperature shield are apart by about 3/16".

Since physical repositioning of the gradient coil system was not a feasible solution on our system, we chose to move the geometric center of compensation electronically. Consequently, the gradient rise time was reduced to within one millisecond over a volume of approximately 10cm *10cm *10cm. The result is shown in Fig.2.

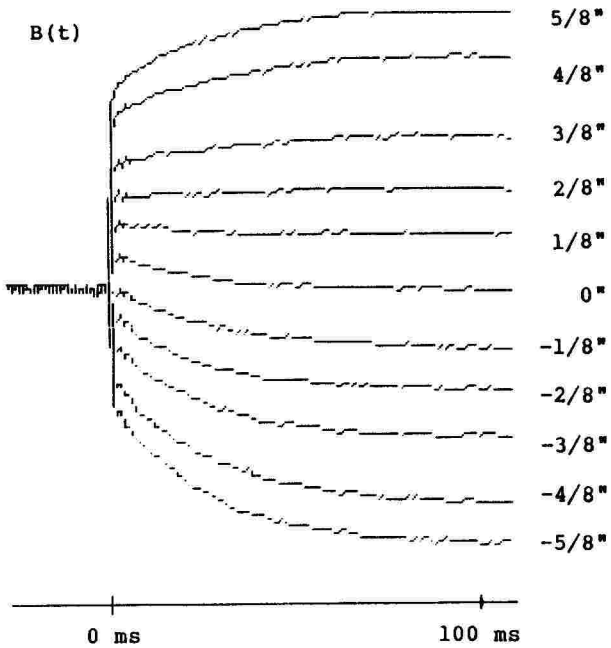

Fig. 1

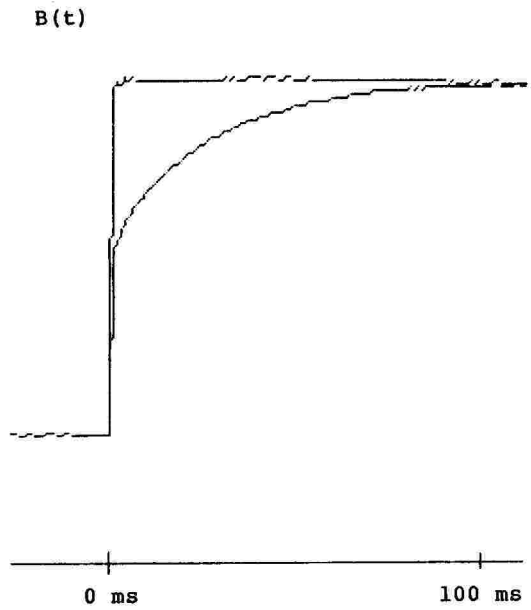

Fig. 2

TECHNICAL ARTIFACTS IN MAGNETIC RESONANCE IMAGES AND THEIR REDUCTION

D.J. Jensen, V.P. Tong, W.W. Brey, P.A. Narayana, J.L. Delayre

The University of Texas Health Science Center Houston
Department of Radiology, 6431 Fannin Street, Houston, TX 77030

During the course of implemention of the two-dimensional spin warp imaging technique on the magnetic resonance imaging spectrometer developed in our laboratory, numerous technical artifacts were encountered, investigated and removed. We would like to present a summary of them, their origins and means of reduction.

Fig.1 shows an image example with two major artifacts. The scan represents a coronal slice through the head of a normal monkey acquired with a spin echo sequence (TE=14ms/TR=800ms/2mm). The RF coil was a 6" slotted tube resonator operating at 85 MHz.

The image shows a severe interference pattern including very high intensity areas on the horizontal image axis. The reason for their appearance is RF field inhomogeneity. To reduce this problem, the phase of the 180 degree pulse is cycled between experiments. Remainders of the interference pattern are moved to the outskirts of the image by changing the phase of the selective 90 degree pulse by 180 degrees from scan to scan. This phase alternation results in an additional 180 degree phase shift between consecutive echoes in the direction of the phase encoding gradient whereas the sign of the interfering signal remains unchanged. The Fourier transform along this axis, therefore, yields a shift of the object about half the spectral width but leaves the projection of the interfering signal in the image center. Swapping the two halves of the image, returns the object and banishes the interference to the periphery.

The second dominant artifact in the image is a stripe through the vertical image center. The reason is a remaining DC component in the acquired time signal which occurs despite the use of quadrature phase detection and a CYCLOPS sequence. Instead of performing a baseline offset correction on individual echoes, the same correction is applied to the entire data array. With a 180 degree phase shift of the selective pulse between scans, residual signal is moved to the periphery as described above. Further reduction is achieved when a second baseline offset correction is performed on the center line in the direction of the phase encoding gradient after the Fourier transform in the first dimension.

Fig.2 shows a coronal section through the head of a normal cat (TE=30ms/TR=500ms/6mm). The image was acquired using the same RF coil as before. The imaging sequence, however, and the data processing were modified as described. Both artifacts are eliminated. Only the well known chemical shift artifact remains.

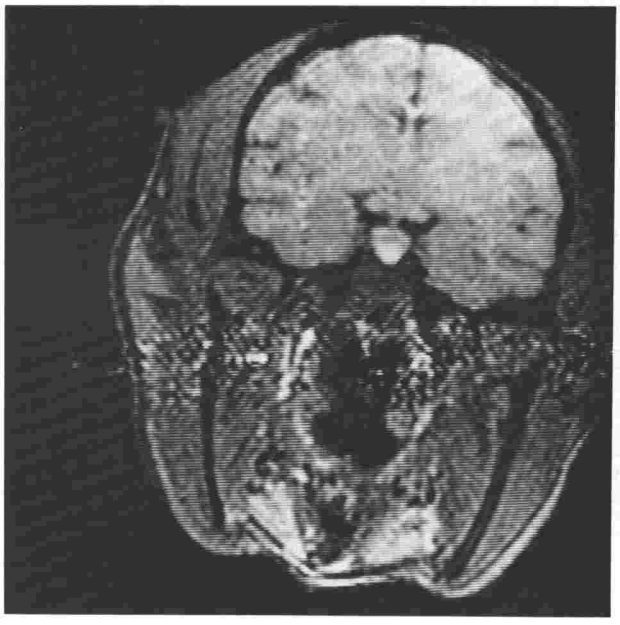

Fig. 1

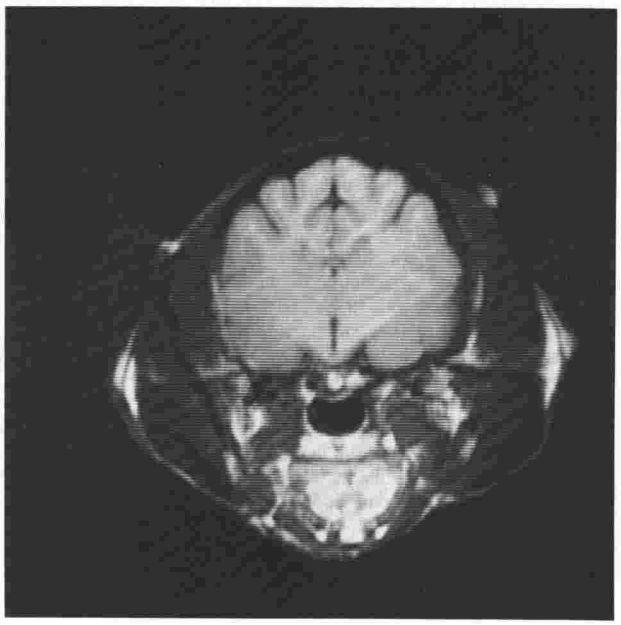

Fig. 2

MAGNETIC RESONANCE IMAGING OF BREAST AND AXILLARY TISSUE AT 0.6 TESLA: A CORRELATION OF SIGNAL INTENSITIES AND RELAXATION TIMES WITH PATHOLOGICAL FINDINGS

Charles W. Merten, M.D., Alexander Chako, M.D., Jonathan I. Wiener, M.D., Stanley Gross, M.D.
Edward L. Coffey, M.D., Alan Wecksell, M.D., Harry L. Stein, M.D.

From the Departments of Radiology and Pathology, North Shore University Hospital, Manhasset, New York, and the Departments of Radiology and Pathology, Cornell University Medical College, New York, New York

A series of both preoperative breast lesions and tissue specimens were examined at 0.6 Tesla utilizing various pulses including both T_1 and T_2 weighted sequences and combinations to investigate the relative efficacy of each in the detection and differentiation of specific benign and malignant processes. Examples of disease including carcinoma, fibroadenoma, benign fibrocystic disease, cystosarcoma phylloides and hemorrhage in preoperative breasts, as well as axillary nodal processes including metastases, infarct and reactive hyperplasia are depicted to illustrate the effect of T_1 and T_2 weighting. Correlative mammograms and histological sections are also included to illustrate the influence of collagen and cellular content of lesions on MRI images and the contribution of MRI to assessment of extent of disease.

THERMAL RESPONSES TO DIFFERENT LEVELS OF RADIOFREQUENCY POWER DEPOSITION DURING CLINICAL MAGNETIC RESONANCE IMAGING AT 1.5 TESLA.

Frank G. Shellock, Ph.D.; Daniel J. Schaefer, Ph.D.*; and John V. Crues, M.D.

Division of Cardiology, Department of Medicine and Division of Magnetic Resonance Imaging, Department of Diagnostic Radiology. Cedars-Sinai Medical Center and UCLA School of Medicine, Los Angeles, CA 90048
*General Electric Company, Medical Systems Group, Milwaukee, WI 53201

In order to operate magnetic resonance (MR) imaging devices as a "nonsignificant risk" to patients, current U.S. Food and Drug Administration guidelines recommend limiting the radiofrequency (RF) power deposition to a specific absorption rate (SAR) of 0.4 W/kg averaged over the whole body. To characterize the thermal responses associated with MR imaging, we evaluated the temperature changes produced by three different specific absorption rates: brain scans - 0.06 W/kg (Group I), knee scans - 0.41 W/kg (Group II), and lumbar spine scans - 0.70 W/kg (Group III). A 1.5 Tesla superconducting magnet operated at 64 MHz for proton imaging was used in this study (Signa MR System, General Electric Company, Milwaukee, WI). Body temperature (Tb) was measured with an electronic thermometer (Mark X, Electromedics, Englewood, CO) placed in the sublingual pocket. Skin temperatures were obtained with a non-contact infrared thermometer (Meditherm, Everest Interscience, Tustin, CA) from the following sites: forehead (Tfh), forearm (Tfa), and the positioning isocenter (Ti; outer canthus for brain scans, mid-patella for knee scans, umbilicus for lumbar spine scans). Ambient conditions were room temperature 20-24°C, relative humidity 40-50%. All measurements were obtained immediately before and after the MR scans.

Results are:

		Tb (°C)	Tfh (°C)	Tfa (°C)	Ti (°C)
GROUP I (N=8)	Pre MRI	36.6±0.3	32.4±0.6	30.7±0.6	31.7±0.8
	Post MRI	36.6±0.2	32.9±0.2*	30.7±0.8	32.8±0.3*
GROUP II (N=7)	Pre MRI	36.6±0.3	33.0±0.6	30.5±0.9	30.1±1.2
	Post MRI	36.6±0.2	33.0±0.5	31.0±0.8	30.4±1.5
GROUP III (N=6)	Pre MRI	36.6±0.1	32.2±0.8	31.0±0.4	33.4±0.6
	Post MRI	36.8±0.1*	32.2±1.0	31.3±0.6	34.1±0.8*

(values are mean±SD, *$p<0.05$, Pre compared to Post MRI).

There was a significant increase in Tb related to MR imaging above the advised SAR, however, this temperature elevation was not considered to be of physiological importance. Skin temperatures increased significantly during the brain and lumbar spine scans, but these temperature alterations were also minimal. We conclude that, at the specific absorption rates we studied, there are slight increases in body and skin temperatures produced by clinical MR imaging that do not appear to be detrimental to patient health.

CHANGES IN CORNEAL TEMPERATURE ASSOCIATED WITH HIGH-FIELD (1.5 TESLA) MAGNETIC RESONANCE IMAGING: EXPERIENCE IN 118 PATIENTS.

Frank G. Shellock, Ph.D. and John V. Crues, M.D.

Division of Cardiology, Department of Medicine and Division of Magnetic Resonance Imaging, Department of Diagnostic Radiology. Cedars-Sinai Medical Center and UCLA School of Medicine, Los Angeles, CA 90048

Radiofrequency (RF) pulses are required for magnetic resonance (MR) proton imaging and the frequency of these pulses are directly proportional to the static magnetic field strength. Exposure to RF power is known to increase tissue temperatures and may be harmful to thermally sensitive tissues. The eye is particularly susceptible to thermal damage, therefore, the purpose of this investigation was to determine the temperature effects of high-field MR imaging on corneal temperature. A 1.5 Tesla superconducting magnet was used in this investigation (Signa MR System, General Electric Company, Milwaukee, WI). A total of 118 patients were studied: 52 males, 66 females, average age 44 years, range 10-87 years old. Corneal temperatures were measured with a non-invasive infrared thermometer (Meditherm, Everest Interscience, Tustin, CA) with a spot size setting of 5 mm (1). Ambient conditions were room temperature 20-24^{o}C and relative humidity of 40-50%. Temperature measurements were obtained immediately before and after MR imaging. The MR scans were obtained for diagnostic purposes, using conventional RF pulse sequences. The estimated average whole body specific absorption rate ranged from 0.06 W/kg to 1.81 W/kg (U.S. FDA advises an analysis of health effects if RF deposition is greater than an SAR of 0.4 W/kg). The average corneal temperature increased from 32.7$\pm$0.7^{o}C to 33.1$\pm$0.6^{o}C ($p<0.001$). The largest change in corneal temperature was 3.0^{o}C and no temperature exceeded 34.8^{o}C. We conclude that MR imaging significantly increases corneal temperature in patients undergoing clinical scans, however, this temperature elevation is far below the threshold for producing thermally-induced damage (2).

1. Shellock FG, Riedinger MS, Adler L: Measurement of corneal and supra-orbital temperatures using a portable infrared thermometer. Clinical Research 32:32A, 1984.
2. Elder JA: Special senses. In, Biological Effects of Radiofrequency Radiation. EPA-600/8-83-026F, pp. 5-64 to 5-69, 1984.

EVALUATION OF THYROID MASSES BY MAGNETIC RESONANCE IMAGING

S.A. Kroop*, D. Margouleff**, I. Zanzi**, M. Susin***, M.A. Goldman* and H.L. Stein*

From the Departments of Radiology*, Medicine** and Pathology***, North Shore University Hospital, Manhasset, New York and the Departments of Radiology, Medicine and Pathology, Cornell University Medical College, New York, New York

Twenty patients with palpable thyroid masses were prospectively evaluated by nuclear medicine, high resolution real-time ultrasound and magnetic resonance imaging (MRI) techniques. All MRI studies were performed with a 0.6 Tesla superconducting magnet utilizing whole body or surface coils and T_1 and T_2 weighted spin echo and inversion recovery pulse sequences in coronal, transverse and sagittal planes. Diagnoses were established by surgery (n=18) or by radiologic/clinical correlation and follow-up of at least 12 months (n=2). There were 6 cases of solitary adenoma, 8 cases of multinodular adenomatous goiter, 3 cases of papillary carcinoma, 2 cases of follicular carcinoma and 1 case of epidermoid carcinoma. MRI detected all lesions. Solitary adenomas were round somewhat inhomogeneous lesions with relatively smooth sharply defined margins demonstrating variable signal intensity on T_1 weighted images and high signal intensity on T_2 weighted images. Adenomatous goiters were characterized by gland enlargement, heterogeneity, and by multiple nodules of relatively low signal intensity on T_1 weighted images and high signal intensity on T_2 weighted images. All malignancies were lobulated heterogeneous masses of relatively low signal intensity on T_1 weighted images and high signal intensity on T_2 weighted images. MRI was useful in depicting lesion margin, lesion extent, tissue heterogeneity, cystic and hemorrhagic regions, cervical lymphadenopathy, invasion or compression of adjacent anatomic structures and additional non-palpable thyroid nodules. Qualitative assessment of MRI signal intensity was not lesion specific with regard to pathologic diagnosis.

MRI OF GYNECOLOGIC LESIONS

Marcia C. Fishman[1], M.D., Harry L. Stein[1], M.D., and John L. Lovecchio[2], M.D.

Departments of Radiology[1] and Obstetrics and Gynecology[2], North Shore University Hospital, Cornell Medical College, Manhasset, New York.

One hundred fifty magnetic resonance imaging scans of the pelvis were performed for a variety of gynecologic lesions on a 0.6 tesla superconducting magnet using both T1 and T2 weighted 2D spin echo technique. Results were compared to computed tomography, clinical staging and surgical findings. MRI was useful to provide not only anatomic but also diagnostic information in evaluating a wide variety of gynecologic neoplasms. The characteristic appearances of the lesions are discussed and reviewed by anatomic location.

(Poster Presentation,
2 viewing surfaces needed,
lighted viewboxes)

IN - VIVO PROTON SPIN LATTICE RELAXATION TIMES IN NORMAL AND DYSTROPHIC MUSCLES

P.A.Narayana, J.L.Delayre and L.K.Misra

Department of Radiology, University of Texas Medical School and Department of Physiology and Molecular Biophysics, Baylor College of Medicine, Houston, Texas 77030

Nuclear Magnetic Resonance (NMR) spectrum of tissue protons generally exhibits two chemically shifted lines originating from water and lipid molecules. Tissue characterization based on spin lattice relaxation times (T1), therefore, requires the determination of T1 values separately for these two types of protons. However, most of the reported T1 values were measured in a relatively low resolution mode. These relaxation times, therefore, represent neither the water protons nor the lipid protons alone but depend on their relative concentrations. This is particularly true in dystrophy as lipids are known to accumulate in the affected muscles(1). In this work, we report the in-vivo T1 measurements of both water and lipid protons in normal and dystrophic pectoralis major muscle in a chicken animal model. This muscle is known to undergo severe degenerative changes with the disease progression.

Four day - to sixty day - old New Hampshire chicks of line 412(normal) and line 413(dystrophic) were used in these studies. The chicks were anesthetized by sodium pentabarbitol(I/V 8 to 12 mg/Kg). Twelve chicks were used in each age group (six normals and six dystrophic). All the NMR measurements were made on a 2T NMR Imager/Spectrometer described elsewhere(2). The magnet has a 25cm clear horizontal bore. The T1 values were measured with a 1" flat circular coil placed directly on the pectoralis major muscle. A 2 θ - TI - θ pulse sequence was used(3). The accuracy of this method was verified by using inversion recovery sequence with separate transmitter and receiver coils. A 5" slotted tube resonator was used as a transmitter coil to provide uniform excitation over the whole sample volume. The receiver coil was a 1" flat circular coil. MR images were used to ascertain that the received signal originated only from the pectoralis major muscle. Good agreement was obtained in the T1 values determined by these two methods. The measured T1 values are shown in Table I. No lipid signal was observed in the 4 day - old chicks and so only their water T1 was reported.

These results indicate that 1) in normal muscles the T1 values of water protons decrease with age while the T1 values for lipid protons increase, 2) in the dystrophic muscles the value of T1 for water protons does not change with age and 3) the T1 behaviour of lipid protons in normal and dystrophic muscles is similar. These results suggest that the measured in-vitro diifferences in the global proton relaxation times between normal and dystrophic muscles(4) reflect the changes in water proton concentration and/or environment. The water proton T1 values of dystrophic muscles at all ages studied are similar to those of the 4 day old normal muscles suggesting a failure of maturation process in the dystrophic muscles.

Table I

T1 values of normal and dystrophic pectoralis major muscles at different ages.

Age (days)	Normal T1(water) (ms)	Normal T1(lipid) (ms)	Dystrophic T1(water) (ms)	Dystrophic T1(lipid) (ms)
4	1500+/-200	-	1300+/-150	-
14	1190+/-150	500+/-60	1450+/-160	500+/-60
40	1150+/-120	700+/-70	1500+/-180	600+/-70
60	1150+/-130	800+/-80	1400+/-150	900+/-100

Refeferences

1. Newman,R.J. et al, Br. Med. J. 284, 1072-1074(1982)
2. Delayre,J.L., Jensen,D.J., Brey.W.W., Tong.V and Narayana,P.A., Soc. Mag. Reson. Abstracts 187-189(1984)
3. Evelhoch,J.L. and Ackerman,J.J.H., J. Mag. reson. 53, 52-64 (1983)
4. Misra,L.K.,Narayana,P.A., Beall,P.T. and Hazlewood,C.F., Mag. Res. Med. 1, 205-206(1984)

DETAIL VISIBILITY ENHANCEMENT IN SURFACE COIL IMAGES

Noever, T., Eisner, RL., Sprawls, P., Coumans, JJ., Hoffman, JC

Department of Radiology, Emory University
School of Medicine, Atlanta, GA 30322

Surface coils have proved to be useful for obtaining increased signal to noise and spatial resolution in magnetic resonance imaging. The improved image quality results from the surface coil's smaller sensitive area and reduced noise pickup when compared to coils encircling large body sections.

The advantage of the surface coil is partially offset by a significant variation in coil sensitivity over the imaged area which produces a large dynamic range in the image intensity data.

The use of conventional grey-scale manipulation techniques cannot provide simultaneous visibility of anatomical detail in both the areas of high and low image intensity. For example, the surface coil image in Fig. 1 (left) shows the signal from fat to be high, and the lower signal region adjacent to it to be poorly visualized. Using operator-interactive window-level controls can provide more contrast and enhanced visibility of detail in the lower signal areas but only with a concomitant loss of contrast in the high signal areas.

The following approaches have been investigated and used to overcome this problem:

1) Global contrast enhancement:

Non-linear image-to-display transfer functions (maps) are used to enhance, globally, the contrast of the lower intensity ranges while decreasing that of the higher ones. These maps are logarithmic functions of the type:

$$D = a * \log^{n}(I) + b$$

where D is the displayed intensity, I is the image intensity, a and b are scale and offset factors, respectively, and n may assume any integral value greater than zero. Note that as n increases the map approaches that of the conventional linear form.

We found that the optimal value of the parameter n is dependent on the exact type of surface coil image under consideration. An example is shown in Fig. 1 (right) where the contrast and resulting image quality of the spine surface coil image is significantly enhanced using b=0 and n=3.

2) Regional contrast enhancement:

An image containing only large-area contrast is generated by digitally blurring the original reconstructed image (R). The blurred image (B) exhibits intensity variations that closely relate to coil sensitivity but contain no small-scale detail. An enhanced image (E) is obtained by scaling each pixel in R by either of two parameters:

$$E = R - a * B \quad (1)$$
$$\text{or } E = a * R/(B + b) \quad (2)$$

Where "a" is a scaling factor, and "b" is a parameter which controls the degree of enhancement in eq. (2). A fourth parameter is the relative amount of blurring required to produce image B.

The specific image processing algorithm and parameter values are selected to optimize detail visibility is the various surface coil applications. Protocols are established for the routine processing of clinical images.

Figure 1. Conventional MRI display (left) and processed image display showing increased visibility of detail throughout image area (right).

POSTER AND PRESENTATION

THE ROLE OF MRI IN THE MANAGEMENT OF INTRACRANIAL ANEURYSMS

M.H. Johnson, M.D., G.J. DeFilipp, M.D., R.H. Rosenwasser, M.D., T.H. Liu, M.D., C.G. Drake, M.D., A.J. Macones, Jr., M.D., W.A. Buchheit, M.D., and J.A. Kenning, M.D.

Temple University Hospital

The Role of MRI in the Management of Intracranial Anerysms

The definitive imaging modality for the evaluation and follow-up of intracranial aneurysms and vascular malformations has remained arteriography despite the advent of newer modalities for intracranial imaging. CT scanning has been adjunctive in management as it is capable of demonstrating aneurysms plus associated hemorrhage and intramural calcifications. We have found MRI with its capacity to demonstrate differences between flowing blood and thrombus as signal intensity differences to be useful in the evaluation and follow-up of certain vascular lesions. Imaging on all cases was performed on a Fonar 0.3 Tesla Mobile MRI unit.

An illustrative case is presented in Figures 1 and 2. The patient was a thirty-eight year old man with ataxia. A CT scan demonstrated a giant basilar trunk aneurysm confirmed by angiography. MRI (Figure 1) with a spin echo sequence of TE 56, TR 2000 demonstrated the aneurysm with a thick wall and central flow. Surgical exploration was performed and a Drake tourniquet placed on the proximal basilar artery creating an angiographically confirmed 90% basilar artery stenosis. Repeat MRI (Figure 2) the same spine echo sequence demonstrates almost complete thrombosis of the lesion with only a small residual lumen.

The capacity of MRI to demonstrate thrombosis is particularly useful in the giant aneurysm situation where an attempt to induce thrombosis rather than clipping is the therapy of choice. Similar results have been identified in a case where arteriographic balloon occlusion of the carotid was utilized for the promotion of thrombosis in a non-clippable carotid cavernous aneurysm.

In patients with associated AVM's and aneurysms which have hemorrhaged, MRI is useful in the evaluation of thrombosis within the aneurysmal component, the usual site of bleeding. In the more usual saccular aneurysms, MRI may demonstrate both the aneurysm and the presence of complete or incomplete thrombosis post hemorrhage. We are currently prospectively evaluating our patient population with documented subarachnoid hemorrhage and negative arteriography to evaluate our capacity for demonstrate thrombosed aneurysms which thrombosed after hemorrhage.

1.5 T MRI OF MUSCULOSKELETAL TUMORS

D. L. Burk, Jr., M.D., E. Kanal, M.D., J. A. Brunberg, M.D., M. A. Goodman, M.D., and G. L. Wolf, Ph.D., M.D.

Pittsburgh NMR Institute and the Departments of Radiology and Orthopedic Surgery, University of Pittsburgh

CT plays an important role in the diagnosis and staging of musculoskeletal tumors, but MRI offers several significant advantages. MRI can provide superior soft tissue and marrow contrast and direct multiplanar images are routinely obtainable. Previous MRI studies have utilized low field strength magnets with limited spatial resolution. High field systems provide increased resolution and improved signal-to-noise ratios with the potential for hydrogen and phosphorus spectroscopy. Using a 1.5 T scanner, we have imaged 30 patients with a variety of benign and malignant tumors. Pulsing sequences (TR/TE) were used with T1 weighting (600 msec/25 msec) for marrow pathology and T2 weighting (2000 msec/25, 50, 75, 100 msec) for soft tissue pathology. A rim of decreased signal intensity was often seen between benign lesions and normal marrow corresponding to reactive bone formation. MRI was superior to CT in demonstrating extension of tumor across growth plates and in defining the relationship of tumors to vessels and joints. Postoperative MRI studies showed less artifact from metallic implants than CT in the evaluation of tumor recurrence. Although calcification could not be readily identified on MRI, fat and hemorrhage could often be specifically characterized.

NON-ANGIOGRAPHIC IMAGING OF THE PULMONARY ARTERIES: CT AND MR IMAGING

Conces DJ, Tarver RD, Augustyn GT

Indiana University Medical Center, Indianapolis, Indiana

The central pulmonary arteries may be involved by a variety of disease processes. Plain film radiography provides limited information on the involvement of the central pulmonary arteries by disease. Traditionally pulmonary angiography was used to evaluate both intrinsic and extrinsic disease processes involving these vessels. Computed tomography (CT) and magnetic resonance (MR) imaging provide additional methods of studying the central pulmonary arteries without resorting to angiography. A series of 21 patients with pathologic conditions involving the pulmonary arteries were studied with both CT and MR imaging. CT and MR imaging demonstrated the pathology involving the vessels in all cases. MR imaging better demonstrated the pathology or identified additional findings in 9 patients. Coronal MR images, which were done on all patients, provided unique information not seen on either CT or transverse MR images in 3 patients. Both CT and MR imaging are useful modalities with which to evaluate the central pulmonary arteries. MR imaging was better able to delineate the extent of disease involving the pulmonary arteries than was CT.

MRI OF THE MEDIASTINUM FOR DETECTION OF THYMOMA IN PATIENTS WITH MYASTHENIA GRAVIS

Poonam Batra, M.D., Christian Herrman, M.D., John Keesey, M.D., Donald Mulder, M.D.

UCLA, Center for Health Sciences, Dept. of Radiological Sciences, Los Angeles, CA. 90024

MRI of the mediastinum was performed in 14 patients with myasthenia gravis, (10 females, 4 males of age 11-69 years) for the detection of thymoma after obtaining chest radiographs and computed tomograms (CT). Using a 0.3 Tesla Fonar permanent magnet imaging system the images were obtained by T_1 weighted spin echo technique (TR 500, TE 28). T_2 weighted images were obtained in 8 patients (TR1500-2000, TE56.) All images were obtained in axial plane, 11 in sagittal and 3 in coronal.

Chest radiographs (posteroanterior and lateral views) detected an anterior mediastinal mass in 2 patients, and diffuse widening of superior mediastinum in one. 10 patients had a positive CT scan (e.g. a nonfat density in anterior mediastinum) and lipomatosis in one. Calcifications not seen on radiographs, was present in one.

On T_1 weighted MRI the signal intensity of the lesion was less than the surrounding fat in 8 and equivalent to fat in 2. In 2 cases a small amount of thymic tissue (1 cm and 1.5 cm) easily seen on CT was indistinguishable from mediastinal fat on T_1 weighted images. Marked increase in signal intensity relative to fat, occurred on all T_2 weighted images. Calcifications were not visualized due to lack of signal.

Nine patients underwent thymectomy. One proved to have invasive thymoma, 1 encapsulated thymoma, 5 hyperplasia and 2 a normal gland. Both cases of thymoma were accurately diagnosed by CT and MRI but thymic hyperplasia and normal gland are histologic diagnosis and could not be distinguished by either CT or MRI.

MRI AND CT OF CRYPTIC STRUCTURAL LESIONS IN REFRACTORY PARTIAL EPILEPSY

Ormson, Mark J., Kispert, David B., Sharbrough, Frank W., Houser, O. Wayne, Earnest, Franklin, IV, Scheithauer, Bernd W., Laws, Edward R., Jr.

Mayo Clinic and Mayo Foundation, Rochester, Minnesota.

Contrast-enhanced computed tomography (CT) and T2-weighted spin-echo magnetic resonance imaging (MRI) scans were correlated with the pathologic findings in 25 patients treated surgically for refractory partial epilepsy. Of 12 pathologic lesions present, MRI detected 10 (83%) and CT detected 7 (58%). Of 9 low-grade gliomas, MRI detected 8 and CT detected 4. A post-traumatic scar (1 patient) and temporal lobe atrophy (1 patient) were better demonstrated by MRI. A small thrombosed arteriovenous malformation was the only lesion detected by CT but not MRI. Both MRI and CT were negative in 13 patients who had only mild gliosis pathologically and in 1 patient with a 1.2-cm grade 1 astrocytoma. Although more sensitive than CT for detection of structural lesions in patients with refractory partial epilepsy, MRI gave a 25% false-negative rate with a TE60 TR2000 pulse sequence. Therefore, multiecho imaging with at least one long echo time may be needed to increase MRI sensitivity in these patients.

ORAL ABSTRACTS

PULSE SEQUENCES

A COMPARISON OF FAST ACQUISITION MODES IN MRI.

M L Gyngell, G L Nayler, N Palmer, M Paley

Advanced Development Group
Picker International Ltd
P O Box No 2, East Lane
Wembley, Middx, UK
HA9 7PR

The use of fast acquisition techniques in NMR Imaging offer the clinical advantage of increased patient throughput, improved patient comfort, and a reduction in motion related image artefacts.

Fast scan methods may be broadly split into two categories. Category 1 fast scans attempt to cover more of k-space in each acquired FID or spin echo than conventional scans which cover only one 'line' of k-space per view. The limiting case of this is EPI where the 'whole' of k-space is scanned in a single FID. Category 1 fast scans suffer from poor signal to noise due to wide acquisition bandwidths, they can, however, be applied to conventional sequences such as SE and IR, thus preserving their contrasts. Hybrid occupies a position midway between conventional scanning and EPI offering SNRs comparable to normal scans combined with reduced scan times.

The second approach (Category 2) is simply to repeat a sequence as fast as possible. However, this alters image contrast, but good SNR's and resolution can be achieved. One such method is the recently described FLASH technique which uses a very rapid FID sequence with low angle (10°) RF pulses.

The Category 1 methods are extremely demanding in terms of the scanner hardware. They require very high gradient strength, good field homogeneity and generally high system specification and also require careful calibration. The Category 2 methods are better suited to routine application and can be implemented easily without increased hardware demands.

A number of gradient strategies have been investigated for application to the Category 2 approach. It has been possible to produce good head and body images with good resolution, with only a small loss in SNR, in as little as 10 seconds for a 256 x 256 data matrix with single acquisition. This enables a body scan to be taken in a single breath hold resulting in image free of motion artefacts.

The following images were taken with a standard Picker 0.5 Tesla Imaging System, both are 256 x 256 images of 2 acquisition per view, the total scan time was 20 seconds for each image.

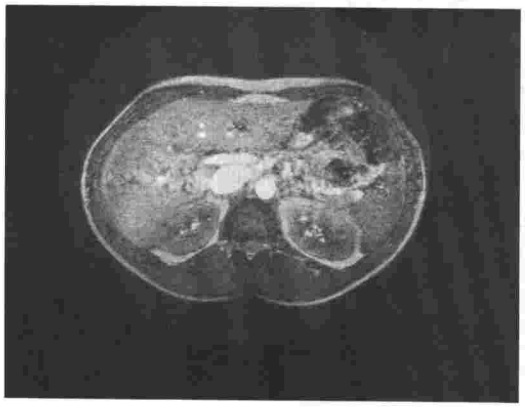

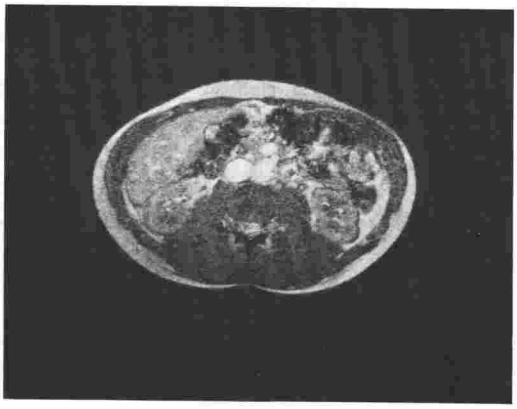

ARTIFACT-FREE MULTIPLE-ECHO IMAGING IN A SINGLE ACQUISITION

D. Lampman and M. Morich

Picker International, Cleveland, Ohio

Multiple echo imaging techniques offer a number of important advantages over single-echo techniques. These advantages include; obtaining a range of T2 contrast images from a single scan, flow imaging, and fast scan techniques. Unfortunately, multiple echo imaging is more susceptible to artifacts due to the increased number of RF pulses involved.

These artifacts may be grouped into three categories:

1) Stimulated Hahn echoes due to refocusing of transverse magnetization from imperfect π pulses (1).
2) Transverse magnetization immediately following imperfect π pulses ("out-of-slice" signal).
3) Steady-state magnetization due to incomplete T2 decay between repetitions.

A commonly used technique to eliminate or reduce these spurious signals is by phase cycling the RF so that unwanted components cancel when averaged together (2,3). However, the requirement of averaging increases the scan time by a factor of N, where N is the number of phase cycles required.

An alternative to phase cycling is to utilize gradient pulses to selectively dephase the unwanted signals while retaining the refocusing of the primary echoes (4,5). However, in order to do this properly with multiple echoes, one must determine the effective flip angles undergone by the magnetization giving rise to the stimulated echoes. These effective flip angles dictate limitations on the symmetry of the dephasing gradients.

We have developed an experimental technique which allows determination of the effective flip angles undergone by the magnetization which appears as stimulated echoes. The technique involves moving the phase encoding gradient to different times in the sequence to determine when this magnetization is in the XY plane. Given this, we have been able to construct appropriate gradient profiles which maximize dephasing of stimulated echoes and out-of-slice signal while still refocusing the primary echo. Figure 1 shows the sequence used for a 4-echo multi-slice sequence.

The third source of artifacts, steady-state magnetization between repetitions, is not amenable to the dephasing techniques described above. However, these artifacts are easily eliminated by the appropriate choice of a spoiler gradient at the end of the sequence.

Using these techniques, we have successfully obtained artifact-free, multi-slice, multi-echo images in a single acquisition (Fig. 2).

REFERENCES:
1)E.L. Hahn, Phys. Rev., 80:580, 1950.
2)D.I. Hoult, R.E. Richards, Proc. R. Soc. Lond. A., 344:311-340, 1975.
3)D.M. Kramer, J.B. Murdoch, L.M. Strenk, SMRM 4th Annual Meeting, 1985.
4)J. Duijn, J. Creyghton, J. Smidt, SMRM 3rd Annual Meeting, 1984.
5)M.L. Gyngell, G.L. Nayler, J.M. McNally, SMRM 4th Annual Meeting, 1985.

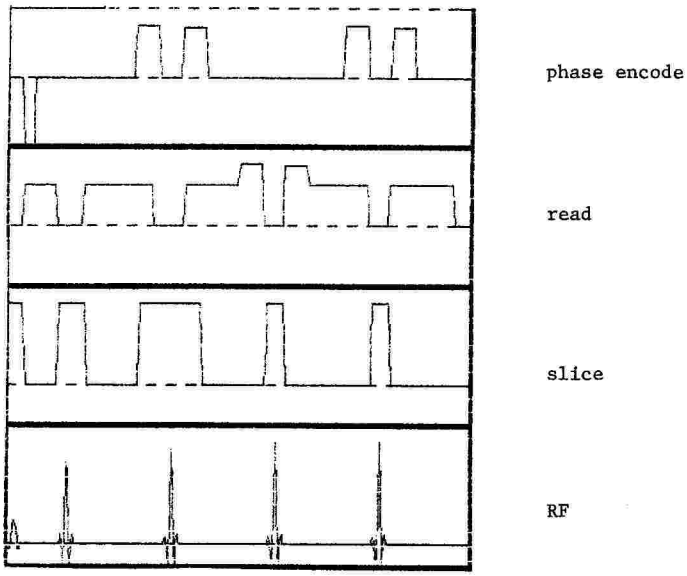

Fig. 1

4 Echo Pulse Sequence

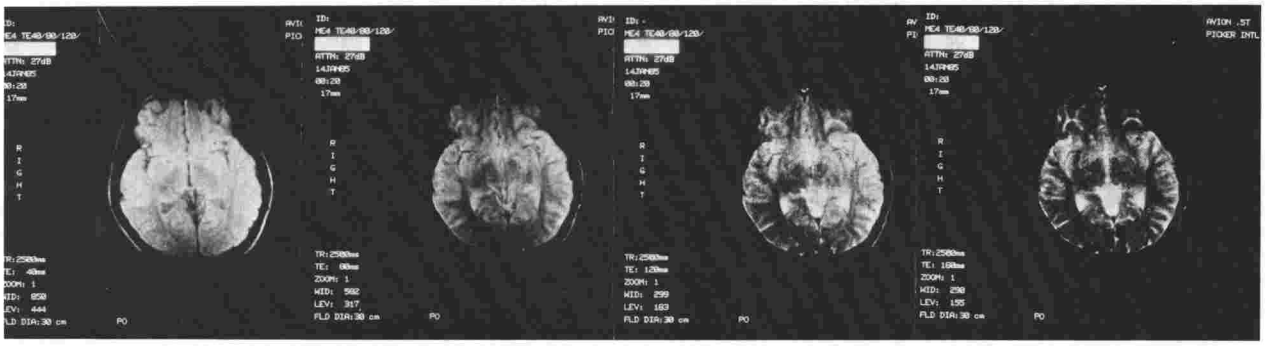

Fig. 2 - 4 echo head images (TEs 40/80/120/160)

FAST HYBRID 3D IMAGING BY SMALL TIP ANGLE EXCITATION

O. Nalcioglu, Z.H. Cho, S.Y. Lee, G. Kashmar and C.B. Ahn

Division of Physics and Engineering, Dept. of Radiological Sciences, University of California-Irvine

We have previously reported a volume imaging method, called the hybrid 3D technique, which combines 2D echo planar method with Fourier imaging. The current work extends the hybrid concept by using the small tip angle excitation technique and homospoiler pulses prior to re-excitation to erase any residual phase memory. The pulse diagram is shown in Figure 1. After a 3D volume is excited by a non-selective α-degree RF pulse the FID signal is encoded in the y-direction with a y-gradient. Subsequently, a sinusoidal x-gradient along with a half-rectified sinusoidal z-gradient are applied to generate the echo planar FID signal. At the end of data collection for a given G_y value, homospoiler pulses are applied to prepare the system for the next RF sequence. The three dimensional volume is reconstructed by applying echo planar reconstruction technique to each G_y(or t_y) plane. The final image is obtained by performing a one dimensional Fourier transform over G_y(or t_y) for all (x,z) coordinate pairs. It can be shown that the reconstructed image is given by

$$I(x,y,z) = \rho(x,y,z)\ \mathrm{Sin}\alpha\{1-E_1(t_R)\}/\{1-\mathrm{Cos}\alpha.E_1(t_R)\} \qquad (1)$$

where ρ density, α tip angle and $E_1(t_R)=\exp(-t_R/T_1(x,y,z))$ with t_R the repetition time.

In order to appreciate the advantage of the new technique we will compare it with the time multiplexed 2D technique in which the time spent waiting for the magnetization to relax within a slice is used to excite other parallel slices within the volume. The maximum number of slices which can be collected by this technique is $N_z=t_R/T_{max}$ where t_R is the repetition time and T_{max} the maximum time required for the encoding and readout. Even though the time multiplexed 2D technique ultimately provides a 3D image, the inherent contrast to noise ratio (CNR) within each slice is low due to the fact that a single slice is excited at any given time. In contrast, the hybrid 3D method excites N_z slices simultaneously (volume excitation). Thus improving the CNR by a factor of $\sqrt{N_z}$. We will now compare the hybrid 3D technique using small tip angle excitation and time multiplexed 2D method using saturation recovery for equal number of slices with the same slice thickness. This will be done in terms of a figure of merit (FOM) per slice which is defined by

$$\mathrm{FOM} = \mathrm{CNR\ (hybrid\ 3D)/CNR(time\ multiplexed\ 2D)} \qquad (2)$$

where CNR is the contrast to noise ratio for a given technique. Using eqs(1) and (2), the FOM is found to be

$$\mathrm{FOM} = f(A,B,t_1,\alpha)\sqrt{N_z}/g(A,B,t_2) \qquad (3)$$

where $g(A,B,t_2)$ = G(A)-G(B) representing contrast of the multiplexed 2D saturation recovery sequence, with $G(j)= \rho_j(1-E_1^j(t_2))$ and j=A,B. In eq.(3) f is defined by $f(A,B,\alpha,t_1)=F(A)-F(B)$ and represents the contrast in the hybrid small tip angle sequence with

$$F(k) = \rho_k \{1-E_1^k(t_1)\} \text{ Sin } \alpha/\{1-\text{Cos}\alpha.\ E_1^k(t_1)\} \quad k=A,B \tag{4}$$

Figure 2 shows the FOM for gray and white matter as a function of flip angle and number of slices simultaneously excited. The employed values were $T_1(G)$=500msec, $T_1(W)$=250msec. The spin densities were taken to be equal. The repetition time for the saturation recovery time multiplexed method was 500msec whereas for the hybrid technique was 50msec. We observe that as the number of slices increases, the hybrid technique provides a CNR higher compared to the time multiplexed method. An additional advantage of the hybrid method lies in its speed which is 10 times faster in the example given above for better CNR and equal spatial resolution.

We have shown that hybrid 3D imaging with small tip angle excitation offers the possibility of obtaining high resolution multislice information in a shorter data acquisition time. We are in the process of applying the hybrid technique to phantom and patient studies.

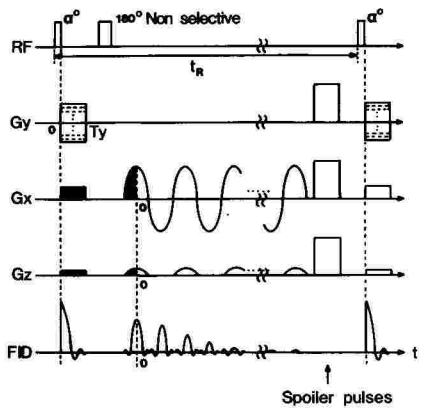

Figure 1. Hybrid 3D pulsing sequence with small tip angle.

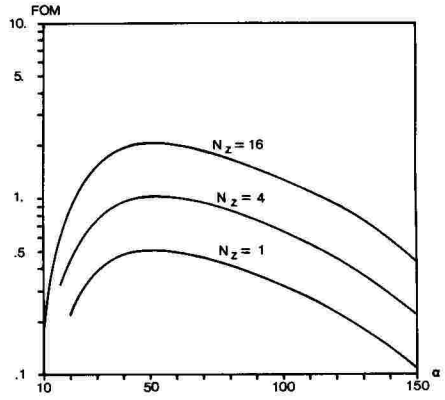

Figure 2. Figure of merit of hybrid 3D method.

FLASH MR IMAGING

J. Frahm, A. Haase, D. Matthaei, W. Hänicke, K.D. Merboldt

Max-Planck-Institut für biophysikalische Chemie, P.O. Box 2841, D-3400 Göttingen, FRG

FLASH (Fast Low Angle Shot) MR imaging is a new technique for high-quality rapid two- and three-dimensional MR imaging. The method employs the detection of the free induction decay (FID) in the form of a gradient echo and takes advantage of excitation pulses with flip angles of the order of 15°. Thus "repetition times" are reduced to about 10 - 20 msec. Typical measuring times are 2 sec for a 128 x 128 2D-image and 4 min for a 128 x 128 x 128 3D data set. The major advantages of the FLASH technique are: (i) a reduction of the measuring time by a factor of 50 - 100, (ii) a solution for all types of motional artifacts without the need of gating or triggering, (iii) high signal-to-noise per unit time, (iv) movie imaging capability for functional MR studies, and (v) rapid isotropic 3D imaging capability even of the abdomen and thorax. Experiments have been carried out on animals and humans.

STIMULATED ECHO MR IMAGING

J. Frahm, A. Haase, D. Matthaei, W. Hänicke, K.D. Merboldt

Max-Planck-Institut für biophysikalische Chemie, P.O. Box 2841, D-3400 Göttingen, FRG

STEAM (Stimulated Echo Acquisition Mode) MR imaging is a new technique for multi-parametric MR studies which takes advantage of the properties of the stimulated echo signal. Stimulated echos are excited by sequence of at least three RF pulses which normally have 90° flip angles. However, special applications such as T1 imaging may benefit from series of pulses with even lower flip angles. In general, STEAM MR imaging offers a variety of new imaging modalities: (i) contiguous multi-slice imaging with arbitrary timings, (ii) continuously variable T1 contrast independent of TR, (iii) simultaneous recording of a set of images describing the spin-lattice relaxation behaviour, (iv) multiple chemical shift selective (CHESS) MR imaging using selective excitation, (v) diffusion imaging, and (vi) flow imaging. Experiments on normal volunteers and patients have been carried out using a 40 cm 2.3 T system and a whole-body magnet.

NON ORTHOGONAL MR IMAGING : TECHNIQUES AND CLINICAL APPLICATION

S.D. Mehta, P.P. Price, M.V. Kulkarni

The University of Texas Health Science Center Houston and Vanderbilt University Medical Center

Although different techniques of non orthogonal Magnetic Resonance (MR) Imaging have been described previously, they frequently involve positioning the patient in oblique position. We have developed an electronic technique to minimize patient discomfort and provide unlimited non orthogonal planes of MR Imaging.

A three dimensional model to explain axes of x, y and z gradient was developed. By changing one or all eular angles, proper non orthogonal plane was acquired. This technique was utilized and images were acquired in 82 patients with cardiac, spinal and abdominal pathology. This included a series of 12 patients who underwent post operative evaluation of mustard and sennings procedure.

Non orthogonal MR Images displayed the anatomy regarding myocardial thickness, cardiac chamber relationships and vascular connection. These images were also useful in obtaining proper cross sectional measurements of vessels at the level of anastomosis. The evaluation of intervertebral discs and their herniation into the spinal canal was felt to be superior with non orthogonal plane rather than the conventional transverse plane. This presentation will explain in detail the methods of obtaining non orthogonal MR images and technique to minimize errors and artifacts associated with non orthogonal MR Imaging. Multiple algorithms were developed to obtain proper imaging planes to evaluate specific organ systems and/or disease processes being studied.

Non orthogonal MR Imaging is superior to conventional orthogonal planes in certain situations. By changing the gradient angles electronically, infinite numbers of imaging planes can be obtained without patient discomfort. With this technique high quality images were obtained without associated artifacts and is particularly well suited for cardiac and lumbosacral spinal imaging in view of their anatomic orientation.

MAXIMIZING SIGNAL-TO-NOISE AND CONTRAST-TO-NOISE RATIOS IN SPIN-ECHO IMAGING USING NON-STANDARD FLIP ANGLES

Terrence J. Provost, M.S.* and R. Edward Hendrick, Ph.D.+

*NMR Advanced Development Group, Picker Corporation, Highland Heights, OH
+Department of Radiology, University of Colorado School of Medicine, Denver, CO

Ernst has shown that the flip angle maximizing the signal-to-noise ratio for a series of θ^{o} pulses with subsequent free-induction decay measurement is given by $\cos(\theta)=e^{-TR/T1}$. It is well-known that the signal-to-noise maximum occurs as $\theta \rightarrow 0$ and $TR \rightarrow 0$ while satisfying the above expression.[2] In this work, we consider a generalized spin-echo sequence: θ^{o}-TE/2-180^{o}-TE/2-measurement-T'... ,where TR=TE+T'. An analytic expression similar to the Ernst expression is derived for the flip angle maximizing signal-to-noise in generalized spin-echo imaging, and the degree of improvement of the signal-to-noise ratio over conventional ($\theta=90^{o}$) spin-echo imaging is quantified. Similar results are reported for the improvement in contrast-to-noise ratios from the generalized spin-echo sequence over that of the conventional ($\theta=90^{o}$) spin-echo sequence. TE, TR, and θ values that maximize the signal-to-noise and contast-to-noise ratios in the generlized spin-echo sequence are given in analytic or parametric form.

In the generalized spin-echo sequence, the signal-to-noise ratio is maximized for $TE=TE_{min}$ and $\cos(\theta_{opt})=-e^{-TR/T1}$. The improvement in signal-to-noise from the generalized spin-echo sequence over that of the standard ($\theta=90^{o}$) sequence for TR fixed is a strong function of TR/T1 and is essentially independent of TE. For TR/T1=.5, $\theta_{opt}=127^{o}$, and a 30% improvement in S/N results. For TR/T1=1, $\theta_{opt}=112^{o}$, and a 7% improvement in S/N results. For TR/T1=3, $\theta_{opt}=90^{o}$, the generalized sequence provides essentially no improvement in signal-to-noise. When TR is varied to optimize signal-to-noise in either the generalized or standard spin-echo cases, then TR_{opt}, θ_{opt}, and the degree of improvement all become functions of TE/T1, with the greatest improvement occurring for small values of TE_{min}, TR_{opt} in the generalized case shorter than in the standard case, and $\theta_{opt} > 90^{o}$.

Contrast-to-noise improvements using the generalized spin-echo sequence also depend on TE/T1. For realistic TE/T1 values, improvement amounts to only a few percent if TR is optimized separately in the generalized and standard cases. For cases where TR is constrained, substantial contrast-to-noise improvements can result by choosing $\theta_{opt} > 90^{o}$.

1. R.E. Ernst, Rev. Sci. Instr. 37, 93 (1966).
2. P. Mansfield and P.G. Morris, Advances in Magnetic Resonance: NMR Imaging in Biomedicine, New York: Academic Press, 192-4 (1982).

THREE SECOND CLINICAL NMR IMAGES USING A GRADIENT RECALLED ACQUISITION IN A STUDY STATE MODE (GRASS)

J.A. Utz, M.D.[1], R.J. Herfkens, M.D.[1], G. Glover, Ph.D.[2], N. Pelc, Sc.D.[2]

[1]Department of Radiology, Magnetic Resonance Imaging Section, Duke University Medical Center, Durham, North Carolina; [2]General Electric Company, Milwaukee, Wisconsin

One limitation of the application of nuclear magnetic resonance (NMR) to clinical imaging is the prolonged imaging time required. A number of new imaging techniques have been introduced to shorten this imaging time. One such technique utilizes an extremely short repetition time (10-20 msec). Since the repetition is much less than the T1 relaxation time of normal tissues, flip angles of less than 90 degrees are utilized to decrease saturation effects. An echo is generated using gradient reversal and images are acquired with conventional 2DFT spin warp technique. This technique enables the acquisition of 3 second clinical images. A review of 100 "GRASS" images obtained in 18 patients, performed on a 1.5 Tesla superconducting magnet (GE Signa System), revealed spatial resolution that was equivalent to normal spin echo images obtained at a TR of 500 and a TE of 25 msec. The images were extremely sensitive to blood flow. This sensitivity permitted quick identification of the vascular nature of indeterminant structures such as varices or aberrant vessels. The differentation of dilated bile ducts from hepatic or portal veins, both of which may have decreased signal on MR images, was facilitated. Additionally, the hypervascularity of abdominal masses was accentuated. Contrast resolution secondary to tissue differences in T1 relaxation times was slightly diminished when a flip angle of 45 degrees was utilized and the GRASS images were compared to spin echo images utilizing a 90 degree pulse. Motion related artifacts were enhanced and evaluation of the left lobe of the liver was compromised by artifact from the pulsatile aorta. The short acquisition times, however, allowed for obtaining images during breath holding in all patients, thus minimizing respiration related artifacts. The technique was sensitive to field nonhomogeneity and metallic artifacts were exaggerated.

Two second GRASS images are extremely useful in anatomic localization. The marked flow sensitivity may assist in the verification of the vascular nature of an area of indeterminant signal intensity as well as in the evaluation of vascular patency.

MULTIPLE ANGLE OBLIQUE MAGNETIC RESONANCE IMAGING

S Smith, R Olsen, R Wolf, D Hertz, M Reicher, Flannigan B, Lufkin R

FONAR Corporation(SS,RO,RW,DH), UCLA School of Medicine(MR,BF,RL)

Multiple angle oblique magnetic resonance images were produced on normal volunteers using multislice 2D-FT spin echo imaging. The technique allows for the choice of slice angle and position individually for each slice in a multi-slice sequence. This was accomplished by appropriate adjustment of the slice select RF pulse frequency and the slice select and readout magnetic field gradients for each image plane. Multiple angle oblique MRI has potential application in studies of the lumbar spine, TMJ, orbits, knees, and other regions where non-parallel oblique scanning is necessary. A practical limitation is that artifacts occur in the region of intersection of multiple planes due to local changes in effective repetition time.

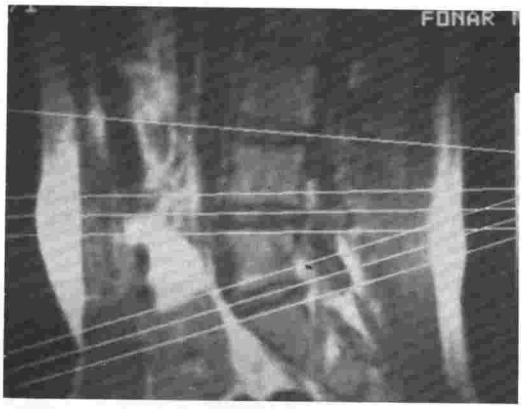

IMAGING OF SELF-DIFFUSION COEFFICIENT BY NMR

C.B. Ahn, S.Y. Lee, O. Nalcioglu and Z.H. Cho

Division of Physics and Engineering, Dept. of Radiological Sciences, University of California-Irvine

The pulsed field gradient (PFG) technique for measuring coefficient of self-diffusion (D), introduced by Stejskal and Tanner, provides a simple and effective means for determining D in small samples. The implementation of the PFG technique for larger objects using an NMR scanner is quite difficult due to various experimental complications. In this paper, we report on a new technique in which the length of the readout gradient is varied for each set of images during data collection. The main advantage of using the readout gradient for diffusion coding is due to the residual gradient fields which arise from eddy currents. The residual gradient in the readout direction is easily measurable and can be corrected for by finding the time position of the echo center, while that in slice selection or coding gradient directions introduces additional signal attenuation by spin dephasing, from which signal decay by diffusion cannot be distinguished. The pulse sequence introduced in this work is shown in Figure 1. It is similar to conventional two dimensional Fourier imaging except that the duration of the readout gradient is varied to encode different amounts of diffusion attenuation. Note that the time position of echo center is constant thus making the spin-spin relaxation effects identical in all experiments. If we denote an image obtained with a specific diffusion encoding time t_k by $I^k(x,y)$, it can be shown that the two dimensional diffusion may $D(x,y)$ is given by,

$$\ln\{I^k(x,y)/I_o(x,y)\} = - D(x,y)C_k \qquad (1)$$

where I_0 is the spin density image without any diffusion effects and

$$C_k = \gamma^2 \sum_{j=1}^{3} \{ \int_0^t (\int_0^{t'} G_j(t'')dt'')^2 dt' \} \quad (2)$$

with $G_1 = G_S$, $G_2 = G_C$ and $G_3 = G_R$. We can eliminate $I_0(x,y)$ using eq.(1) with two images obtained with different readout gradient durations. The result is,

$$\ln\{I^m(x,y)/I^n(x,y)\} = -D(x,y)\{C_m - C_n\} \quad m \neq n \quad (3)$$

The above described technique was tested experimentally with a 0.6T whole body NMR scanner with three orthogonal gradient fields of strength 0.25G/cm. In the experiments a phantom which contained distilled water, acetone and DMSO in separate compartments was used. The repetition time was taken to be 2 seconds.

Four diffusion coding steps were used, i.e. k=1,2,3. and 4 in eq.(1). Figure 2 shows one of the images. A two dimensional absolute diffusion map (see Figure 3) was computed using the four images and eq.(3). In Figure 3, the displayed gray levels are equal to the coefficient of self-diffusion within the slice. The brightest circular region is acetone. The background area is distilled water. The darker circular region on the right side is DMSO. The measured diffusion coefficients for the three materials are: $D(H_2O)=2.16\pm 0.20$, $D(\text{Acetone})= 4.4\pm 0.26$ and $D(\text{DMSO})=1.19\pm 0.15$, all in 10^{-5} cm^2/sec. For comparison, the diffusion coefficients for water and acetone measured by others are 2.5×10^{-5} and 4.50×10^{-5} cm^2/sec, respectively. Thus, our results obtained from the two dimensional diffusion map of the phantom agree well with measurements obtained by other techniques.

We have shown that the new imaging technique is capable of providing accurate diffusion coefficient maps of materials. It would be interesting to apply this technique to human subjects. Tissue characterization by diffusion map has hardly been tried in humans but may have a potential in future studies.

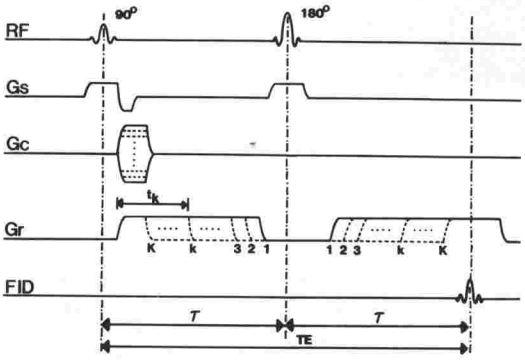

Figure 1. Pulsing Sequence

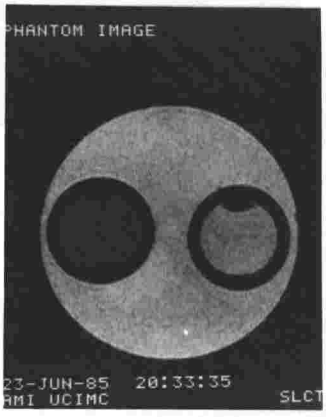

Figure 2. Phantom Image

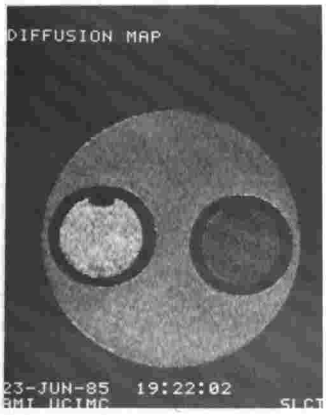

Figure 3. Diffusion Map

FAST SCAN 2DFT IMAGING AT 0.15T BY FIELD ECHOES AND SMALL PULSE ANGLE EXCITATION.

N.G. Kumar, N. Karstaedt, and P.R. Moran

Department of Radiology, Bowman Gray School of Medicine, Winston-Salem, North Carolina 27103

Many clinical applications of 2DFT MR imaging need very fast scanning time. One of the major limitations is long relaxation waiting period (TR) between differently phase-encoded data aquisition cycles. By using a small tip angle (Fig. 1), one can use fast pulse-cycle repetition times and pulse fast without saturating the NMR signals. The relationship between α (pulse angle or Ernst angle), TR and T_1 is given by: $\alpha = \cos^{-1}[\exp(-TR/T_1)]$; $TR = T_1(1-\cos\alpha)$. For example, using a 30°rf-pulse (Fig. 1) the detected signal is reduced to sin (30°) = (0.5) relative to a 90° rf-pulse ($M_{xy} = M_o \sin\alpha$). The magnetization left behind (cos 30°) is 0.87, hence only 13% of the coherence has been destroyed ($M_z = M_o(1-\cos\alpha)$) and one can pulse six times faster because smaller TR time is required to reestablish equilibrium along the z-axis. The gain in scan time by a factor of six can more than offset the loss of signal by a factor of two.

In 2DFT MRI, spatial information is encoded in terms of frequency in one axis (t_2) and in terms of phase in the other (t_1). In Fig. 1, selective small angle excitation by $(\pi/6)_x$ pulse ($\alpha = 30°$) or by $(\pi/4)_x$ rf-pulse ($\alpha = 45°$) brings the longitudnal magnetization initially present along the z-axis into the y-axis of the rotating frame and in the presence of gradient G_z^+ defines a slice in the x-y plane (TRANS image plane; Figs. 2 and 3). The slice select gradient pulse G_z^+ applied during the rf-pulse has the effect of dephasing the magnetization. Therefore, a gradient of opposite sign (bipolar) G_z^- is required to rephase the spins across the thickness of the slice. The spins are dephased along the y direction by G_y^- and are rephased by a readout gradient G_y^+ giving rise to a field-echo at time TE by gradient-reversal. In order to discriminate structures in the x-direction, phase-encoding gradient G_x is applied and this sequence is repeated N times with identical G_y and G_z waveforms (N = 128 (Fig. 2); N = 256 rows (Fig. 3)) but the gradient G_x has different amplitude each time. The individual amplitudes of the G_x phase-encoding pulse vary linearly with the sequence number (N) during the evolution period t_1.

The fast scan breast images of a patient, (Figs. 2 and 3; FOV = 350 mm, slice thickness = 10 mm, one repetition, bandwidth = 10 KHz), were obtained in 12 sec (128 x 128) and 24 sec (256 x 256 resolution) by using the small tip-angle pulse sequence and gradient-reversal echoes (Fig. 1) at 0.15T (6.3855 MHz) Picker resistive imaging system. We have shown that 2DFT images of diagnostic quality of a single slice can be obtained in a time well below the nominal breath-holding limit of 18 sec at 0.15T. The clinical applications of this (Fig. 1) and other fast scan pulse sequences in the areas of flow and motion, (respiratory, cardiac etc.), where image quality is limited by slow motion, are under investigation. Low RF energy deposition in the patient at higher magnetic field is an added advantage of this fast scan pulse technique.

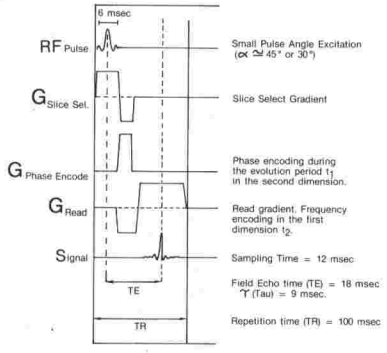

Fig. 1. Small Tip Angle Pulse Sequence

Fig. 2. 2DFT Trans breast image. 128 x 128. TR = 100 msec., $\alpha = 45°$, Total scan time = 12 sec., S/N = 9.

Fig. 3. 2DFT Trans breast image. 256 x 256. TR = 100 msec., $\alpha = 45°$, Total scan time = 24 sec., S/N = 7.

NON-PROTON IMAGING AND SPECTROSCOPY

SPECTROSCOPIC IMAGING BY QUADRATURE MODULATED ECHO TIME SHIFTING

C.B. Ahn, S.Y. Lee, O. Nalcioglu and Z.H. Cho

Division of Physics and Engineering, Dept. of Radiological Sciences, University of California-Irvine

A new proton spectroscopic imaging technique, for resolving fat and water simultaneously, is proposed and experimentally confirmed. The new method is a variation of the echo time encoded spectroscopic imaging technique which has a unique advantage for providing images with high spatial resolution [1]. The basic idea of this technique is to shift the echo signal from the rephasing point, hence generating different phase codings for different compounds. If the time shift, ΔT, and difference in the precession frequency, Δf, of the two compounds due to chemical shift satisfy the following relationship

$$\Delta T \cdot \Delta f = 1/4 \qquad (1)$$

then the two compounds will have orthogonal phases. Since the density map is a real function, we can readily resolve the two compounds using quadrature information. As shown in the experimental pulse sequence (see Figure 1), the echo shifting is made by adjusting the amplitude of the dephasing readout gradient. Once the FID is separated into water and fat, chemical shift artifact correction is performed by moving each image by a known amount in the direction of readout gradient [2].

Since the quadrature modulation is applied to water and fat within the same slice, phase error due to the T_2 relaxation time (in this case the reconstructed image becomes a complex function) or phase coding by blood flow is less severe compared to the quadrature dual slice technique [3]. As is in other application areas, decomposition or demodulation of the reconstructed image into two parts is the essential part of the new technique. In order to accomplish the separation, a small reference tube is placed near the object, and zeroth and first order phase corrections are performed observing the projection data until reference material is projected completely on either the real or imaginary axis. The use of a predetermined correction factor by some other technique is also possible [3].

The new technique was experimentally tested using a phantom which contained water and salad oil at 0.6T with a whole body NMR scanner. The real part of the FID corresponded to water and imaginary part to oil. Figure 2 shows an image of the water component. The oil image is shown in Figure 3. Finally, a composite image of oil and water corresponding to a conventional image is shown in Figure 4.

The advantage of the new technique is the imaging of water and fat with one measurement, hence reducing the scan time. Although it has no signal to noise ratio(SNR) gain, it is attractive in high field imaging systems where FID averaging is not necessary. Also this technique is quite stable against motion artifacts, since it involves images obtained within a relatively short measurement time.

References

1. W.T. Dixon, Radiology 153, 189 (1984)
2. Z.H. Cho, O. Nalcioglu, H.W. Park, J.B. Ra, and S.K. Hilal, Magn. Reson. Med. 2, 253 (1985)
3. J.B. Ra, S.K. Hilal, H.W. Park, M.H. Cho, and Z.H. Cho, Quadrature multiplexed pulse sequence for dual slice NMR imaging. To be published in Magn. Reson. Med.

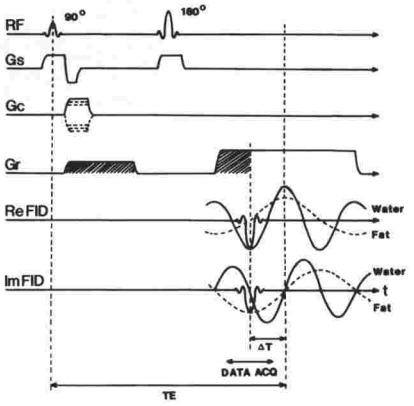

Figure 1. Pulse sequence.

Figure 2. Water.

Figure 3. Oil.

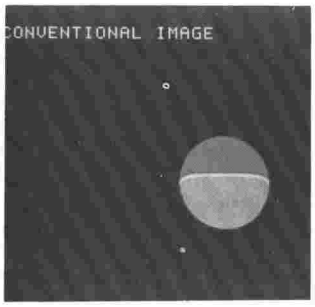

Figure 4. Combined image.

UTILIZATION OF PROTON SPECTROSCOPIC PHASE CONTRAST IMAGES

Charles Spritzer, M.D., Leon Axel, Ph.D., M.D.,
Herbert Y. Kressel, M.D.

Hospital of the University of Pennsylvania, Philadelphia, PA 19104

Over 20 patients with a variety of abnormalities were examined using the "out of phase" contrast image technique first described by Dixon.(1) Twelve patients with bone marrow abnormalities including avascular necrosis (7), osteomyelitis (3) and miscellaneous (2) were examined. The extent of osteomyelitis was better appreciated with the out of phase images. Delineation of fatty from hemopoietic and abnormal marrow was enhanced in the patients with avascular necrosis. Out of phase images may help increase tissue specificity. In 3 lipomas the cancellation of signal at the interface of the aliphatic and water tissues created a loss signal which appeared as a dark ring surrounding the tumors. This ring confirmed the fatty nature of the tumors. The presence or absence of this ring has helped in distinguishing between fat and hemorrhage in a variety of situations including metastatic tumors and ovarian masses. Proton spectroscopic phase contrast imaging promises to be a useful technique in magnetic resonance imaging.

1. Dixon WT. Simple proton spectroscopic imaging. Radiology 1984; 153: 189-194

AN EVALUATION AND COMPARISON OF METHODS FOR LOCALIZED IN VIVO HIGH RESOLUTION SPECTROSCOPY

Hong Yan and John Gore

Department of Diagnostic Radiology, Yale University School of Medicine, New Haven, Connecticut 06510

High resolution NMR spectra obtained in vivo from tissue reveal a variety of useful biochemical information, such as the relative concentrations of high energy metabolites depicted in a P^{31} spectrum. The successful application of spectroscopic techniques in large animals relies on developing methods for localizing the volume that gives rise to the signal. We are studying the relative performances of such methods. Most work to date has used simple surface coils with inhomogeneous RF fields to define the sensitive region, but by suitably modulating the amplitudes and phases of sequences of pulses a better degree of localization can be achieved. Such depth pulses however are impractical for deep structures while experiments and simulation show unwanted signals contaminate the desired response. The use of multiple coils introduces phase errors which may however be reduced by modifying the pulse cycle. Several methods can be adapted that use spatially selective pulses in the presence of magnetic field gradients. In principle orthogonal

gradients applied in succession with a sequence of echo refocusing pulses or selective excitations can give accurate spatial localization. However, the detailed spectrum and volume shape are affected by instrumental factors such as off-resonance effects, RF field inhomogeneity and phase imperfections. We have developed a computer simulation of these methods in order to study their behavior and develop criteria for their relative performances. In studies of the effects of system imperfections we demonstrate that echo techniques in particular are susceptible to errors and propose a modification to the simple volume selection techniques to provide localization more immune to such effects. The ability to perform more elaborate experiments in the region of interest, such as solvent suppressed proton NMR, is also being evaluated.

BIOENERGETICS OF ALCOHOLIC LIVER DISEASE IN THE RAT: COMPARISON OF ^{31}P NMR SPECTROSCOPY WITH HPLC

J.H. Helzberg[1], M.S. Brown[2], D.J. Smith[1], J.C. Gore[2], E.R. Gordon[1]

Liver Center[1] and Department of Diagnostic Radiology[2], Yale University School of Medicine, New Haven, CT

Previous investigations have variably demonstrated decreases in liver ATP content in rats chronically fed ethanol. The technique usually used for assessment of hepatic ATP, ADP, and AMP levels has depended on freeze clamping the liver. This method has the disadvantage of sampling a small piece of tissue at an isolated time. Furthermore, phosphate bonds are readily lost with hypoxia. In this study, ATP/ADP ratios obtained by HPLC after liver freeze clamp were therefore compared to values obtained by ^{31}P NMR spectroscopy in vivo.

Hepatic ATP/ADP ratios were obtained by in vivo ^{31}P NMR spectroscopy performed on rats fed for six weeks with a nutritionally adequate liquid diet containing either 36% of calories as ethanol or a liquid control diet. Ethanol fed animals received three grams of ethanol per kilogram body weight by gavage immediately prior to investigation. A small surface coil was placed on the liver of ethanol fed and control rats through a midline laparotomy with ketamine/xylazine anesthesia. Spectra were obtained at 34 MHz using a short 90 pulse preceeded by low level presaturation of the broad phosphorus baseline. Hepatic ATP/ADP ratios as assessed by ^{31}P NMR spectroscopy were 6.5:1 in the control animals (N=5) and 3.2:1 in the ethanol fed rats (N=5, $p<.01$). Values obtained by this technique were compared to ATP, ADP, and AMP levels measured on HPLC of freeze clamped liver (-70°C). ATP levels were significantly decreased in the ethanol fed rats ($p<.01$), and AMP and ADP levels were increased, though only the former increased significantly ($p<.05$). ATP/ADP ratios by HPLC were 3.2:1 in the control animals and 1.3:1 in the ethanol fed rats ($p<.05$).

Conclusion:

Hepatic ATP/ADP values were found to be decreased by both ^{31}P NMR spectroscopy and HPLC in rats chronically fed ethanol. The difference in absolute ATP/ADP ratios by the two techniques is probably explained by breakdown of high energy phosphate bonds during freeze clamp extraction. Alternatively, an increase in ATP/ADP levels obtained by ^{31}P NMR spectroscopy may result when ADP is rendered partially invisible to NMR by binding effects with proteins. Further experiments to unravel the cause of such discrepancies and the effect of ethanol on phosphorylation will be presented.

BLOOD PO_2 IMAGING BY ^{19}F MRI

J.E. Fishman[1], T.F. Floyd[2], H.A. Sloviter[3], M. Ziegler[2], and P.M. Joseph[1]

Departments of Radiology[1], Surgery[2], and Harrison Department of Surgical Research[3], University of Pennsylvania School of Medicine, Philadelphia, PA 19104

Dissolved molecular oxygen is paramagnetic and thus enhances the spin-lattice ($1/T_1$) relaxation rates of neighboring nuclei. The amount of influence depends on the ratio of oxygen molecules to susceptible nuclei in the sample. Fluorinated blood substitutes such as perfluorotributylamine (FTBA) have oxygen solubilities greater than ten times that of water or plasma. The ^{19}F spin-lattice relaxation rates of such compounds vary linearly as a function of PO_2 (1), and the T_1 values exhibit much larger changes per change in PO_2 than do protons. This phenomenon raises the possibility of assessing blood and organ oxygenation via T_1 differences in ^{19}F images. We have developed an FTBA-perfused kidney preparation which can be imaged with ^{19}F MRI. By increasing the flow rate of perfusate, the arteriovenous O_2 difference decreases; this is reflected by a decrease in T_1 in both venous perfusate samples and the organ image.

The renal artery and vein of a New Zealand rabbit were catheterized and a recirculating perfusion of emulsified FTBA was begun at pH 7.4 and 22°C. The reservior was bubbled with 95% O_2-5% CO_2. The kidney and catheters were transferred to a 1.4 Tesla MRI (55.6 MHz) where the kidney was perfused at various flow rates. At each flow rate, arterial and venous samples were obtained for T_1 measurements. The kidney was imaged using a partial saturation pulse sequence, T_E 6.7 msec. Two images were obtained: one at T_R 400 msec and another at T_R 2000 msec. By forming a divided image (400/2000) the resultant image is heavily T_1 dependent (shorter T_1 values appear brighter); image T_1 can be calculated from the divided image pixel intensity.

The Table presents T_1 values obtained from arterial and venous perfusate samples at 2 different flow rates. As a reference, the T_1 of 100% O_2 - saturated FTBA is 260 msec; deoxygenated FTBA has a T_1 of 690 msec (both measured at 55.6 MHz and 22°C). The venous T_1 decreased as flow rate increased, reflecting a diminished A-V O_2 difference at the higher flow rate. Also tabulated are whole-kidney image T_1 values calculated from the divided images. The image T_1 is seen to track the venous sample T_1 value closely. The divided images show an overall higher intensity at the higher flow rate, reflecting a lower T_1; furthermore, the cortex is selectively enhanced as the flow rate increased.

Fluorinated blood substitutes are potentially valuable as PO_2 imaging agents using ^{19}F MRI. Our results demonstrate that fluorine images can track the changes in perfusate PO_2 which occur when flow rate to an organ is changed. We are currently investigating the use of other fluorinated compounds which may provide even more sensitive estimates of blood PO_2 than does FTBA.

TABLE

Flow Rate	Sample	T_1, msec
2.5 ml/min	Arterial	276
	Venous	532
	Image	526
8.0 ml/min	Arterial	349
	Venous	373
	Image	368

^{19}F Divided Images of Rabbit Kidney

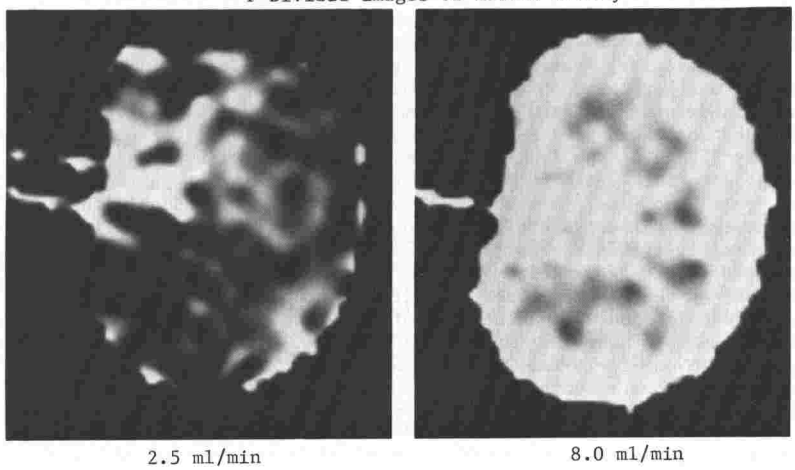

2.5 ml/min 8.0 ml/min

(1) Parhami, P. and Fung, B., J. Phys. Chem. 87, 1928-31 (1983).

31-P SPECTROSCOPY OF RENAL EFFECTS FROM LITHIUM ISOTOPES

Patrick T. Cahill, Tom Vullo, John A. Markisz, Michael J. Hennessey,* Michiko Okamoto, Bradford A. Bottger, Peter Stolle, Peter E. Stokes, Joseph P. Whalen, and R. James R. Knowles

The New York Hospital-Cornell Medical Center, 525 E. 68th St., New York, N.Y. 10021
*Intermagnetics General Corporation (RPI), Troy, New York 12180

In order to quantitate differences in the degrees of renal toxicity caused by 6-Li and 7-Li, we analyzed in vivo 31-P NMR spectra of rat kidneys. Male Wister rats were injected subcutaneously with either 6-Li or 7-Li chloride solutions (1mg/kg twice daily) for a period of two weeks. In vivo 31-P NMR spectroscopy at 2.2 T was performed on the intact, surgically exposed kidney, placed on a specially designed surface coil. 31-P spectra of control rats typically demonstrated seven peaks: three associated with beta, alpha and gamma ATP phosphate groups; a fourth displaying a small level of phosphocreatine (PCr); a phosphodiester peak; an inorganic phosphate peak; and a sugar phosphate peak. Spectra of 6-Li treated rats exhibited a markedly elevated PCr level and a decrease in the level of sugar phosphates, relative to the

controls (using total areas). Rats treated with 7-Li had spectra which were similar to those of controls, except for elevated phosphodiester levels. Thus the 31-P biochemical processes of rat kidneys treated with 7-LI are closer to those of the control rats than are those of the 6-Li treated group, and 31-P spectroscopy appears to be a very sensitive method for quantifying the effects of the different lithium isotopes.

IMAGING THE VASCULAR SYSTEM USING ^{19}F MRI

P.M. Joseph[1], J.E. Fishman[1], B. Mukherji[2], and H.A. Sloviter[2]

Departments of Radiology[1], and Surgical Research[2], University of Pennsylvania School of Medicine, Philadelphia, PA

Fluorinated blood substitutes such as perfluorotributylamine (FTBA) are heavily fluorinated and are amenable to ^{19}F NMR imaging. ^{19}F MRI using such compounds has been proposed for investigations of the vascular system, both because of the absence of naturally-occurring fluorine and the fact that emulsified fluorochemicals remain in the circulation after infusion. However, significant difficulties exist for the imaging of fluorine in moving blood. The NMR spectra of fluorinated compounds are typically complex; for example, FTBA has four peaks. Second, moving blood dephases rapidly, especially in a gradient field. We have developed a new technique which uses spectrally selective excitation and spin-echo RF pulses for imaging FTBA. High-quality images of the vascular system in a living rat infused with FTBA are made in 8 minutes or less.

Imaging was performed on a 1.4 Tesla, animal-sized MR imager. The spin warp imaging technique was used, with pulse bandwidths modified for ^{19}F imaging of FTBA as follows. The spectrum of FTBA contains four peaks: a pair of peaks separated by 2 ppm which contain 56% of the fluorine signal between them, and two upfield peaks separated by 36 and 44 ppm from the downfield pair. Using a newly developed technique we selectively imaged the pair of downfield peaks by suppressing the upfield peaks in two ways. The 90° excitation pulse was enveloped by a sinc waveform such that its bandwidth included only the imaging peaks. For slice selective imaging, however, selective excitation would excite each spectral line in a different plane. In this case, spectral selectivity was accomplished by limiting the bandwidth of the 180° pulse to refocus signals from the imaging peaks only. Results from phantom tests indicated that the ratio of signals from the undesired spectral lines to that of the imaging lines was within 2.5% in all cases (including slice-selective scans). Rats (250-350g) were infused with a quantity of 36% FTBA emulsified in lecithin equal to 3% of body weight, and were imaged within 6 hours of infusion. A partial saturation, spin echo pulse sequence was used for imaging, with T_R=500 msec and T_E=15 msec. Data was taken on a 64x64 pixel grid, and images were formed in 8 minutes.

The figure shows a coronal, non-slice selective image of a rat after infusion of FTBA. The heart and liver are labelled at the left. Several vessels are seen in the upper body, including the external jugular veins (labelled). There is a background ^{19}F signal from the animal, probably representing fluorine in vessels too small to be resolved. An exactly corresponding proton image was made (not shown), which lacked the vascular information present on the ^{19}F scan. Fluorinated blood substitutes may have potential as NMR contrast agents, particularly in the cardiovascular system.

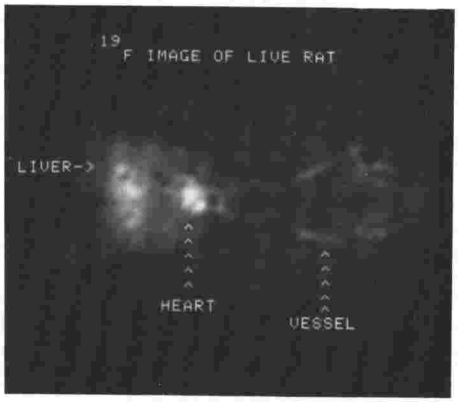

INITIAL CLINICAL EXPERIENCE WITH SPECTROSCOPIC IMAGING BY QUADRATURE MODULATED ECHO TIME SHIFTING

R. Friedenberg, D. Katz, H. Pribram, O. Nalcioglu, H. Fritts

University of California, Irvine

Examples of normal and abnormal multiple organ scans including brain, liver, and kidney will be shown utilizing a new proton spectroscopic imaging technique for resolving fat and water simultaneously. This new method is a variation of the echo encoded imaging technique which has high spatial resolution. The technical aspects of Spectroscopic Imaging by Quadrature Modulated Echo Time Shifting are being presented separately. The technique was initially tested with phantoms and then on normal brain and abdominal organs and finally on appropriate lesions which benefit from fat and water shift. The authors feel that this technique, when compared to the Dixon technique, reduces scan time, provides less motion and chemical shift artefact, and provides better spatial resolution.

VOLUME SELECTIVE ^{1}H NMR SPECTROSCOPY WITH SOLVENT SUPPRESSION

D. Lampman, G. Hurst, J. McNally, and M. Paley*

Picker International, Cleveland, Ohio *Wembley, U.K.

Introduction - In vivo ^{1}H NMR spectroscopy requires spatial localization as well as suppression of the very large water signal. Techniques which rely on the field profile from a surface coil to achieve spatial localization have several drawbacks, including: 1) The coil must be physically moved to change the localization coordinates which it determines; 2) The size and shape of the localized region are not clearly definable, and vary with position of the region relative to the coil; 3) If the surface coil is used for transmit, there is a chemical shift dependence in the spatial response [1], which further complicates the definition of the localized region.

In order to avoid these localization problems, we have developed a pulse sequence which combines selective excitation volume selection with solvent suppression techniques.

Method - Solvent suppression is achieved by using a $1\bar{3}3\bar{1}$ pulse to selectively excite the desired bands in the spectrum [2]. The $1\bar{3}3\bar{1}$ pulse is followed by three selective π pulses. Each selective π pulse is applied in the presence of a separate slice selecting gradient pulse along one of the three orthogonal axes (x,y,z) [3]. Thus, the third echo of the Carr-Purcell series contains signal only from unsuppressed resonances, and is confined to the region where the three selected planes intersect. Stimulated echoes which arise due to imperfect π pulses are dephased by using symmetric gradient pulses around each of the π pulses. The location of the region of interest is controlled by the transmitter frequency during each of the selective π pulses, thereby allowing completely flexible electronic positioning with respect to each of the orthogonal axes. Similarly, the thickness of the selected region along each axis is determined by the gradient strength and selective excitation bandwidth of each of the three π pulses.

Results - The technique was implemented on a Picker 1.5T whole body imager. The sample used was a 3500 cc solution of water and acetone. Suppressed and unsuppressed spectra from an 8 cc selected volume are shown in Figure 1. The water peak in the suppressed spectrum has been reduced by a factor of about 200. Localization was verified by imaging the selected volume.

Conclusions - Effective solvent suppression is obtainable in conjunction with multiple echo volume localization. This allows us to avoid the localization problems inherent in surface coil dependent techniques. The major drawback with multiple echo localization is the relatively long time to the third echo. This impacts observations of resonances with short spin-spin relaxation times. As with planar slice selection for imaging, there are tradeoffs between minimum echo time, the width and sharpness of selected slices, and available gradient strength and RF power.

REFERENCES: [1] P. Blondet, et al., S.M.R.M. 4th Annual Meeting, 1985.
[2] P.J. Hore, J. Mag. Res., 54, 539-542, 1983.
[3] R.E. Gordon, R.J. Ordidge, S.M.R.M. 3rd Annual Meeting, 1984.

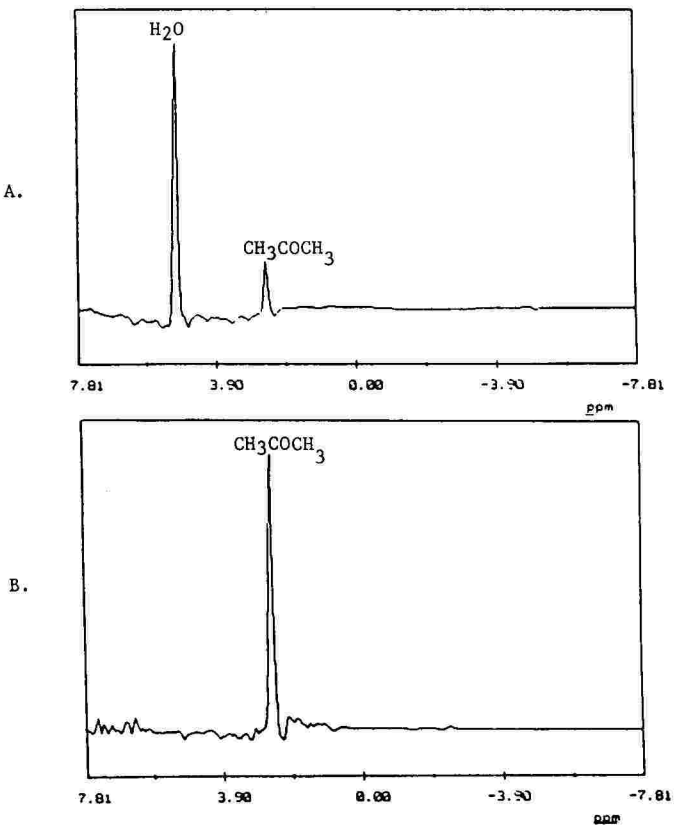

Figure 1 - Spectra from an 8 cc selected volume of a water/acetone phantom A. no suppression; B. 1331 suppression.

ASSESSMENT OF CEREBRAL ENERGY METABOLISM AND INTRACELLULAR pH IN ISCHAEMIC NEONATAL PIGLETS USING IN VIVO P-31 NMR

R.J.T. Corbett, H.T. Nguyen, A.R. Laptook and R.L. Nunnally

Departments of Radiology and Pediatrics, University of Texas Health Science Center at Dallas, Dallas, Texas, 75235

We describe a model for the study of the effects of transient global ischaemia on the cerebral metabolism of neonates measured nonivasively using P-31 NMR spectroscopy. Eleven piglets (5 to 14 days) were paralyzed (D-tubocurare Cl) and ventilated (70% N2 and 30% O2). Piglets were placed inside a 30 CM. bore 1.9 T magnet with the head fixed over a 4 cm. diameter single turn surface coil tuned to the P-31 frequency. Mean arterial pressure (MAP; mmHg), heart rate, arterial blood gases, pH (pHa) and O2 content, as well as plasma concentrations of glucose and lactate were monitored throughout the experiment (left common carotid artery). For 5 piglets analogous measurements were made on cerebral venous blood (sagittal sinus). After the collection of control P-31 spectra (8 mins/spectrum) blood was withdrawn until MAP decreased from 88 +-11 to 33 +-5 (X +-SD). Previous studies (ARL; Pediatr. Res. 17:77-80, 1983) have shown that a MAP of less than 45 exceeds the limits of cerebral autoregulation, resulting in reduced cerebral blood flow. A spectrum was obtained after 7 to 10 minutes of hypotension. Thus the total duration of hypotension was 15 to 18 minutes. All removed blood was reinfused rapidly (3 minutes) and 11 spectra were collected during a given recovery period (90 minutes).

During hypotension, the intensity of the resonance peak corresponding to PCr decreased (62% +-10) with a simultaneous increase in Pi (157% +-31) and slight decrease in ATP (82% +-12) compared to levels at control (100%). Intracellular pH (pHi) was estimated from the chemical shift difference between PCr and Pi. pHi decreased from control levels of 7.06 +- 0.07 to 6.59 +- 0.31 during hypotension. In comparison, pHa changes from 7.37 +- 0.05 at control to 7.16 +- 0.15 during hypotension. Cerebral arteriovenous differences of glucose increase while remaining unchanged for O2. Accordingly, the glucose/O2 quotient increased by more that 10 fold during hypotension. During recovery, levels of PCr, Pi and ATP all return to within 10% of control by 24 min (post-reinfusion). pHi also returned to within 0.10 of control over this time period; in contrast pH a remains low and arterial plasma lactate elevated for up to 90 min. during recovery.

Reduced levels of ATP, brain acidosis and the increased glucose/O2 quotient are all consistent with the notion of higher degrees of anaerobic metabolism during hypotension and the initial stages of recovery. It is apparent that cerebral pHi and metabolites return to control levels prior to clearance of systemic acidosis. Reductions in ATP even though PCr is present suggests that there is a cellular pool of PCr which is not utilized during hypotension. A high inter-animal variability was observed in the ratio of PCr/Pi for the piglets during control (1.78 +- .55). However, the control PCr/Pi does not show a linear correlation with pHi during control (r=.2) or hypotension(r=.4). This suggests that the utility of PCr/Pi values at control as a predictor of the extent of brain acidosis during an ischaemic insult is questionable. During hypotension both PCr/Pi and pHi decrease in a linear fashion (r=.7); thus pHi has a biphasic relationship with PCr/Pi showing a downward break for PCr/pi ratios of less than one.

This model and the results described should provide a basis for determining the effect of pre-insult treatments on the extent and onset of brain acidosis and changes in cerebral metabolites during and after ischaemia.

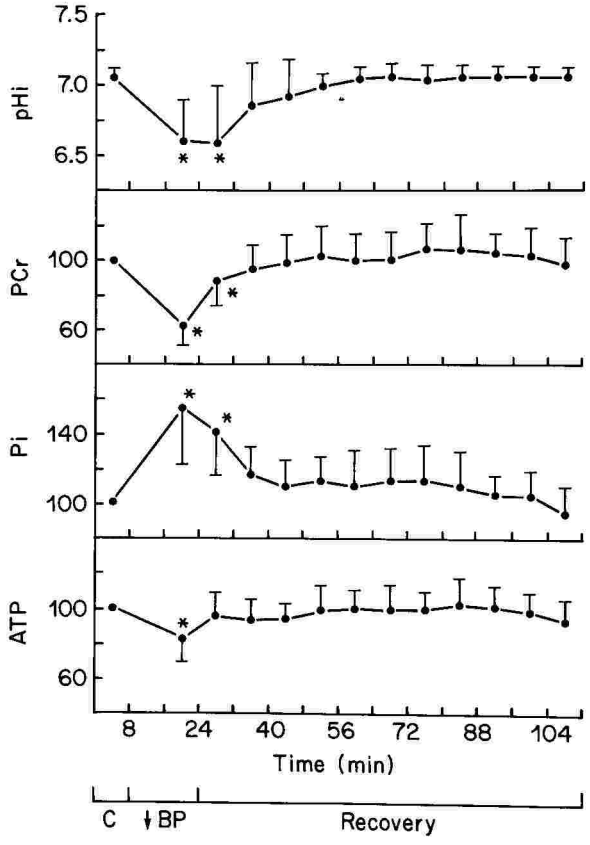

Figure shows changes in levels of cerebral intracellular pH and metabolites for neonatal piglets (n=11) during and after a transient ischaemic insult. The data are plotted at midscan of each 8 minute NMR spectrum. Values for PCr, Pi and ATP are represented as percent changes ($\bar{x}$ +-SD) relative to levels at control (100%) (* p . 05 relative to control). C and ↓BP refer to control and hypotensive periods, respectively.

MULTIPLE-OUTPUT CHEMICAL SHIFT IMAGING (MOCSI) -- A RAPID METHOD FOR CHEMICAL-SHIFT IMAGING AND LOCALIZED MODERATE RESOLUTION NMR SPECTROSCOPY

D. B. Twieg* and G. C. McKinnon
Philips GmbH Forschungslaboratorium Hamburg,
Vogt-Koelln-Strasse 30, D-2000 Hamburg 54, Federal Rep. of Germany
(*on leave of absence from Dept. of Radiology, Univ. of Texas Health Sci. Center at Dallas)

A new rapid method for imaging multiple chemical shifts and measuring localized NMR spectra is being developed at Philips Forschungslaboratorium Hamburg (PFH) using the 2 Tesla whole-body MRI system. Using periodically varying gradient fields during data acquisition, the new method requires only 5 to 8 minutes to obtain a set of 128x128 planar images representing up to 30 frequencies within a spectral bandwidth of 5.9 ppm (for protons) at 2 Tesla. Alternatively, 30-point NMR spectra may be produced for any picture element, or for selected regions of interest. By doubling acquisition time, spectral bandwidth can be doubled (to 11.7 ppm for protons, 28.6 ppm for 31P at 2 Tesla). For the patient study shown here, 24 frames were reconstructed within the 5.9 ppm bandwidth.

MOCSI is a Fourier method intermediate between Fourier spectroscopic imaging methods for high-resolution NMR spectroscopy at low spatial resolution (E.g., Brown et al.1982, Maudsley 1983), and Fourier methods which acquire high spatial-resolution images at very low (two-point) spectral resolution, such as the "fat/water" imaging method of Dixon et al. (1984). It produces a set of multiple frames as does the method of Sepponen et al. (1985), but with a briefer acquisition time per frame. A method developed for a smaller MRI system by Matsui et al.(1985) is similar, but uses spin-echoes.

In most whole-body imaging systems, the time required to switch large gradient fields is significant, occupying a significant portion of the potential signal-acquisition time in a gradient-switching method such as MOCSI. MOCSI's novel reconstruction technique makes use of data gathered throughout the NMR signal, even during the periods of gradient switching. It can be shown that one can improve spatial resolution by using this gradient-switching data in the reconstruction rather than ignoring it.

As a method for producing "fat" and "water" images, MOCSI has some advantages over the two-echo methods (e.g., Dixon's). Because one acquires a large number of individual spectral frames, each with a narrow response width (<.25 ppm), and adds them to form composite fat and water images, one can select more precisely the spectral band to be included in each image, and the net spectral response of each composite image is more sharply defined as well. This decreases the degree of contamination of the "fat" image by the water distribution (and vice-versa), especially in the presence of large field inhomogeneity or susceptibility variations.

Because the breadth of the water and fat features in the spectrum from each pixel are inversely related to the respective net transverse relaxation times, it is possible to compute T2-sensitive images (e.g., synthetic "spin-echo" images) from the pixel spectra. The method can also be used to rapidly map magnetic field variations due to main field inhomogeneity and effects of susceptibility variations within the patient.

Acknowledgments: We wish to thank Dr. H. Weiss and Dr. M. Kuhn for making this work possible, and members of the PFH NMR group for their cooperation and assistance. We thank Dr. Traupe of the University Clinic Hamburg for the opportunity to perform the patient study shown here.

References:

TR Brown, BM Kincaid, and K. Ugurbil, Proc. Natl. Ac. Sci. USA 1982, 79, 3523
WT Dixon, Radiology 1984, 153, 189
S Matsui, K Sekihara, and H Kohno, J. Am. Chem. Soc. 1985, 107, 2817
AA Maudsley, S Hilal, W Perman, H Simon, J. Magn. Reson. 1983, 51, 147
RE Sepponen, Magn. Reson. Imaging 1985, 3, 163

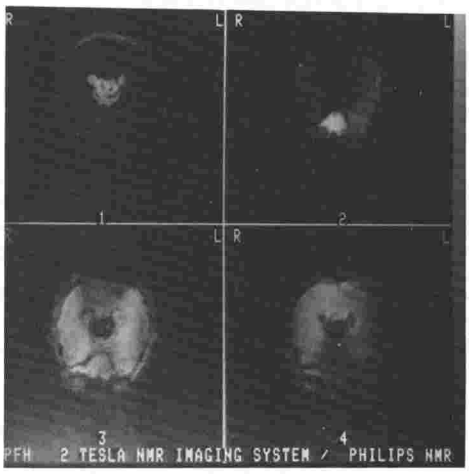

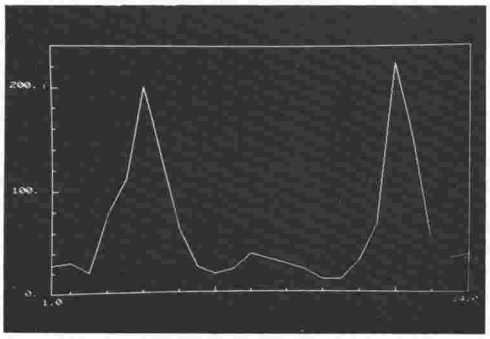

Figure 1: Transverse cross-section images from a patient with cerebral lipoma -- Four selected frames from among 24 representing distinct frequencies about .24 pp m apart. Frame 1 is one of the frames containing the "fat" resonance, in which the lipoma is seen. Frames 8, 10 and 12 (labeled 2,3,4 respectively) are among the frames containing "water" resonance. Note the peak of the water resonance occurs at different frame numbers for different pixel locations, due to inhomogeneity and susceptibility effects. Adding frames 8 through 13 gives the "water" image. Figure 2: a 24-point spectrum from a single pixel at the edge of the lipoma. The left and right peaks represent "water" and "fat" respectively.

CONTRAST MECHANISMS

AN INTEGRATED EXPERT SYSTEM ARCHITECTURE FOR MRI SCAN SETUP AND OPTIMIZATION

Thomas M. DeDonno, Picker International, Highland Hts., OH
Raymond E. Gangarosa, Picker International, Highland Hts., OH
Edward A. Patrick, University of Cincinnati, Cincinnati,OH
Andrew S. Green, Picker International, Highland Hts., OH

An expert system design is desired to obtain automated setup of all scan parameters for users with varied backgrounds, individualized to the examination requirements and consistent with overall scheduling considerations. A number of formidable obstacles must be overcome, relating both to performance and user interface. Potential performance obstacles relate to: (1) a combinatorial explosion which would result from consideration of all possible scan parameter settings, (2) varied examination requirements for different patients, (3) exceptional intrinsic flexibility of MR imagers, and (4) ideally, the desireability of a scan optimization approach. Potential user interface obstacles include: (1) widely varying user background and experience with MR techniques and (2) a strong subjective component to the process of scan setup.

A unique conceptual framework was developed to implement this expert system. The salient features of this expert system[1,2] include (1) separation of the clinical and physical models, (2) identification of MR performance indices, (3) explicit consideration of tradeoffs for each performance index (4) option for user to bypass directly any part of the expert system, i.e., to set any scan parameters ($\underline{p}$) or tradeoffs explicitly. Eight performance indices are identified: (1) examination time, (2) lesion-to-background contrast, (3) signal-to-noise ratio (S:N), (4) spatial resolution, (5) slice thickness, (6) survey length, (7) field of view, and (8) motion artifact rejection. Tradeoffs are expressed as priorities ($\underline{\lambda}$) and constraints ($\underline{c}$) for each of the performance indices. The system input from the user is a description of the clinical setting ($\underline{x}$), obtained via interview, and/or direct settings (any combination of $\underline{\lambda}$'s or $\underline{c}$'s and/or $\underline{p}$'s) specified by the user (see fig. 1). The system output is a set of optimized scan parameters given the clinical setting and constraints, or an indication that no solution is possible (if the problem is overconstrained).

The implementation, shown in fig. 1, consists of (1) a network of CONSULT-I^{R}[3] expert systems, (2) a mathematical model and optimization algorithm, and (3) a user override option. As refinements, separate expert systems may be used (1) to generate estimated scan parameters which may improve convergence characteristics of the optimization algorithm and (2) for scheduling considerations.

The mathematical model consists of simplified equations that describe each of the performance indices in terms of scan parameters, eg., TR, number of views, number of excitations, hybrid echo planar factor, coil characteristics, motion rejection techniques, etc. The optimization procedure performs a process commonly described as mathematical programming.

The advantages of this integrated expert system over conventional approaches relate to both performance and ease of use. The performance advantages are: (1) use of an explicit, testable model, (2) adaptability to an empirical expert system (CONSULT LEARNING SYSTEM^{TM}[3]), (3) possibility of modular debugging of the subjective (expert system) and objective (mathematical model) components, (4) synthesis of stored and calculated operations which prevent combinatorial explosions and nonconvergence problems, and (5) adaptability to scheduling. Ease of use results from (1) a novel conceptual framework, (2) "anthropomorphic design" (which separates a "clinician" module from a "physicist" module), (3) adaptability to a wide range of users, and (4) a user-friendly interface.

References:

(1) Gangarosa RE, Patrick EA, Fattu JM, Green AS. Patent applied for.

(2) Gangarosa RE, Patrick EA, Fattu JM, Mohapatra RN, Bellon EM, Mohapatra SN. An integrated expert system for MRI scan optimization: A conceptual model and feasibility study. Submitted to Radiology.

(3) Patrick EA, Fattu JM. Artificial Intelligence with Statistical Pattern Recognition, Prentice-Hall, 1986.

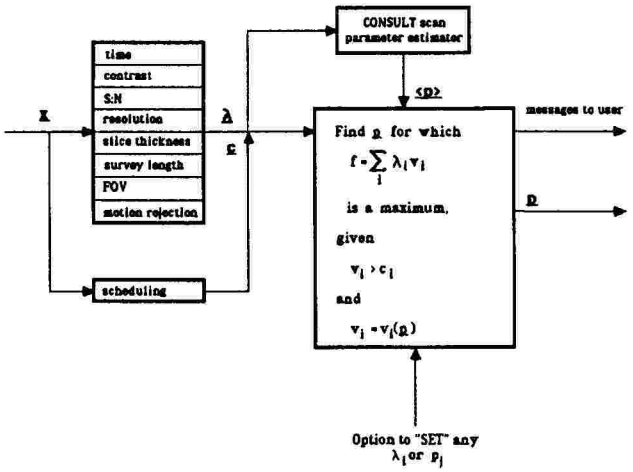

STABILITY OF PROTON SPIN-LATTICE RELAXATION TIMES IN EXCISED RAT MYOCARDIUM

Cam F. Campbell, Gerald A. Pearson, Steve M. Collins, David J. Skorton

The Cardiovascular Center and Departments of Internal Medicine, Chemistry, Electrical and Computer Engineering, and Radiology, The University of Iowa, Iowa City, IA

Nuclear magnetic resonance (NMR) is a new imaging and analytic modality which has the potential for myocardial tissue characterization. At present, the fundamental relationships between NMR image patterns and tissue composition are incompletely defined. Therefore, several investigative groups are concentrating on in vitro experiments on excised tissue specimens, in an attempt to understand more fully the tissue determinants of proton spectra and relaxation times. An assumption made in these in vitro studies is that NMR variables, such as proton spin-lattice (T1) relaxation times, remain stable for periods of time after excision sufficient to perform NMR spectroscopy. Although this assumption appears to be valid for several mammalian tissues, including skeletal muscle, no data are available concerning the dependence of myocardial T1 on time after excision. The purpose of our study was to evaluate the changes in T1 of rat myocardium, measured at two NMR field strengths, at serial time intervals up to 72 hours after excision.

Six Sprague-Dawley rats, weighing 300-399 grams, were anesthetized with a 10:1 mixture of ketamine and acepromazine. The rats had ad lib access to food and water prior to operation. After induction of anesthesia, the chest was entered via a midsternal incision. The great vessels were clamped, the heart excised and immediately placed onto a watch glass. The right ventricle, both atria, and great vessels were removed, leaving only the left ventricle (LV) intact. The LV was divided into two halves along its long axis, incising through the interventricular septum. Half of the LV was used for NMR studies; the other half was used to determine water content and evaporative loss.

The LV sample was prepared for NMR spectroscopy by dividing it into 2-mm cubes using a clean scalpel blade. The tissue was inserted into NMR sample tubes with care to avoid fluid extravasation. NMR sample tubes were covered and stored at room temperature. The process of anesthetization, cardiac excision, dissection, and preparation of sample tubes was accomplished in less than 30 minutes per heart.

Proton T1 relaxation times were measured at 90 MHz (JEOL FX90Q) and 360 MHz (Bruker WM360) using a modified inversion-recovery pulse sequence. T1 values were measured at 1, 3, 6, 18, 24, 48 and 72 hours post-excision.

Water content and evaporative loss for each specimen were determined by measurement of sample weight before each NMR determination, and by measurement of sample weight before and after desiccation at the completion of the studies.

Statistical analyses were performed by analysis of variance. The required level for statistical significance for comparisons of T1 at different times was $p<.0083$ using the Bonferroni correction for multiple comparisons.

Results. The figure shows the values for T1 at 90 MHz (A) and 360 MHz (B). The rate of change of T1 over time at 90 MHz was not significantly different from that at 360 MHz. The table shows that the mean T1 fell from 1.162 ± .040 (SD) seconds at one hour to 1.081 ± .038 seconds at 72 hours at 90 MHz ($p<.0049$); at 360 MHz, T1 fell from 1.411 ± .049 seconds to 1.326 ± .039 seconds over the same interval ($p<.0081$). Although T1 decreased over time, compared to the value obtained at one hour, T1 did not become significantly different until 72 hours after excision, regardless of whether T1 was obtained at 90 MHz or 360 MHz. Note that T1 values were significantly greater at 360 MHz than at 90 MHz for any given time after excision ($p<.0001$). The mean evaporative water loss of the tissue sample over 72 hours was .61 ± .41%.

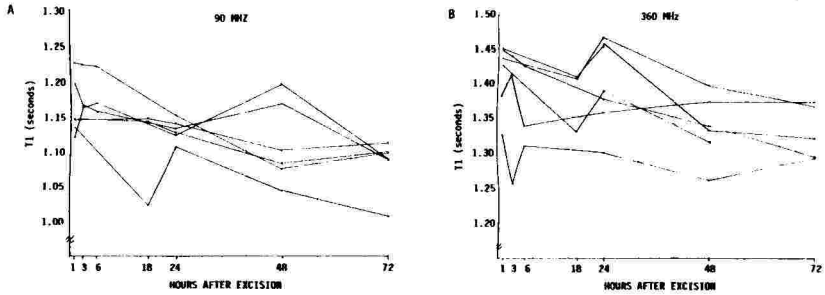

Time After Excision (Hours)	Field Strength (MHz)	Mean T1 Value ± SD (Seconds)	Significance Compared to T1 at 1 Hour
1	90	1.162 ± .040	--
	360	1.411 ± .049	--
24	90	1.130 ± .015	p<.0522
	360	1.388 ± .061	p<.2735
48	90	1.110 ± .058	p<.0608
	360	1.333 ± .048	p<.0257
72	90	1.081 ± .038	p<.0049*
	360	1.326 ± .039	p<.0081*

*T1 significantly different than at one hour

Conclusions. We conclude that: (1) myocardial T1 varies directly with NMR field strength, (2) myocardial T1 decreases slowly after excision, (3) the rate of T1 decrease does not appear to be field-strength dependent, (4) T1 values obtained up to 24 hours after excision are not significantly different from those obtained at one hour after excision, (5) T1 values obtained 72 hours after excision are significantly different from those obtained at one hour. These findings suggest that physiologically meaningful data may be obtained with in vitro NMR studies of the myocardium if performed within 24 hours of excision. However, because of the steady decrease in the T1 value after excision, it is important to note the time after excision at which T1 is obtained.

DETERMINATION OF OIL AND WATER IN RESERVOIR CORE SAMPLES USING MAGNETIC RESONANCE IMAGING

Nicida L. Maerefat, Ph.D.*; Iain Palmer, Ph.D.*; William S. Yamanashi, Ph.D.**; and Patrick D. Lester, M.D.**

*National Institute for Petroleum and Energy Research, Bartlesville, Oklahoma; **City of Faith Medical and Research Center, Oral Roberts University School of Medicine, Tulsa, Oklahoma

Laboratory core experiments consistently required the measurements of fluid saturation which are continuously changing along the length of the core sample. These measurements supply important information for defining core heterogenity and sweep efficiency of different injection fluids. In this work, the magnetic resonance imaging has been used to estimate the amount of oil and water present at different locations in 1" long, 1½" diameter resevoir core sample (Cleveland core). The oil phase used is Soltrol-220 (C13 - C17, mainly C14 and C15) and the water phase is 1% NaCl. The results show that the fluid saturations using this technique can be measured within experimental error. The measurements were identified by making use of the existent difference of the null point in the inversion recovery (where the magnetization crosses the null intensity point) between the water and the oil. The actual imaging pulse sequence was an inversion recovery followed by a short spin echo sequence, typical of those used by majority of commercial MR imagers. Measurements on Berea and Chalk cores were also made.

Picker MR VISTA 2055 scanner operated at 0.5T (21.3 MHz) was used in conjunction with a laboratory built solenoid receiving coil.*

*B.A. Baldwin, W.S. Yamanashi and P.D. Lester, Magn. Reson. Imag. 3, 180-181 (1985).

STUDIES OF THE EFFECT OF STRESS ON PROTON RELAXATION TIMES (T1 AND T2) OF RAT LIVER.

Ramesh Chandra, Ph.D., and Donald J. Pizzarello, Ph.D.

Department of Radiology, New York University Medical Center

The longitudinal relaxation time, T1, of protons in rat liver has been shown to increase after partial hepatectomy as well as after sham operations (abdominal incision, liver handled but none removed). It has been suggested that "surgical stress" which includes tissue trauma and causes a variety of biochemical changes in liver, plays a role in this increase. The present study was undertaken as part of a continuing effort to determine whether stress alone accounts for the effect or if tissue trauma is an essential component. Three types of stressful situations were used. (1) Rats were made to swim to the point of exhaustion. This presumeably produces physical and emotional stress. (2) An intradermal injection of the hormone ACTH was given. This chemically mimics the reactions often produced by situations resulting in fear and flight. (3) Rats were fasted for a period of time reported sufficient to reduce glycogen levels in liver by an order of magnitude.

Methods
(a) Care and Maintenance of Rats: Male Sprague Dawley rats weighing approximately 100 - 130 gms. each were used in all experiments. Food and water were always available except in the experiment involving fasting where food was withheld. The light cycle was 12 hours light, 12 dark, lights on at 7:00 a.m. EDT.
(b) Swimming: Three rats at a time were placed in a large sink filled with enough water to force them constantly to swim. When they appeared very fatigued, usually after 1 or 2 hours, they were removed and placed in a cage. Some were removed for sacrifice at 15 minutes, 2 and 24 hours after the end of the exercise.
(c) ACTH: One unit of ACTH each was injected intradermally in the flanks of a group of rats. Twenty-four hours later this group was sacrificed.
(d) Fasting: Food was withheld for a period of either 24 or 48 hours from a group of rats. Water was available, in the same way as it was to other rats.
(e) Controls: For each set of experiments, a group of rats was used as control. These handled in an identical manner in all respects to the stressed animals except the stress was omitted.
(f) Sampling of liver: Rats were placed under heavy ether anesthesia. An abdominal incision was made and a small sample (0.5-1 gm) of liver taken, placed in a preweighed NMR glass tube for T1 and T2 and water content measurement. The glass tube was corked and kept corked for the duration of T1 and T2 measurement.
(g) T1/T2 Measurements: Measurements of T1 and T2 were performed at room temperature (22+0.5°C) using a commercial pulsed NMR spectrometer which operates on a fixed frequency of 10.7 MH_Z (0.25T - magnetic field) within 5 to 15 minutes of the removal of tissue samples from the animals. Pulse sequence, data acquisition and analysis were controlled by a dedicated micro computer. T1 was determined by a saturation recovery pulse sequence; i.e., 90°-t-90°. Thirty sequentially increasing pulse delays (step = 15 msec) were used and each point was an average of three measurements (spectra). The pulse repetition time (TR) was 1 sec. These measurements described the recovery of longitudinal magnetization as a function of time. A least-squares single exponential fit was made to these data by computer which then printed the relaxation time and the correlation coefficient of the fit to the data. T2 was measured immediately following the measurement of T1 using Hahn's spin echo sequence; i.e., 90 °-t-180°. The effect of diffusion on the pulse echo was found to be negligible as was evident from the observed mono exponential decay of echo amplitude with pulse delay. Again, 30 sequentially increasing pulse delays (step = 2 msec) were used, and each point was averaged from three measurements. T2 was calculated by computer by a least-squares fit to a single exponential.
(h) Water Content: After the T1/T2 measurement, the tube was uncorked and weighed, thus determining the wet weight of the tissue. They were put in a hot air oven at 55 °C and weighed periodically until no further weight change was noted. This dry weight was subtracted from the wet weight, the difference being the weight of water evaporated from the liver piece, and the result expressed as percentage wet weight.
(i) Analysis of Data: Group means and their standard deviations (S.D.) were computed and the significance of the differences between means was determined using student's t test for two groups.

Results: Mean values of T1 of liver protons for control rats, and rats after 1 hour's exercise at 15 minutes, 2 and 24 hours of post exercise were 221.5, 238.7, 209, and 222 msec respectively. Statistical analysis showed no significance of the difference in these mean values. Similar results were obtained for T2. For the ACTH experiment, mean values for control and ACTH injected rats are 221.5 and 227.7 msec respectively. No significance was obtained for the differences of the two means. For the fasting experiment, the mean values of T1, for control, 24 and 48 hours fasting rats are 210.8, 215.9 and 212.6 msec respectively. Again no significance of the differences in the means of these groups was observed.

Conclusions: In light of these negative results, the increase in T1 of liver protons after partial hepactectomy or sham operation can not be explained by the physical, emotional, or metabolic stress alone. It seems that tissue trauma is an essential element in the elevation of T1 of liver protons.

CONTRAST-DETAIL PHANTOM ANALYSIS FOR MAGNETIC RESONANCE IMAGING

William H. Hinson, M.Sc.; P. R. Moran, Ph.D.

Bowman Gray School of Medicine, Wake Forest University, Winston-Salem, North Carolina

Contrast-Detail analysis is a general and powerful quality-control test, performance assessment procedure, and system intercomparison tool for imaging systems. This technique, however, has been largely neglected for MRI systems, mainly due to the lack of a suitable phantom. We propose an indirect method of obtaining contrast-detail analysis plots without construction of a low contrast phantom. The analysis involves "digital" construction of low contrast images from scans of the original high contrast phantom, in analogy to radiographic template-phantoms. Contrast-Detail plots obtained from the "digital" phantom give significant and sensitive indicators of all basic aspects of imaging system parameters and functions. One advantage of this indirect method is that it provides specific information on the level, texture, and relative components of the noise within the system, as well as its resolving power, while excluding complications due to the overall contrast rendition and linearity of the system.

Figure below shows "digital" phantom constructed with (left to right) 3%, 7.5%, and 20% contrast between cylinders and background.

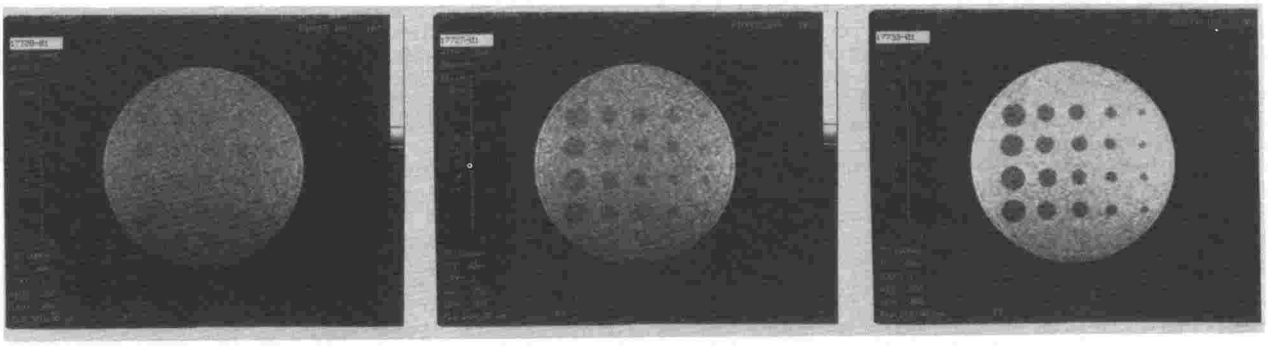

NMR SPECTRA OF CULTURES OF RAT TUMOR CLONES AND Vx2 TUMORS ISOLATED FROM VARIOUS ORGANS OF THE RABBIT.

J.W. Frazer, S.P. Tomasovic, L. Dennis*, C. Hazlewood**, K. Burton, M. Hebert, S.D. Bines, P.A. Steck, and A.W. Boddie, Jr.

M.D. Anderson Hospital & Tumor Inst., Houston, TX; Exxon Research & Eng. Corp., Baytown, TX*; Baylor University School of Medicine, Houston, TX**.

Our laboratories have been engaged in NMR, biological and biochemical investigations of malignant cells and tumors for some years. We have examined NMR spectral differences between clones of rat mammary carcinoma 13762-NF having low (MTPa), intermediate (MTC) and high (MTLN3) metastatic potential in particular culture passages. Our previous examinations of similar clones (Bines et al, Jour Surg Res 38 546-552 1985) showed there was a small but significant downfield shift in water spectrum in non-metastatic clones, and that there were alterations in spectra of isolated lipids. That work was done with a Varian EM360L 60 mHz CW spectrometer. We have repeated these observations with a Varian XL200 Fourier transform spectrometer obtaining spectra of peaks at 3.14 and 3.75ppm, difference spectra apparent at 1.2 and 2.0 ppm with greater expression in metastatic clones. There were also differences at 7-8 ppm. 13C spectra of metastatic and low metastatic clones have also been obtained, though these are somewhat suspect because of the long aquisition time necessary for spectral accumulations with natural 13C abundance.

We have preliminary indications some of these NMR characteristics may be related to biochemical properties of these clones. For example, certain cell surface glycoproteins have been associated with metastatic potential in these clones (Steck and Nicolson, Exptl Cell Res 147, 255, 1983), and several proteolytic enzymes are known to be in greater abundance in clones with higher metastatic potential (Nakajima et al in: "Cancer Metastasis: Experimental and Clinical Strategies", Welch, D.R. ed., Alan R. Liss, N.Y. in press 1985) than in clones with low metastatic potential.

In separate studies of in vivo rabbit Vx2 tumors, investigation of alterations in spectral signature with different anatomical location of the tumors in rabbits utilized the Varian EM360L proton spectrometer. Alterations in signatures associated with lipids were found as well as signatures at 3.5 ppm which might be associated with glycoproteins. These alterations resembled neither the parent tumor nor the tissue of metastatic residence.

The ability to contrast and compare NMR spectra to reproducible biochemical and biological properties of well-characterized metastatic tumor models like the 13762NF adenocarcinoma appears to offer the opportunity to identify NMR spectral characteristics associated with malignancy and may enable us to extend some NMR observations of malignant characteristics to less well-characterized tumors growing in vivo.

Partially supported by USPHS grants CA32745 (SPT) and CA28844 (awarded to G. Nicolson and supporting P.A.'s).

PROBABILISTIC MODELING OF NMR TISSUE CHARACTERISTICS: APPLICATION TO MRI SCAN OPTIMIZATION USING AN INTEGRATED EXPERT SYSTEM

Raymond E. Gangarosa, Picker International, Highland Hts., OH
Ram N. Mohapatra, University of Central Florida, Orlando, FL
Edward A. Patrick, University of Cincinnati, Cincinnati, OH
Mary H. Regier, American University of Beirut

The role of contrast is particularly important in MRI because of the complexity of the behavior governing image contrast and the potential pitfall of image contrast crossover[1]. Previous discussions of proton MR image contrast using analytical modeling of NMR characteristics of tissues have been limited in (1) modeling tissues as deterministic points[2,3] or measured ranges[4] and (2) considering optimization of contrast alone[1,2,3,4]. This discussion introduces the analytical use of probability density functions (p.d.f.'s) for NMR tissue characteristics, in the context of overall scan optimization with an integrated expert system[5]. We further discuss the concept of relative risk of contrast loss in different scan strategies for given clinical settings.

Our integrated expert system consistes of two major components in series: (1) a CONSULT-I^R expert system[6] used to generate priorities λ_s and constraints c_s for each of s=8 performance indices V_s (exam time, contrast, signal-to-noise ratio, resolution, slice thickness, survey length, field of view, and motion rejection) given a description of the clinical features $\underline{x}$. and (2) a mathematical modeling and optimization system which transforms those priorities and constraints into a set of scan parameters $\underline{p}$ which maximize the functional

$$f = \sum_s \lambda_s V_s = \sum_s f_s$$

given the mathematical model $V_s = V_s(\underline{p})$ and the constraint relationships $V_s \geq c_s$. Thus, this system performs tradeoffs which achieve the best overall response.

We further refine this model here by (1) mapping from clinical features to p.d.f.'s for NMR tissue characteristics of lesion f_ℓ and background f_b and (2) subdividing the contrast performance index v_2 into two components, each with their own priorities and constraints expressing the relative requirements for minimizing risk (f_{2a}) and for maximizing expected gain (f_{2b}). For the sake of simplicity, we restrict our discussion to consider only T_1 and T_2 characteristics, monoexponential curves, and pulse sequences for which intensity I can be modeled analytically as a function of scan parameters $\underline{p}$ and tissue T_1 and T_2. We identify that region $\mathcal{L}$ in (T_1,T_2)- space for a given set of scan parameters $\underline{p}$ with $I \leq I_{threshold}$ = constant, i.e., where signal is below the noise level. Then the minimum risk performance index f_{2a} is given by

$$f_{2a} = -\lambda_{2a} \iint_{\mathcal{L}} (f_\ell + f_b)\, dT_1\, dT_2$$

and the maximum gain performance index by

$$f_{2b} = \lambda_{2b} \iint_{\text{all } T_1,T_2} I(T_1,T_2)\,(f_\ell(T_1,T_2) - f_b(T_1,T_2))\, dT_1\, dT_2$$

As above, we seek to find scan parameters $\underline{p}$ which maximize the expression for f, which now substitutes $f_2 = f_{2a} + f_{2b}$.

These results can be extended to multiple lesions and/or backgrounds, consideration of selective tissue suppression techniques, and estimation of the probability of an avoidable "missed lesion". Methods for expediting the computation will also be discussed, including lookup tables, offline training of expert systems, construction methods, and linearization techniques. Furthermore, the empirically-oriented CONSULT LEARNING SYSTEM^R expert system is well-suited to collection of data about NMR tissue characteristics for determining p.d.f.'s used in this analysis.

References:

(1) Droege RT, Wiener SN, Rzeszotarski MS. A strategy for magnetic resonance imaging of the head: results of a semi-empirical model. Parts 1 and 2. Radiology, 153, 419-433 (1984).
(2) Mitchell MR, Conturo TE, Gruber TJ, Jones JP. Two computer models for selection of optimal magnetic resonance imaging (MRI) pulse sequence timing. Invest Radiol, 19, 350-360 (1984).
(3) Droege RT, Wiener SN, Rzeszotarski MS, Holland GN, Young IR. Nuclear magnetic resonance: a gray scale model for head images. Radiology, 148, 763-771 (1983).
(4) Davis PL, Kaufman L, Crooks LE. Tissue characterization, pp. 53-77 in Clinical magnetic resonance imaging, Margulis AR, Higgins CB, Kaufman L, Crooks LE (eds.) (San Francisco, 1983).
(5) Gangarosa RE, Patrick EA, Fattu JM, Mohapatra RN, Bellon EM, Mohapatra SN. An integrated expert system for MRI scan optimization: A conceptual model and feasibility study. Submitted to Radiology.
(6) Patrick EA, Fattu JM, Artificial Intelligence with Statistical Pattern Recognition, Prentice Hall 1986.

NMR DISPERSION IN REGENERATING RAT LIVER

C.F. Pope,[1] M.S. Brown,[1] J.C. Gore,[1] S. Yu,[2] S.H. Koenig,[3] R. Brown III,[3] and W. Flye[2]

Department of Diagnostic Radiology[1] and Liver Transplantation Laboratory[2], Yale University School of Medicine and IBM Thomas Watson Research Center, Yorktown Heights[3]

The differences in relaxation rates between tissues form the basis of MR image contrast so it is important to understand their underlying mechanisms. The field dependence of $1/T_1$ of protons in tissue (the dispersion of T_1 or NMRD) has been shown to be a useful approach to elucidating the nature of relaxation processes in macromolecular solutions. In this study we investigated the in vitro relaxation rate dispersion of freshly excised rat liver that was regenerating following a 70% hepatectomy. Five pairs of adult male Sprague-Dawley rats (total 10) were sacrificed by craniocervical dislocation at the following time points: 1, 3, 5, 7 and 14 days. One rat had the relaxation rate ($1/T_1$) dispersion of the liver measured using a variable field spectrometer (relaxometer) operating at 37°C. The other rat of the pair had T_1 and T_2 measured at 37°C and 14-24 hours later than the above points respectively on an IBM spectrometer operating at 20 MHz. Standard gravimetric analyses were performed on the second set of samples to determine % of H_2O and % lipid. The % lipid in particular varied considerably from 18% (Day 1) to 9% (Day 14). The shape of the dispersion profiles were similar to normal liver, but the magnitude of the dispersive component dominating the rate at low fields (<1 MHz) increased with time following hepatectomy from 31.0 (Day 1) to 42 (Day 14). The variations of the parameters describing the NMRD profiles and their possible interpretations will be presented. Regeneration is a complex process involving cellular hypertrophy and hyperplasia, during which profound alterations of synthetic and differentiated functions of the liver occur. The regenerating liver represents a useful laboratory for studying basic relaxation processes in tissue.

STUDIES OF RELAXATION IN BILE: EFFECTS OF PHYSIOLOGICAL CHANGES AND IMPLICATIONS FOR GALLBLADDER IMAGING

Young S. Kang, John C. Gore, Chris F. Pope, Mark S. Brown

Department of Diagnostic Radiology, Yale University School of Medicine
New Haven, CT

While proton relaxation times of biological tissues show wide variations between specimens in various pathological categories, values for most normal tissues exhibit remarkable consistency at the gross level when parameters such as frequency, temperature, and handling are taken into account.

One notable exception is bile: values for T_1 in the literature range from 300 msec to over 2000 msec at current imaging field strengths. Much of this spread seems to result ultimately from the intrinsically variable composition of bile, affected by factors such as the biliary anatomy of the given species, and the location and timing of sample collection. Recent works[1,2] focusing on differences in MR appearance of normal and diseased human gallbladder between fasting and non-fasting states provided some evidence that MR may be a viable modality for detecting cholecystitis.

The purpose of our study is two-fold: 1) to chart longitudinally the postprandial alteration in relaxation times of bile accompanying its normal physiological change in vivo using MR images of the canine gallbladder, and 2) to better understand the nature of the bile signal intensity by spectroscopic analysis of bile in dogs and rats and solutions simulating bile.

Normal adult dogs underwent MR imaging with a resistive unit operating at 6.35 MHz at several time points over a 24-hour period after a fatty meal. From images generated with various pulse sequences including partial saturation, multiple spin echo, and inversion recovery, T_1 and T_2 of the gallbladder were computed using single exponential fits to 4-8 data points for each relaxation curve.

Progressive monotonic shortening of gallbladder relaxation times was observed, which leveled off by 6-8 hours. The magnitude of these changes was, however, smaller than would be inferred from earlier work: T_1 decreased from 500-900 msec initially to 250-400 msec at 8 hours, and T_2 from 130-190 msec to 50-100 msec. In most dogs, the gallbladder remained hypointense relative to the surrounding liver tissue on T_1-weighted images, and hyperintense on T_2-weighted images, reflecting the fact that T_1 and T_2 of gallbladder stayed longer than those of liver despite the demonstrated change.

In view of the lack of contrast reversal between gallbladder and liver as bile concentrates for most pulse sequences employed, the clinical detection of the abnormal functioning gallbladder might best be accomplished by establishing a range of T_1 and T_2 for normal concentrated bile to which the patient's values may be compared at a predetermined time after the last meal. Measurements at 37 C on aspirated bile samples from imaged dogs using a spectrometer operating at 20 MHz, revealed values consistent with normal dispersion, suggesting partial volume averaging or pulse rotation errors were not large in generating in vivo values.

To further understand the mechanism of the relaxation changes seen, proton spectra were obtained at 85 MHz on bile samples from dogs and rats, with the simultaneous biochemical determination of their consituents. T_1 relaxation curves of water and lipid peaks were also separately obtained with the inversion recovery technique. The presence of cross relaxation between the two moieties was evident, and this has been incorporated into a quantitative analysis of the relaxation mechanism of bile which is reported in an accompanying abstract.

References:
1. Hricak, Het al., Radiology 147:481-484, 1983
2. McCarthy, S et al., Program SMRM IV, 1179-1180

A CORRECTION SCHEME FOR IMPROVED ESTIMATES OF T_2 FROM MULTIECHO MRI IN THE PRESENCE OF SYSTEM IMPERFECTIONS

S. Majumdar*, A. Gmitro, J. Gore, S. Orphanoudakis and D. Reddy

Section of Applied Physics* and Department of Diagnostic Radiology,
Yale University, New Haven, Connecticut 06510

MRI techniques that use multiple spin echoes are important because successive echoes may be added to enhance the signal to noise ratio whereas comparisons between echoes permit quantitative estimates to be made of the intrinsic tissue spin spin relaxation time, T_2. Accurate measurements of T_2 may in principle be used to quantitatively characterize different tissues and diseased states. However the accuracy of such estimates depends on several instrumental factors such as imperfections in the applied RF pulse and off-resonance effects arising from static field inhomogeneities. We have previously reported how such imperfections modify the amplitudes of successive echoes and are compounded in a complex fashion (1). The spin echo amplitude as a function of echo number n becomes

$$M_n = M_o \exp(-n.TE/T_2)\, f_n(\theta, \Delta H)$$

where ΔH is the inhomogeneity in the static magnetic field and θ denotes the angle of nutation produced by the RF refocussing pulses. The form of the function f_n has been determined both analytically and by simulation and confirmed experimentally using imaging studies of phantoms. The nature of the function suggests a scheme which permits more accurate estimates of T_2 to be made even in the presence of severe imperfections. By examination of echo ratios that are independent of T_2 a matrix can be derived which estimates the RF and static field deviations at each pixel. This matrix can then be applied to correct for such effects. The improved estimates that result will be demonstrated. The correction scheme can also be implemented to improve the appearance and accuracy of late echo images in a multiecho sequence, and the beneficial effects of such processing have been confirmed in experimental 8 echo studies at 6.35 MHz with RF and static field imperfections deliberately introduced. A further application is the mapping of the static field distribution from a single multiecho imaging study of a uniform object which permits rapid evaluation of the magnetic field homogeneity.

1. Errors in the measurement of T_2 using multiple-echo MRI techniques; I. Effects of RF pulse imperfections
Majumdar S, Orphanoudakis S, Gmitro A, O'Donnell M and Gore JC
Magnetic Resonance in Medicine, 1986 (in press).

RELAXATION IN BILE: EVIDENCE AND ANALYSIS OF CROSS-RELAXATION BETWEEN WATER AND LIPID PROTONS

Mark S. Brown, John C. Gore, Ian M. Armitage, Chris Mizumoto, Young S. Kang

Department of Diagnostic Radiology, Yale University School of Medicine, New Haven, CT

As an ancillary study to imaging of gallbladder in vivo, the proton spin-lattice relaxation of bile has been studied by high-resolution NMR. Selective inversion experiments reveal a homonuclear Nuclear Overhauser Effect (NOE) between the water protons and the protons of the lipid constituents showing that magnetic exchange, or cross-relaxation, occurs between the two proton populations. The lipid protons thereby provide a relaxation "sink" for the water protons so that the water proton relaxation rate

$1/T_1$ is faster than in the absence of the magnetic cross-exchange. The size of the cross-relaxation term may reveal important information about the molecular dynamics at the water-lipid interface. Qualitatively similar relaxation behavior occurs in simple aqueous solutions of polyethylene glycol (PEG). Since such solutions are inexpensive, stable and more easily handled than bile, techniques and analysis were developed for this simple model system. Techniques for elucidation of the contribution of the cross-relaxation term include the use of selective inversion and the measurement of deuterium relaxation times in PEG/D_2O solutions. Deuterium is a quadrupolar nucleus with no dipolar coupling to protons, and thus the deuterium relaxation times reveal the water rotational correlation time. This can be used to predict a water proton relaxation time in the absence of cross-relaxation. The predicted times are compared to the measured water relaxation times to obtain estimates of the cross-relaxation. The system can be modeled using Solomon type coupled differential equations. Different pulse sequences help differentiate between mechanisms. For example, selective inversion of water only results in a "growing in" of the methylene peak after which it returns to equilibrium, even though it is unperturbed by the pulse sequence. The Solomon model has been incorporated into a fitting routine to obtain more precise estimates of the various relaxation parameters. The results demonstrate the possible importance of cross-relaxation between water and lipids, and implications for imaging will be discussed.

EFFECTS OF EVOLUTIONARY DISUSE, GENETIC SELECTION, AND SEVERITY OF DISEASE ON MUSCLE T1 AND T2

L.K. Misra, W.K. Vijjeswarapu, G.W. Parker, Jr., D. W. Bearden and C. F. Hazlewood

Department of Physiology and Molecular Biophysics, Baylor College of Medicine, Houston, Texas 77030

The degenerative changes in the avian model of muscular dystrophy generally occur in the fast-twitch fibers. However, all fast-twitch muscles are not affected by the disease to the same extent. The pectoralis major is the most severely affected muscle. The other commonly used fast-twitch muscle, the posterior latissimus dorsi (PLD) is less severely affected, and its synergistic slow-tonic muscle, the anterior latissimus dorsi (ALD), is not at all affected in the early stages of dystrophy. Biceps brachii and patagialis (PAT) are fast muscles of wings. The severity of fiber destruction in these two wing muscles is determined by background genes, and therefore varies in different genetic lines. Serratus metapetagialis (SMP) is a cutaneous muscle whose function is to maintain tautness of skin covering the wings during flight. Because chickens lost their ability to fly, SMP became vestigeal due to disuse. However, the normally unaffected type 1 fibers show degenerative changes in SMP, and it is proposed that disuse of muscle predisposes it to dystrophy. The slow tonic metapatagialis latissimus dorsi (MLD) remains functional and could serve as the unaffected internal control to SMP. The objective of our study was to test the hypothesis that the evolutionary-, genetic-, and disease-induced changes in the skeletal muscles alter their NMR characteristics.

Ten week-old chicks from the normal (412) and dystrophic (413) lines were anesthetized by Ketamine (100 mg/Kg, I/M). The seven muscles listed above were dissected and transferred to Wilmad NMR tubes. The proton NMR relaxation times, T1 and T2, were measured by the inversion recovery and Carr-Purcell-Meiboom-Gill methods at 20 MHz using a microprocessor-controlled NMR spectrometer (IBM instruments Inc., Danbury, CT). Water and fat contents were determined by gravimetric method for all the samples.

The proton T1 and T2 values of various muscles are summarized in Table 1. The T1 and T2 values of all dystrophic muscles are significantly higher than their corresponding normal muscles. The relative differences in the T1 and T2 values between the normal and the most severely affected pectoralis major muscles are 10.5% and 23.4%, respectively. The less severely affected wing muscles (PLD, Biceps and PAT) show approximately 7% increase in T1 and 12 to 20% increase in T2 values compared to the corresponding normal muscles. While the evolutionary disuse apparently did not change the T1 and T2 of SMP, myopathic processes increased its NMR relaxation times. The T1 and T2 values of ALD and MLD of normal and dystrophic chicks are similar. These results suggest that the increase in the NMR relaxation times of muscles is disease-specific and, also, that the relative differences in the T1 and T2 values between the dystrophic and its corresponding normal muscle reflect the severity of muscle damage. (Supported by RO1-AM35479-01)

Table I

The NMR Relaxation Times of Muscles in Normal and Dystrophic Chicks[1]

Muscle	T_1[2] (ms) Normal	T_1 (ms) Dystrophic	T_2[2] Normal	T_2 Dystrophic
Pectoralis	506 ± 12	559 + 14**[3]	47 ± 5	58 ± 5**
PLD	539 ± 15	578 ± 27*[4]	50 ± 3	60 ± 5**
ALD	534 ± 11	539 ± 16	61 ± 3	60 ± 4
Biceps	526 ± 16	567 ± 17*	46 ± 4	54 ± 5*
PAT	563 ± 28	600 ± 6*	52 ± 4	56 ± 4
SMP	523 ± 26	573 ± 49*	52 ± 4	58 ± 3*
MLD	531 ± 9	553 ± 28	53 ± 4	51 ± 10

1. 6 chicks each from normal and dystrophic lines were used.
2. Mean ± S.D.
3. Significant at $P < 0.01$
4. Significant at $P \leq 0.05$

PIXEL INTENSITY AND CONTRAST VALUES AS FUNCTIONS OF RELAXATION TIMES AND PULSE INTERVALS IN SEVERAL COMMERCIAL MR IMAGERS

David W. Anderson, Ph.D.; William S. Yamanashi, Ph.D.; John W. Ross-Duggan, M.D.; Patrick D. Lester, M.D.; Steven E. Harms, M.D.*; Wei Kom Chu, Ph.D.+; Richard A. Suss, M.D.++; Rajendra Shenoy, Ph.D.** and Kenneth Maravira, M.D.***

City of Faith Medical and Research Center, Tulsa, Oklahoma 74137-1270; *Baylor Hospital, Dallas, Texas; +University of Nebraska Medical Center, Omaha, Nebraska; ++Arlington Diagnostic and Treatment Center, Arlington, Texas; **NMR System, Inc., Amityville, New York; ***University of Texas Health Science Center, Dallas, Texas

When a radiologist requests a patient scan with a given pulse sequence and pulse interval, he may expect that the image contrast obtained from his scanner is the same as that obtained from any other scanner. If there is a difference, is it significant? In order to answer these inquiries, investigators in several medical centers have participated in a study of images of a relaxation time phantom. The phantom has several chambers filled with paramagnetic solutions in various concentrations so that relaxation times cover the typical tissue T_1 and T_2 ranges. Spin echo and inversion recovery images were compared with respect to pixel intensity and contrast values as functions of relaxation time T_1 and T_2, and pulse intervals TE and TI with TR held constant. Imagers used are: Picker MR VISTA 2055 at 0.5T, Technicare Teslacon at 0.6T, General Electric Signa at 1.5T, FONAR 3000 Beta at 0.3T and Siemens Magnetom at 0.3T§. Experimental data were compared with theoretical plots of pixel and contrast values derived from the Bloch equations. Since T_1 varies with magnetic field, the computed pixel values were obtained using T_1 values initially measured with a pulse spectrometer at 10 MHz and those obtained from extrapolation using Bottomley's equation relating T_1 and the B field. Deviation from the theoretical Bloch (exponential-like) behavior in different commercial imagers were observed. We suggest that some standardization of parameters such as RF pulse width, attenuation, contour, gradient pulse on-time, etc. be agreed upon so that T_1 and T_2 dependence would be more uniform for different scanners.

References

P.A. Bottomley, T.H. Foster, R.E. Argersinger, L.M. Pfeifer, Medical Physics 11, 425-448 (1984).
P.A. Hardy, M.J. Bronskill, R.M. Henkelman, Med. Phys. 12, 581-585 (1985).
F.W. Wehrli, J.R. McFall, T.H. Newton in Advanced Imaging Techniques, ed. T.H. Newton, Clavadel Press, New York, pp. 81-117, 1985.
W.S. Yamanashi, D.W. Anderson, P.D. Lester, et al, Physiol. Chem. Phys. Med. NMR 17, 81-100 (1985).

§data from Diasonic 0.5T unit are also included.

SELECTIVE SUPPRESSION OF SIGNALS IN MR IMAGING OF THE SPINE

Shmuel Albert, D.Sc., Clinical Science Center, Picker International

Spin-echo (SE) sequences with long echo times (TE=60 - 120 ms) and long repetition times (TR=1500 - 3000 ms) are usually used to identify intervertebral disk diseases by MRI.[1-3] However, this method requires a relatively long imaging time, and the resolution is not always satisfactory. The use of proton MR chemical shift imaging techniques was found to be helpful in identifying diseases of the intervertebral disks and the vertebrae.[4] We have developed a different approach that is based on the use of inversion recovery (IR) sequences with short inversion times (TI=50 - 200 ms).

The IR pulse sequence allows suppression of undesirable components within the image. This technique exploits the differentiation between the spin-lattice relaxation times (T_1) of the various tissues. Zero magnetization of any component with a particular T_1 value is accomplished by choosing an appropriate inversion time (TI) in the IR sequence according to:

$$TI = T_1 \ln [2/(1 + e^{-TR/T_1})]$$

This suppression technique was used to remove or partially remove the fat component, which has a relatively short T_1 value, and also to obtain images solely of the fat component.

The lumbar and cervical spines of volunteers and patients have been studied with these IR sequences using a 0.5T superconducting imager (Picker International VISTA^{TM} MR 2055) and compared with conventional SE T_2-weighted images. The fat-removed multisection images show high contrast between the spine tissues. The intervertebral disks and the spinal cord were clearly visualized, while the vertebral morrow signal was partially suppressed. The fat images have also been used to evaluate abnormalities. It is also possible to highlight the back muscle or any specific part of the spine. The imaging time was 6 - 11 minutes with our conventional body coil (6 - 8 slices of 10 mm thickness).

We have also used surface coils in conjunction with these IR sequences. Excellent images of thin slices (5 mm thickness) have been obtained, especially with a cervical spine coil. The resolution and contrast of the IR images are much better than the corresponding conventional T_2-weighted images. We have been able to identify degenerated disk, infected interspace, disk herniation, osteomyelitis; and to observe more pathological detail than offered by conventional spine images.

REFERENCES:

1) Aquila, L.A., Piraino, D.W., Modic, M.T., Dudley, A.W., Ducheseau, P.M. and Weinstein, M.A., Radiology 155, 155-158 (1985).

2) Edelman, R.R., Shoukimas, G.M., Stark, D.D., Davis, K.R., New, P.F.J., Saini, S, Rosenthal, D.I., Wismer, G.L., and Brady, T.J. American Journal of Roentgenology, 144, 1123-1129 (1985).

3) Modic, M.T., Feiglin, D.H., Piraino, D.W., Boumphrey, F., Weinstein, M.A., Duchesneau, P.M., and Rehm, S. Radiology, 157, 157-166 (1985).

4) Rosen, B.R., Wismer, G.L., McFarland, E., and Brady, T.J. presented at the Annual Meeting of the RSNA, Washington, D.C. November 25 - 30, 84. Radiology 153(P), p. 292.

STRATEGIES FOR SURFACE COIL IMAGING OF THE CERVICAL SPINE

R. Edward Hendrick, Ph.D.* and Charles E. Seibert, M.D.+

*Department of Radiology, University of Colorado School of Medicine, Denver, CO
+Department of Radiology, Swedish Hospital, Denver, CO

A double-looped cervical spine coil has been constructed and used during the past year for clinical imaging on a Picker 0.15 Tesla magnetic resonance imaging unit. Performance of the double-looped cervical spine coil is compared to that of the manufacturer-provided coils, particularly the Picker body coil, which is the primary alternative for cervical spine imaging. Performance is compared using cervical spine images of a normal volunteer as a function of slice thickness, number of sequence averages, number of phase encoding steps, and gradient strengths. Comparison of identical imaging techniques shows the signal-to-noise ratio from the double-looped cervical spine coil to be a factor of 1.43 to 7.7 better than the signal-to-noise ratio from the body coil, with 5 mm slice widths requiring the use of the cervical spine surface coil for adequate signal-to-noise ratios at 0.15 Tesla.

An evaluation of the normal volunteer images acquired with the double-looped cervical spine coil by a group of radiologists suggests an appropriate imaging strategy to take advantage of the signal-to-noise improvement of the cervical spinal coil. Measured signal-to-noise ratios are also shown to be in good agreement with theoretical expectations as slice width, number of averages, number of phase encoding steps, and gradient strengths are varied in surface coil imaging.

EVALUATION OF MAGNETIC RESONANCE FOR THE DETECTION AND STAGING OF HEAD AND NECK PATHOLOGY

Madeleine R. Fisher, M.D., Richard M. Gore, M.D.,
Robert L. Vogelzang, M.D., Lee Sider, M.D., Raja Atiyah, M.D.
George Sisson, Sr., M.D.

Northwestern Memorial Hospital, Department of Radiology
710 N. Fairbanks Court
Chicago, Illinois 60611

Staging of head and neck pathology is of critical importance in decisions regarding appropriate therapy. A retrospective study was performed to evaluate the potential of magnetic resonance (MR) in detecting pathology within the head and neck, to assess the extent of disease, and to evaluate the accuracy of staging using the TNM system compared to the clinical stage and pathologic findings. Correlation to computed tomography (CT) was performed when available. Twenty-one patients, ranging in age from 14 to 73, were evaluated using a 1.5 tesla system, operating at 0.5 tesla. In all 21 patients the head and neck pathology was detected. Comparison of staging between MR, CT, and the clinical stage showed: lesions invading the posterior fossa were better delineated with MR; sinus lesions were equally well seen with MR and CT, but the bone involvement was better depicted with CT; detection and extent of lesions of the salivary glands were better with MR; small lesions arising from the epiglottis, pharynx, and larynx were not well seen with either MR or CT and were better assessed with endoscopy: intra-thyroid lesions were better seen with MR as were lymph node metastases. Preliminary results suggest MR is a promising modality for detection and staging of head and neck pathology.

MRI EVALUATION OF THE PARASPINAL NEUROGENIC TUMOR

Anthony R. Lupetin, M.D.; William E. Rothfus, M.D.; Ziad L. Deeb, M.D.; Richard H. Daffner, M.D.; Rolf L. Schapiro, M.D.;

Allegheny General Hospital, Pittsburgh, Pennsylvania

PURPOSE: To demonstrate the usefulness of MRI in the evaluation of the paraspinal neurogenic tumor; specifically, can MRI detect the intraspinal extension of this lesion?

METHODS: Ten surgically-proven paraspinal tumors of neurogenic origin were studied with MRI using conventional T1 and T2-weighted spin echo pulse sequences obtained on a cryogenic magnet at field strengths of 0.35 and 0.5 Tesla.

RESULTS: We encountered lesions in the cervical (2); thoracic (5); lumbar (2) and sacrococcygeal (1) regions. Nine lesions were benign neurofibromas or schwannomas. One neuroblastoma (malignant) was encountered. In 2 of 10 cases, tumors extended into the spinal canal at surgery - MRI did successfully detect the presence or absence of this key finding in each case.

We will demonstrate the T1 and T2 appearances of neurogenic tumors and show how MRI will successfully preoperatively stage the paraspinal/intraspinal and bony manifestations of these lesions.

CONCLUSION: MRI may play an important future role in the preoperative assessment of paraspinal neurogenic tumors.

MAGNETIC RESONANCE IMAGING OF THE LUMBAR FACET JOINTS

F. Reed Murtagh, M.D.; H. Norman Schnitzlein, Ph.D.; John A. Arrington, M.D.; J. Daniel Jones, III, M.D.; Brian P. Cornnell, M.D.

University of South Florida College of Medicine

The ability to image in the sagittal and coronal plane adds much to the examinaton of the lumbar facet joints. These structures are at least as well seen on MR as on CT and the additional information provided by the sagittal and coronal planes can be extremely helpful. MR imaging of lumbar facets in the axial plane can be as useful, if not yet as detailed, as CT.

Anatomical material in the planes noted above will be presented with corresponding MR scans and clinical correlation.

SHORT TI INVERSION RECOVERY (STIR) IMAGING OF THE ORBIT AT 3.4 MHz.

F. W. Smith, G. Crosher, T.W. Redpath.

Department of Nuclear Medicine, Aberdeen Royal Infirmary, Aberdeen, Scotland.

Using the Aberdeen University designed and built 3.4 MHz MR imager and surface coils, 35 patients with orbital disease have been studied. Inversion Recovery sequences using a fixed TR of 1000 ms and a TI which may be varied from 50 - 500 ms are used. The spin-warp method of imaging is used with readout pulses every 1000 ms with alternate readout pulses preceded by inversion, giving a pulse sequence of interleaved saturation recovery and inversion recovery pulses.

Short TI sequences are those where the TI value is below 200 ms, medium TI being between 200 - 500 ms. Short TI sequences are sensitive to changes in both T1 and T2 and because many pathological conditions produce an increase in both T1 and T2 the addition of these two types of contrast with STIR sequences produces a very high net tissue contrast. Furthermore when the T1 and T2 decays of structures under examination are significantly different, very strong contrast between them is possible, very often more than would be possible using the equivalent spin-echo sequence. STIR sequences are particularly useful in displaying retinal detachment and choroidal haemorrhage which are not displayed using medium TI sequences.

The suppression of the signal from fat which occurs using STIR sequences improves the image quality adjacent to the surface coil. It also provides for better contrast between orbital structures and orbital fat allowing the easy demonstration of occular muscles, orbital vessels and the display of intra and extra conal tumours.

We are surprised that very little attention has been paid to these sequences by most groups performing MRI, who use spin echo sequences almost exclusively. We believe that in the use of STIR sequences any spatial resolution that is sacrificed is compensated for by the improved contrast resolution between normal structures and the greater contrast between normal and abnormal tissues.

MRI OF THE INTRATEMPORAL FACIAL NERVE USING SURFACE COILS

Teresi L, Kolin E, Lufkin R, Wortham D, Ward P, Hanafee W

UCLA School of Medicine(LT,RL,DW,PW,WH), Mount Sinai School of Medicine(EK)

Five normal volunteers and 36 patients with pathology of or involving the facial nerve were studied with a 0.3 Tesla permanent magnet MR system. Images were obtained with surface coils using various 2D-FT spin echo pulse sequences. 5mm thick sections with 0.5 mm pixels on a 512x512 acquisition matrix were used whenever possible.

The normal MR images were correlated with thick cryosection specimens of fresh human cadavers. The seventh nerve was followed from its nucleus in the brainstem through the temporal bone to the styomastoid foramen. The entire labyrinthine and tympanic portions, as well as the geniculate

ganglion could be shown with appropriate scan planes. Examples of brainstem and cerebropontine angle pathology affecting the facial nerve and nucleus, facial neuromas, and other pathology were studied.

Magnetic resonance produces excellent images of the facial nerve with high contrast resolution. Unlike CT, there is no beam-hardening artifact from the temporal bone. MR provides valuable information for the surgical and medical management of pathology affecting the facial nerve.

HIGH RESOLUTION SURFACE COIL MRI OF THE ORAL CAVITY AND LARYNGOPHARYNX

D Wortham, R Lufkin, L Hoover, E Abemayor, W Hanafee

UCLA School of Medicine, Los Angeles, CA 90024

Ninety patients with pathology of the oropharynx, hypopharynx, larynx, or tongue were studied with magnetic resonance (MR). Four millimeter thick axial, coronal, and sagittal scans were obtained with a pixel size of .75 x .75 mm. Both T1 and T2 weighted spin echo sequences were used. Sixty of these patients had computed tomography (CT) scans. Thirty-nine went to surgery and the specimens were obtained for organ sectioning. Correlation was made between these three studies as well as with clinical history, physical examination, and endoscopic photography. In those patients with all three studies, the ability to detect mandible involvement, cartilage invasion, adenopathy, and intra-organ and extra-organ spread of disease was compared.

Neither CT or MR was able to recognize histology or detect microscopic spread of disease. Both studies were less effective in the post-operative or post-irradiation neck. The use of direct coronal and sagittal scan planes on MR allowed the visualization of intrinsic laryngeal musculature which was important in recognizing subtle tumor extension.

In the oropharynx and tongue base, T2 weighted MR images showed high signal with tumor and provided much better tumor contrast than either T1 weighted images or double contrast CT. Like CT, MR did not show histology and many inflammatory and reactive processes produced similar high signal areas on T2 images. Post-surgical changes and atrophy were also high signal on T2 and T1 images but could be differentiated from neoplasm which was lower intensity on the T1 images. The ability to obtain coronal and sagittal planes was also a distinct advantage in recognizing intrinsic tongue musculature and assessing tumor volume and spread.

In general, MR using surface coils was superior to CT for imaging the oral cavity and laryngopharynx and is the imaging study of choice at our institution.

PREDICTING DEPTH OF INVASION OF ENDOMETRIAL CARCINOMA BY MRI

Marcia C. Fishman[1], M.D., Harry L. Stein[1], M.D., John L. Lovecchio[2], M.D.

Departments of Radiology[1] and Obstetrics and Gynecology[2], North Shore University Hospital, Cornell University Medical College, Manhasset, New York

MRI on the 0.6 tesla superconducting magnet accurately demonstrated the depth of myometrial invasion on T2 weighted images in 18 of 24 cases of surgically proved endometrial carcinoma. Twelve cases had full thickness invasion. Two cases had invasion deep to the stratum basale. Four lesions were confined to the endometrium. MRI was superior to CT scan in defining the location and extent of adenocarcinoma in 14 of 24 cases. Associated findings included parametrial extension, adenopathy, and bladder involvement. Three cases status post TAH-BSO had recurrent or metastatic disease. MRI offers the unique advantage of visualizing endometrium separate from myometrium. Relaxation rate differences afford characterization of pathologic tissue such as depth of invasion of endometrial carcinoma. MRI is superior to CT scan for localization of uterine malignancy within pelvic viscera.

(Oral Presentation)

THE VALUE OF MRI IN EVALUATING PERIRECTAL DISEASE

Marcia C. Fishman, M.D., Harry L. Stein, M.D., Bruce Javors, M.D., James Naidich, M.D.

Department of Radiology, North Shore University Hospital, Cornell University Medical College, Manhasset, New York

Twelve cases of perirectal disease were studied on a 0.6 tesla superconducting magnet. MRI with its multiplanar imaging capability accurately defined the location and extent of perirectal lesions including primary rectal carcinomas. Posterior extension of tumor from cervical carcinoma (three cases), and ovarian carcinoma (one case) was detected. A huge perirectal arteriovenous malformation was well documented by MRI, but was mistaken for recurrent endometrial carcinoma by CT scan. Inflammatory bowel disease was detected but findings were non-specific. MRI was particularly useful in providing not only anatomic but also diagnostic information in perirectal disease and holds great promise for complete staging of pelvic neoplasms.

(Oral Presentation)

STAGING OF CARCINOMA OF THE CERVIX BY MRI

Marcia C. Fishman[1], M.D., Harry L. Stein[1], M.D., John L. Lovecchio[2], M.D.

Departments of Radiology[1] and Obstetrics and Gynecology[2], North Shore University Hospital, Cornell University Medical College, Manhasset, New York

Twenty five patients with carcinoma of the cervix were studied on a 0.6 tesla superconducting magnet. MRI was superior to CT scan in 15 of 19 cases with CT correlation for localizing the primary lesion to the cervix rather than the uterus. Two patients with stage Ib occult cervical carcinoma showed no definite focal lesions by MRI. MRI correctly showed parametrial extension (six cases), rectal invasion (two cases), bladder invasion (three cases), and vaginal extension of tumor (two cases), but is probably less reliable than CT scan for detection of adenopathy due to lack of bowel contrast agents. On T2 weighted images, ten cervical carcinomas were of intense signal and seven cases were mixed in signal. Nine patients had an enlarged uterus with a distended endometrial cavity. MRI was more useful than CT scan for localization of tumor within pelvic viscera.

(Oral Presentation)

CORRELATION OF MRI, ULTRASOUND, AND NECROPSY IN THE EVALUATION OF STILLBORN FETUSES

Rita Gottesman[1], M.D., Marcia C. Fishman[1], M.D., Ellen Kahn[2], M.D., Mitchell Goldman[1], M.D., Steven A. Kroop[1], M.D., and Harry L. Stein[1], M.D.

Departments of Radiology[1] and Laboratories[2], North Shore University Hospital, Cornell University Medical College, Manhasset, New York

MRI of ten stillborn fetuses was performed on the 0.6 tesla superconducting magnet prior to necropsy. Ultrasound was correlated in seven cases. There were five male and four female fetuses, and one with ambiguous genitalia. Gestational ages ranged from 14 weeks to term. Anatomical detail was seen in the liver, kidneys, spleen, heart, and lungs. Pleural effusions and ascites were readily visible. One case thought to have renal agenesis by sonography had normal appearing kidneys by MRI. Other anomalies well visualized by MRI were a posterior fossa cyst, two cystic hygromas (one with trisomy 21, and one with Turner's syndrome), omphalocele, and two very low signal livers (histologically-proved hemosiderosis and and congenital hepatic fiborosis). MRI has multiplanar imaging capability, absence of ionizing radiation, and excellent contrast discrimination. Through ultrasound remains the procedure of choice for fetal and obstetrical survey, MRI provides a potential alternative for safe and accurate imaging. MRI has the added advantage of tissue characterization as demonstrated by this series.

(Oral Presentation)

MAGNETIC RESONANCE APPEARANCE OF THE PELVIC DERMOID

Anthony R. Lupetin, M.D.; Nilima Dash, M.D.; Irwin Beckman, D.O.; Lidia Linetsky, M.D.;

Allegheny General Hospital, Pittsburgh, Pennsylvania

PURPOSE: To demonstrate the usefulness of MRI in the detection of the pelvic dermoid tumor.

METHODS: Twelve patients with surgically-proven pelvic dermoid tumors were studied with MRI preoperatively. Conventional T1 and T2-weighted spin echo pulse sequences were utilized in each case in axial and coronal sections using a cryogenic magnet operating at either 0.35 or 0.5 Tesla.

RESULTS: All 12 lesions were identified with MRI. In 4 cases, a pathognomonic, triple-intensity pattern secondary to the combined presence of fat, fluid, and bony components allowed a specific diagnosis. Totally cystic dermoid tumors exhibited a T1 and T2 intensity pattern not separable from other cystic pelvic masses. Mainly, fatty dermoid tumors demonstrated a high signal intensity on T1 scans. In our experience, this appearance can only be seen otherwise in endometrioma. The MRI appearance of the dermoid capsule and all forms of internal or peripheral calcifications will also be demonstrated.

CONCLUSION: MRI will consistently and occasionally specifically diagnose pelvic dermoid tumors.

PELVIC TUMOR RECURRENCE: EVALUATION WITH MR AND CT

Mary Victoria Marx MD, Javier Beltran MD, Barry S Rose MD, Edward W Martin MD, Daniel P McCabe MD

Departments of Radiology (MVM, JB, BSR) and Surgery (EWM, DPM), Ohio State University Hospitals

Evaluation of the pelvis for tumor recurrence in people with primary gastrointestinal malignancies who have had previous surgery and radiation therapy is a complex problem. Because CT is felt to underestimate the extent of pelvic recurrence, second-look laparotomy continues to be necessary in the follow-up of many patients. This study investigates the role of MRI in the evaluation of pelvic tumor recurrence.

Sixteen patients (15 with colo-rectal cancer and one with small bowell carcinoma) with rising serum CEA levels were imaged with magnetic resonance. All had had previous resection of primary tumor and five had undergone perioperative radiation therapy. MR imaging was performed on a GE Signa 1.5 Tesla magnet using a partial saturation pulse sequence (TR 800msec/TE 25msec) in the sagittal plane and a spin echo pulse sequence (TR 2500msec/TE 35,70msec) in the axial and coronal planes. 15/16 patients had comparison CT. The CT and MR examinations were first interpreted in a double blind fashion, and subsequently examined together. Surgical and pathologic correlation is available in 11/16 patients. Of the other five, two were deemed to have unresectable disease on the basis of the imaging procedures, two were found to have metastatic disease

to the lungs, and one currently awaits second-look laparotomy.

Five patients with negative CT and MR studies had no evidence of pelvic tumor at laparotomy. In three patients, the extent of recurrent tumor was correctly predicted by both MR and CT. In one of these, done in the first half of the series, correlation with the CT was helpful in accurately interpreting the MR. Tumor recurrence was predicted by MR but not by CT in one patient. Two patients had recurrent tumor that was not apparent on either imaging study: in one, malignant infiltration into pelvic fat was evident only microscopically and in the other, a mass was obscured by surrounding bowel.

On MR, tumor recurrence most frequently presented as an irregular mass with a prolonged T2 signal. The abnormal signal made differentiation from adjacent muscle obvious - a major advantage over CT. Marrow involvement was also easily identifiable. The sagittal and coronal imaging planes did not appear to increase the diagnostic accuracy of MR over CT, but they were perceived as useful by surgeons planning operative intervention. Changes attributable to previous radiation therapy included prolonged T2 signal in fascial planes along the pelvic sidewalls, prolonged T2 signal throughout the pelvic fat, and increased signal in the bladder wall and sacral marrow.

In this preliminary study, magnetic resonance imaging has advantages over CT in selected cases. Results are promising, but MR is not yet a substitute for second-look laparotomy.

Coronal plane, spin echo image (TR2500/TE35) Tumor mass in left iliacus muscle in a patient status post partial left colectomy for adenocarcinoma in the descending colon (arrows).

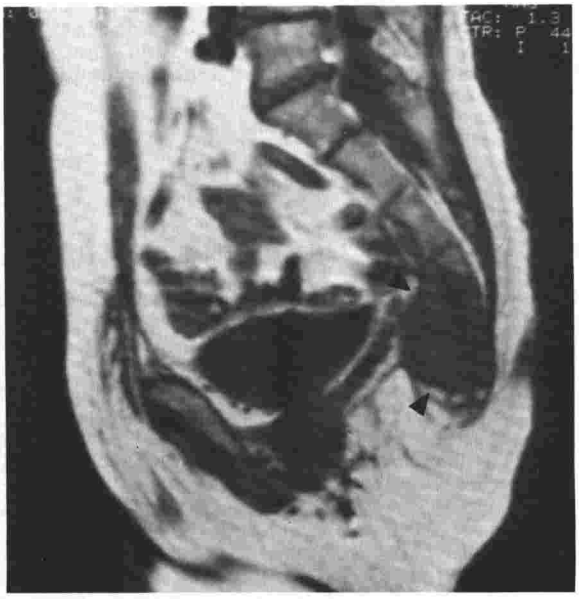

Sagittal plane, partial saturation image (TR800/TE35) Tumor mass invading the sacrum in a patient status post abdomino-perineal resection for adenocarcinoma of the rectum (arrows).

MAGNETIC RESONANCE IMAGING OF VARIATIONS IN FEMALE PELVIC ANATOMY DURING THE MENSTRUAL CYCLE AND WITH ORAL CONTRACEPTION

Shirley McCarthy, M.D., Ph.D.[1], Cheryl Tauber, RT[2], John Gore, Ph.D.[1]

1. Department of Diagnostic Radiology, Yale University School of Medicine New Haven, CT 2. General Electric Research Division, Milwaukee, WI

Twenty-one women in different phases of the menstrual cycle were imaged with magnetic resonance. Nine females were taking oral contraceptives whereas 12 were not taking any hormonal medication. Three were menstruating. A 1.5T G.E. Signa system was utilized. Sagittal spin echo images (TR2000, TE40,80) of the pelvis were obtained to assess the conspicuity and dimensions of the corpus uteri, cervix, vagina and their component tissues. On both the first and second echo images, the endometrium, junctional zone, myometrium, cervical canal, fibrous stroma, and vaginal canal were seen in 21/21 (100%) of the women. The anterior fornix was seen in 19/21 (90%) and the posterior fornix was seen in 20/21 (95%) of women. The vesicovaginal septum, the rectovaginal septum and levator ani were seen in 19/21 (90%) , 18/21 (86%) and 21/21 (100%) of the females, respectively.

The uterus was retrodisplaced in 4/21 (19%) of the women. In the non-pill group, endometrial width was significantly larger ($P < .025$) in the secretory phase (mean=5 mm.) than in the follicular phase (3.1 mm.). In the pill group, endometrial width was 1.1 mm. in the follicular and in the secretory phases, significantly smaller than in the non-pill user ($P < .025$ follicular phase, $P < .0005$ secretory phase). Junctional zone width was significantly smaller in the pill group ($P < .005$). Corpus width ($P < 0.5$) and length ($P < .025$) was significantly smaller in the pill group. Qualitatively, myometrium was relatively brighter at TE 80 in the pill group compatible with the known edema which occurs with oral contraception. We conclude that MR can reliably demonstrate gynecological structure and the anatomical changes which occur in the menstrual cycle and under the hormonal influence of oral contraception.

SHORT TI INVERSION RECOVERY (STIR) IMAGING IN HUMAN PREGNANCY.

F. W. Smith and H. W. Sutherland.

Depts. of Nuclear Medicine and Obstetrics, Aberdeen Royal Infirmary, Aberdeen, Scotland.

The use of Short TI Inversion Recovery (STIR) pulse sequences in the study of human pregnancy has been developed using the 3.4 MHz M.R. Imager designed and built at the University of Aberdeen. Using the Spin-warp method of imaging with a fixed TR of 1000 ms, images of the fetus, using TI valves between 100 and 500 ms have been studied.

One hundred and fifty examinations on one hundred and twenty-eight pregnant patients have been performed. As well as a series of normal pregnancies which have been studied at 4 weekly intervals from 24 week gestation to term, patients with diabetes mellitis, Intra-uterine growth retardation, pre-eclampsia and known fetal abnormality have been studied.

STIR images using TI values below 200ms are useful for the demonstration of fetal organs especially the heart and lungs, and for the demonstration and localisation of the placenta. Placental localisation, especially in cases of posterior placenta, using STIR sequences is particularly valuable in cases of suspected placenta praevia.

Using Medium length inversion recovery sequences TI = 300 - 500 ms the fat signal which is suppressed using TI values below 150 ms become enhanced. Using TI values of 500 ms accurate measurements of fetal subcutaneous fat, which correlate with both skin fold measurements and birth weight are possible. These are particularly useful in the evaluation of the fetus of the diabetic mother when planning obstetric management. Measurements of the fetal shoulder width are also possible providing a safe method of diagnosing shoulder dystocia.

GENERAL

A STEREOTAXIC SYSTEM AND ITS APPLICATION USING MAGNETIC RESONANCE IMAGING

John W. Ross-Duggan, M.D.; Angelo A. Patil, M.D.; William S. Yamanashi, Ph.D.; Jimmie L. Valentine, Ph.D.; Deborah L. Hill, S.S. and Patrick D. Lester, M.D.

City of Faith Medical and Research Center, Oral Roberts University School of Medicine, 8181 South Lewis, Tulsa, Oklahoma 74137-1270.

A CT and MR guided neurosurgical stereotaxic system has been used frequently in brain biopsy, aspiration of cysts and abscesses, in interstitial and intracavitory radiation, and functional neuro and radio surgery[1]. It requires no modification of the scanner, no special software modifications, measures coordinates directly from a single slice, and is portable. This versatility is possible secondary to the use of no feromagnetic materials. The ability to localize lesions with both scanners is advantageous in that both modalities are complimentary in delineating pathology.

In MR stereotaxis, the patient is positioned and MR image is targeted in the region of interest, with the x and y coordinate measurements determined using the cursor and viewer software. The z coordinate is determined using a special paramagnetic reference marker positioned in the stereotaxic system. The patient is taken out of the MR scanner and the procedure (biopsy, cysaspiration, etc.) is performed in an adjacent prepared site.

Reference

A.A. Patil, Acta Neurochirurgie, vol. 68, 19-26, 1983.
A.A. Patil, Neurosurgery, Vol. 15, 410-114, 1984.

THE DEVELOPMENT OF COMPUTER ALGORITHMS FOR ACCURATE REGRIDDING OF RECTANGULAR ARRAYS OF PIXEL VALUES

John H. Letcher, III, Ph.D., William S. Yamanashi, Ph.D.* and Patrick D. Lester, M.D.*

University of Tulsa, Department of Computer Science, 600 South College, Tulsa, Oklahoma 74014; *City of Faith Medical and Research Center, Department of Radiology, 8181 South Lewis, Tulsa, Oklahoma 74137.

In NMR, CT and ultrasound scanners, image data are normally saved as rectangular arrays of pixel values. Some of these data are known with fifteen-bit resolution, a gray scale of -8000 to +8000 (e.g. Picker MR VISTA series MR 4 and 5).

For the purpose of (1) comparing two or more images where the patient has moved or (2) altering absolute scale for magnification (reduction) of the image, redefining the grid is desirable. Computer programs MRITAPE and UPLOAD have developed to move binary pixel images from the magnetic tapes and to make these images available for manipulation on another computer.

The regridding procedure is accomplished by fitting the rectangular array of pixel values to a third order polynominal at each point of the array using four nearest neighbors selected in the x-plane. Then using the appropriate polynomial expansion coefficients for the four nearest neighbors in the y-plane, the function value for any desired point is readily obtained. The computer subroutines have been written intentionally in a machine independent language (FORTRAN) so that parting of this software may be readily accomplished.

ACQUIRING TECHNOLOGY IN THE NEW HEALTH CARE ENVIRONMENT: MAGNETIC RESONANCE IMAGING

Bruce J. Hillman, M.D. (1), C. Richard Neu, Ph.D. (2), John D. Winkler, Ph.D. (2), Jerome Aroesty, Ph.D. (2), Richard A. Rettig, Ph.D. (3), Albert P. Williams, Ph.D. (2)

(1) Department of Radiology, University of Arizona College of Medicine and University Hospital, Tucson, AZ 85724, (2) The Rand Corporation, Santa Monica, CA, (3) Department of Social Sciences, Illinois Institute of Technology, Chicago, IL

Recent changes in the reimbursement and regulation of health care are intended to provide incentives for more efficient and less costly use of technology, and to increase price competition among providers as a means of cost-containment. The effects of the changes are expected to be enhanced by an impending surfeit of doctors and facilities, as well as the increasing presence of health care corporations and entrepreneurs. These changes are expected to alter providers' motivations and behavior with respect to acquiring new technologies. To see how these environmental changes were affecting the early diffusion

of a particularly prominent innovation -- magnetic resonance imaging scanners (MRI) -- we conducted a study focussing on the influences encouraging and discouraging MRI acquisition.

We adopted a case study approach, conducting in 1984-85, 74 confidential personal interviews. Respondents included physicians, administrators, and representatives of regulatory agencies and third party payors from five states that span a stringent-lenient regulatory/reimbursement spectrum. We also interviewed representatives of MRI manufacturers, physician and commerical organizations, and federal regulatory agencies having an interest in MRI.

What we found was a near universal enthusiasm among respondents for the clinical potential of MRI, that was a major force promoting acquisition. Except for certificate of need regulations -- in states where CON was stringently enforced -- regulatory influences and anxieties over reimbursement for MRI scanning had little effect upon providers' decisions to acquire the technology. However, many respondents indicated that of equal or of even greater importance than technological considerations to their acquisition decisions were perceptions of local competition. Three forms of competition were evident with respect to MRI: 1. Direct competition over MRI services; 2. How MRI might be useful in gaining an advantage over other providers for non-MRI services; and competition among specialties and over referral sources. Competition was promoting more rapid diffusion of MRI, impelling some providers to acquire the technology sooner than they would have liked or knowing that MRI would likely represent a financial loss. The harsh competitive environment was also resulting in the adoption of practices contrary to those traditionally accepted among physicians.

The findings of our study suggest that changes in the health care environment are not having the effect intended with respect to MRI -- namely to promote more cautious behavior in technology acquisition. This may be because providers have not fully adapted to the changes that have occurred or that may occur in the immediate future. More plausibly, much of what we observed may be an appropriate response to the mixed signals of a health care system in transition. Possible implications for physicians and patients of the phenomena surrounding the acquisition and operation of MRI will be discussed.

HEAT DEPOSITION EFFECTS IN NUCLEAR MAGNETIC RESONANCE IMAGING IN 550 PATIENTS

Emanuel Kanal, M.D., Gerald L. Wolf, Ph.D., M.D.

Pittsburgh NMR Institute and the Department of Radiology, University of Pittsburgh

Much has been written concerning the possible effects of heat deposition during clinical Magnetic Resonance Imaging, with concern voiced about power deposition limitations in systems of higher magnetic field strength. While numerous studies have been reported discussing the effects of heating in animals, human data with large populations studied in a controlled manner during MR imaging are notably lacking. We report the results of an ongoing study where, to date, 550 patients have undergone head, body, and/or surface coil magnetic resonance imaging with specific absorption rates up to 1.5 W/Kg. Patient temperature, pressure, and pulse were measured before and after MRI. These measurements were also correlated with measurements of ambient atmospheric humidity and temperature in the magnet room itself. A mild yet statistically significant fall in patient temperature ($-0.176 \pm 0.032^{o}F$, $p < 0.005$) was found in 347 patients post-MRI at ambient temperatures of $67^{o}F$. Since this temperature decrease could reflect relatively greater body cooling due to ambient temperature than body heating due to RF power deposition, we raised ambient temperature to $72^{o}F$ and studied another group of patients. At this ambient temperature, in 207 patients temperature still decreased but not significantly ($-0.029 \pm 0.043^{o}F$, $p > 0.05$). Furthermore, at the higher ambient temperature, the fall in body temperature was significantly less ($p < 0.007$) than the fall in body temperature of the group studied at lower ambient temperature. In neither group was there evidence of an increase in pulse or decrease in blood pressure signaling a compensatory thermoregulatory response.

These results suggest that the limitation of 0.4 W/Kg placed on routine MRI by the FDA may indeed be far lower than necessary from the standpoint of patient safety and heat deposition. It may be possible to screen individual patients for potentially significant abnormalities in their compensatory thermoregulatory mechanisms prior to MRI. This may aid in detection of that limited segment of the patient population that may indeed require a lower SAR ceiling than the general populous. The generally untapped potential for increased ambient climate control may further enable studies with higher SAR's to be performed with no deleterious effects upon the patient.

MAGNETIC RESONANCE IMAGING SIMULATOR FOR INSTRUCTION IN PULSE SEQUENCE SELECTION

Rhodes M,Lufkin R, Keen R, Quinn J, Glenn W, Hanafee W

Multiplanar Diagnostic Imaging(MR,JQ,WG) and UCLA School of Medicine(RL,RK, WH)

An ordinary desk top microcomputer was programmed to simulate MR images for any specified spin echo pulse sequence. Model pixel maps of proton density, T1, and T2 relaxation times were created from published values for different regions of human anatomy. Images were then generated and displayed from the model maps and user specified pulse sequence parameters(TR, TE) in less than 30 seconds per image.

Models for various pathological conditions including calcification, subacute hemorrhage, porencephaly, fat, and multiple sclerosis were superimposed on the images of normal anatomy to create unknown cases. The effect of pulse sequence selection on the contrast of normal structures as well as the pathological conditions is easily demonstrated with these devices. The use of simulated images is an excellent technique to provide experience in pulse sequence selection. Low cost microcomputers can provide adequate image detail and reasonable image calculation and display time of synthetic MR images for teaching purposes.

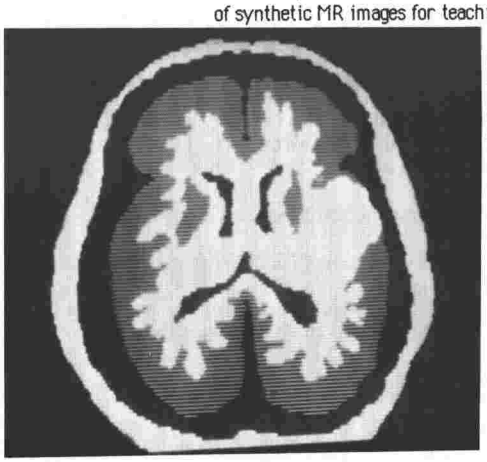

Fig. 1. Simulated SE/150/20 image of a patient with a subacute hemorrhage in the left cerebral hemisphere.

Fig. 2. Simulated SE/1500/56 image of a patient with basal ganglia calcification.

TRUNCATION ARTIFACT SIMULATING MOTION IN MAGNETIC RESONANCE IMAGING

E Pusey, R Lufkin, D Stark, R Brown, B Leikind, W Hanafee

UCLA School of Medicine(RL,EP,RB,BL,WH), and Massachusetts General Hospital(DS)

A ringing artifact similar in appearance to artifact produced with patient motion but unrelated to movement is present on magnetic resonance images. The phenomenon was investigated using doped water phantoms and normal volunteers. All images were obtained on 0.3 Tesla permanent and 0.6 Tesla superconducting MR imagers with varying phase and frequency sampling rates.

The artifact appeared in both the phase and frequency axes as parallel lines or ringing adjacent to borders or tissue discontinuities. Increasing the sampling rates from 128 to 512 resulted in higher frequency ringing and more rapid dropoff in amplitude. Low pass digital filtering also diminished the ringing at the expense of fine detail. The truncation of the infinite Fourier series necessary to encode edges to the 128 to 512 terms used for most MR imaging produces the artifact. It is important to recognize this common artifact of the 2D-FT technique and not mistake it for patient motion or pathology.

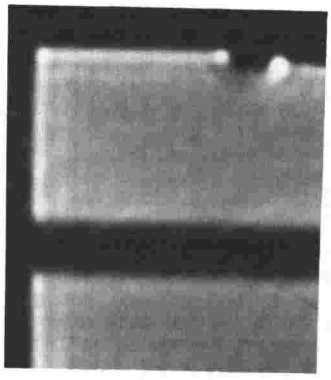

Fig. NiCl (2.5 mM) phantom imaged with symmetrical data acquisition (phase=frequency sampling rates) shows effect on truncation artifact. The signal intensity across the line is plotted on the graph.

A)128 x 128 level- pronounced ringing is present.

B)256 x 256 levels- the artifact is diminished.

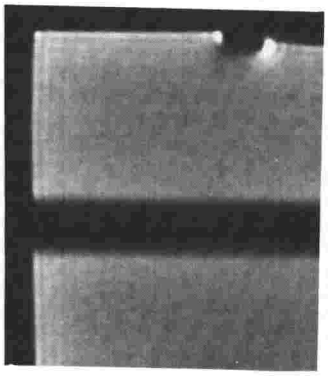

THE ROLE OF MAGNET DESIGN IN MOBILE MRI SYSTEM ECONOMICS

G.R. Morrow, W.D. Markiewicz, C.L. Linkinhoker

Intermagnetics General Corporation, Guilderland, New York 12084

"Up Time" or system availability is a significant factor in determining the economic viability of magnetic resonance imaging as a diagnostic procedure. Nowhere is "up time" so severely challenged as in the mobile system environment, where the demands on the magnet system are particularly severe.

A significant number of mobile MRI units are now in service and under evaluation as experimental devices. The design requirements imposed on the MRI magnet system in the mobile configuration are reviewed as they relate to "up time". Design solutions that address the mechanical, electrical, cryogenic, and field uniformity issues are described and their potential for application to siting options other than mobile is discussed.

Data from field experience with mobile units is reported to support the conclusion that with careful design, the magnet sub-system need not be the limiting factor in determining imaging system "up time".

EFFECTS OF LEAD PLACEMENT ON ECG RECORDING IN A 1.5 T FIELD

Laurence W. Hedlund, Ph.D., Richard Dimick, B.S., Robert J. Herfkens, M.D.

Department of Radiology, Duke University Medical Center, Durham, North Carolina

Blood flow in the magnetic field induces potentials which distort the ECG recording and can interfere with cardiac gated acquisitions. The distortion is especially prominent during the S-T segment and appears to be related to systolic blood flow.

The purpose of this study was to systematically examine the changes in the ECG pattern in volunteers in a magnetic field and determine which lead placement minimizes the flow potential distortion and maximizes the QRS wave.

Standard 12 lead ECG was recorded from normal volunteers (N = 5) while in a 1.5 T imaging magnet and again outside the magnet. The amplitudes of the ECG segments (QRS, T, P) were then compared.

The most apparent magnetic field-flow related distortion of the ECG was an elevation of the T. Such distortion was detected on all 12 leads. It was maximal in leads I, V3, and V4. This suggests that the vector for the flow potential is directed left lateral and slightly anterior from center chest. The magnitude and direction of the QRS segments were not changed by the magnetic field. Other, less definable distortion was seen in the baseline from the T to the P interval. The least distortion of the T and T to P segments was observed in the AVF lead. This suggests that the AVF lead vector is perpendicular to the major flow potential vector.

Since the AVF leads show the least distortion in the magnetic field, this may be the most useful configuration for cardiac gated MR imaging. These results from normal volunteers are being compared to recordings from patients with cardiac pathology.

THE IMPACT OF SPECTROMETER DYNAMIC RANGE, NOISE FIGURE, AND INTERNALLY GENERATED DISTORTION PRODUCTS ON IMAGING SYSTEM PERFORMANCE

George J. Misic, Ricardo Becerra, and Dr. Mehrdad Mehdizadeh

Picker International, Cleveland, Ohio

The proper design of an NMR receiving system requires attention to details far beyond the use of a low noise preamplifier. In order to extract the best possible signal-to-noise ratio in combination with very low distortion of the high signal levels encountered in imaging experiments calls for careful attention to gain distribution, active device selection, and proper parameters for mixer operation. Since internally generated distortion within the receiver caused by harmonic distortion or intermodulation distortion products will appear as noise or other artifacts in an image, it is important to design the receiver system to minimize these products as well as achieve very low noise performance at low signal levels.

To understand and optimize the performance of an NMR receiver for imaging purposes, a total RF/IF/AF system approach must be taken. A discussion of the design parameters and considerations necessary to achieve optimal system performance by definition of the requirements for each building block of the receiver is undertaken. An interpretation of the impact of dynamic range and third order intercept points is given, particularly as they relate to the specific requirements of NMR spectrometers. Both a single stage and a systematic analysis are shown. The selection of appropriate IF frequencies is discussed along with methods of eliminating the reception of undesired noise at the image frequencies. Methods of terminating diode ring doubly balanced mixers to optimize their dynamic range are given; the effects on receiver performance of this factor is illustrated. A discussion of IF and audio filter parameters relates the interaction of these specifications, and considers how they impact NMR imaging systems. The compromises between optimum signal-to-noise ratio versus obtainable dynamic range are discussed; recommendations for parameter selection for specific applications are included.

Proper receiver design, therefore, is a task which must be considered at the system level, rather than as a mere assembly of discrete building blocks. To aid in comprehension of these concepts, a typical receiver design for high performance imaging at medium field is illustrated, with a discussion of the rationale behind the selection of parameters used. Test results verifying the quality of performance achieved are included.

SUPER-PARAMAGNETIC PARTICLES AS T2 CONTRAST AGENT IN PROTON MR-IMAGING

Magnus B .E. Olsson, Bertil R.R. Persson, Leif G. Salford, Ulf Schroder

Lund University, S-221 85 Lund, Sweden.

The magnetic microsphere we used consists of a biodegradable starch gel matrix with a diameter of about one micrometer, containing small grains of magnetite (iron oxide Fe3O4) with diameter of about 10 nanometer. The magnetized vector of these small grains fluctuates in the same way as for paramagnetic ions but, has much larger magnetic moments and is therefore called "super-paramagnetic".

In vitro measurements were carried out in a Praxis II NMR analyzer at a magnetic field strength of 0.25 tesla and at a temperature of 37oC. The effect of the microspheres on the T1 and T2 relaxation times were studied in a solution of 8% (by weight) bovine serum albumin, at pH 7. Albumin solution was chosen instead of plasma and serum because it contains proteins of only one kind and will thus be reproducible from time to time. Free magnetite particles and three different preparations of microspheres were studied which contained 2.7 wt%, 1.0 wt% and 0.4 wt% magnetite respectively. The measuring volume was always 1 ml, and the samples were carefully suspended before measurement. Due to their small size, the particles were easily maintained in suspension during the period of measurement.

In vivo NMR-measurements were performed in an experimental imaging system, based on an iron-core window-frame magnet with a magnetic field of 0.07 tesla. Anesthetized wistar rats with an average weight of 380 +/-16 (1SD) g were used. The spheres contained as much as 20 wt% Fe2O3 in order to be able to move in an applied external magnetic gradient field. Thus the right hemisphere of the rat was placed in a magnetic gradient field of 200 tesla per meter and microspheres were injected through the

external carotid artery. After six minutes, the magnetic field was turned off and after another six minutes the rats were sacrificed and examied in the NMR-imager. The image show a "black hole" that the sphere were accumulated in the muscle and not in the brain. In vitro measurements, however, show that the T2-relaxation time is lowered in the right hemisphere which indicates the magnetic microsperes are targeted to this area.

In another series of experiments magnetic microspheres were injected through vena femoralis , and the rat was examined in the NMR-imager 10 to 20 minmutes after injection. In the NMR-image thus obtained the liver is clearly seen as a "black hole"

Conclusion: By introducing a starch gel matrix with entrapped magnetite, we have created a specific contrast agent for T2 NMR-imaging of the reticulo-endothelial system. The possibility of targeting the spheres with various pharmaceuticals might make these spheres useful as contrast agents for other organs and as therapeutic agent as well.

A COMPARISON OF THE PROTON RELAXATION ENHANCEMENT PROPERTIES OF IRON (III) AND MANGANESE (III) $TPPS_4$ IN SOLUTION AND TISSUE.

R.J. Fiel, T.M. Button, D. Musser, S. Gilani, N. Razack, E. Mark and R. Kurland*

Roswell Park Memorial Institute
Buffalo, New York
and
*Geisinger Medical Center
Dannville, Pennsylvania

Iron (III) and manganese (III) meso-tetraphenylporphine sulfate ($TPPS_4$) have been investigated for their potential as magnetic resonance imaging contrast agents. Both porphyrins demonstrate marked relaxivity (R) in aqueous solutions. Measured at 10.7 MHz, the value for R was found to be 3.0 mM^{-1} sec^{-1} and 12 mM^{-1} sec^{-1} for $Fe(III)TPPS_4$ and $Mn(III)TPPS_4$, respectively.

Previous studies of the acute toxicity of $Fe(III)TPPS_4$ in mice give an LD_{50} of >600 mg/kg, (i.p.). Our studies show that this porphyrin has an LD_{50} of <200 mg/kg when administered i.v. The toxicity of $Mn(III)TPPS_4$ appears to be much less with an LD_0 of >300 mg/kg, (i.v.).

Biodistribution studies were carried out on both porphyrins with DBA/2 mice bearing L1210 solid tumors using a tissue extraction procedure. This procedure involves an ammonium hydroxide/methanol extraction of trichloroacetic acid (TCA) precipitates of tissue homogenates. Preliminary measurements indicated that this procedure can recover 100% of $Fe(III)TPPS_4$. The tumor to tissue ratios for lung, kidney, liver and muscle were found to be 1.2, 2.9, 5.1 and 11, respectively. In the case of $Mn(III)TPPS_4$, preliminary measurements indicated that only 85% could be recovered with the extraction procedure and that in some tissues, the porphyrin was partitioned between the TCA precipitate and supernatant fraction. Within this limitation the tumor/muscle ratio was found to be 7.0 at 3 hrs. post injection of 50 mg/kg.

Relaxation measurements of excised tissues from L1210 tumor bearing mice indicated that no significant effect could be demonstrated for $Fe(III)TPPS_4$ in any tissue, including tumor, for doses of 25 to 200 mg/kg. The highest dose was found to be lethal within a 1 hour period. In contrast to this, $Mn(III)TPPS_4$ demonstrated a marked reduction in relaxation time for all tissues, except muscle. Doses up to 200 mg/kg were used with time points of 3 and 24 hrs. For tumor, an ED_{50} (dose required to give a 50% reduction in T_1) was found to be approximately 38 mg/kg and >>200 mg/kg for muscle at 3 hours. A simple calculation for 24 hour results based upon a spin echo pulse sequence indicates that a dose of 200 mg/kg would enhance the contrast between tumor and muscle by 350%.

It appears from these results that although $Fe(III)TPPS_4$ is unsuitable as a contrast agent, $Mn(III)$-$TPPS_4$ shows considerable potential as a tumor specific agent. It can also be noted that this porphyrin might be useful in a more general application as a tissue contrast agent since its tissue relaxivity compares very well with several other recently tested paramagnetic agents.

PARTICULATE IRON OXIDE (MAGNETITE): A RETICULOENDOTHELIAL SYSTEM SPECIFIC LIVER MR CONTRAST AGENT

Sanjay Saini, M.D., David D. Stark, M.D., Joseph T. Ferrucci, Jr., M.D., Joseph Sullivan, B.S.*, Jack Wittenberg, M.D.

Massachusetts General Hospital, Harvard Medical School, Boston, MA and Advanced Magnetics, Inc.*, Cambridge, MA

INTRODUCTION: Magnetite is a naturally occurring form of iron which is commercially available (BIOMAG*) for use in magnetically targeting chemotherapeutic drugs and **in vitro** techniques of protein separation. Aqueous preparations of crystalline aggregates (.5-1.5 u) can be injected intravenously in rats without demonstrable acute toxicity and become sequestered in the reticuloendothelial system. Due to the very large magnetic moment produced by the magnetite particles (superparamagnetism), induced local magnetic field inhomogeneities create marked shortening of the T2 relaxation times. The superparamagnetic relaxation properties and selective RES uptake of these iron oxide particles offer significant potential for achieving enhanced tumor-liver contrast in MRI of liver cancer.

METHODS AND RESULTS: We performed **in vitro** magnetic resonance spectroscopic studies (.5 Tesla) and **in vivo** imaging (1.4 Tesla) in 55 Fisher 344 female rats surgically implanted with mammary adenocarcinoma. The tumor model is particularly suitable for experimental imaging of liver metastases because the adenocarcinoma grows rapidly to a size of 1-2 cm in 14 days after implantation and recapitulates the MR imaging features of human metastatic liver cancers by virtue of prolongation of tumor T1 and T2 relaxation times. Microscopic (EM; iron stain) studies demonstrate that magnetite is localized in the Kupffer's cell of normal liver but not in neoplastic tumor nodules. Spectroscopic and time-dosage response studies also confirm prompt RES removal of the particles from circulating blood without significant retention, lung or kidney. A 50% reduction liver T2 with no change in T1 relaxation time can be achieved with very small dose (1.2 mg of magnetite/kg of rat weight).

In vivo MRI studies demonstrate profound tumor-liver contrast enhancement on pulse sequences with T2-weighting (spin echo = TR greater than 500 msec; TE greater than 30 msec).

Sequence	SD/N**	
	Pre	Post
SE 1500/60/2	21.2	27.7
SE 500/30/3	1.3	15.2
SE 250/15/3	-5.0	+6.5
IR 1500/450/15/2	-9.0	-4.0

**SD/N = [SI tumor - SI liver]/SI background
Corrected for uniform imaging time

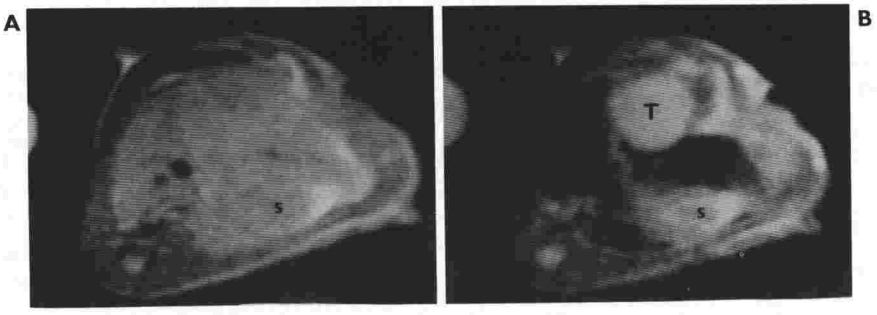

SE 500/30/3 Pre and Post magnetite injection MR images of a tumor bearing rat abdomen. (a) Tumor and liver are indistinguishable on the pre-contrast image. (b) After administration of magnetite (2 mg) there is a pronounced increase in the tumor-liver signal difference due to the precipitous drop in signal from normal liver. (T=tumor nodule; S=stomach).

CONCLUSIONS: Magnetite enhanced MR images provide an increase in tumor-liver contrast because magnetite is accumulated only in normal liver parenchyma (RES) and not in tumor. The tissue specificity of magnetite and its large magnetic moment make it a powerful liver contrast agent. Our studies indicate that magnetite enhanced MRI can greatly improve the detectability of liver cancer.

IMAGE ARTIFACTS IN MAGNETIC RESONANCE IMAGING

R. James R. Knowles, John A. Markisz, Thomas P. Callahan, Richard J. Fischer, Joseph P. Whalen, and Patrick T. Cahill

The New York Hospital-Cornell Medical Center, 525 E. 68th St., New York, N.Y. 10021

Magnetic Resonance Imaging has produced a new generation of image artifacts, recognition of which is essential for proper interpretation of diagnostic studies. All artifacts can be divided into two broad categories: (a) artifacts associated with the patient and (b) artifacts associated with the MRI system itself. Patient associated artifacts include random motion and foreign bodies, which may either simply create voids in the image (if non-magnetic) or cause image distortion (if magnetic). Personal articles (keys, hairpins, jewelry, cosmetics, etc.), prosthetic devices (artificial hips, shoulders, eyes, etc.) and medical/surgical implants (clips, sutures, valves, plates, etc.) are the most common causes of image degradation. Respiratory, cardiac and bowel motion are physiologic factors that affect image quality by producing blurring and displaced signal (particularly in the direction of the phase encoding gradient). The first two of these can be minimized with proper gating techniques, while the administration of glucagon may lessen the latter. Specific types of image artifacts associated with instrumental failures can be traced to problems with gradients, shims, RF and computer hardware. Artifacts inherent in the imaging process include chemical shifts at fat/soft tissue interfaces and a wide variety of flow related artifacts. Recognition and classification of the types of MRI artifacts are essential not only for proper clinical interpretation but also for the evaluation of system performance.

PERIPHERAL PULMONARY EMBOLI DEMONSTRATED USING MAGNETIC IMAGING.

Carl Olof-Ovenfors, M.D.

University of California, Los Angeles, Dept. of Radiological Sciences, Los Angeles, CA.90024

Earlier experimental studies have shown that large barium tagged emboli can be visualized on MR scans as areas of increased signal. (Gamsu et al, Radiology 153:467, 1984). Correlation was done with CT scans and scout films. Pulmomary angiograms were not performed.

In the present study pulmonary angiograms were done for localization of the boiled autologous clots after embolization. Smaller approximately 2 X 10 mm and larger, 4 X 10 mm clots were used.

Eight dogs were embolized and studied with MR scanning using a 0.3 Tesla permanent magnet scanner and spin echo sequences (TE=28 msec, TR=499 msec). EKG gating was used in all experiments.

MR scans were obtained in transaxial and coronal planes. Areas of increased signal were present on all scans corresponding to the embolized areas seen on the angiograms.

In conclusion, pulmonary emboli at the segmental and subsegmental levels can be demonstrated in the dog by MR scanning as areas of increased signal. A clinical study seems to be warranted to evaluate the method of use in patients.

MRI IN THE EVALUATION AND FOLLOW UP OF COARCTATION OF THE AORTA IN CHILDREN

Marcia C. Fishman[1], M.D., Harry L. Stein[1], M.D., Robert A. Boxer[2], M.D., Michael A. LaCorte[2], M.D., Rubin S. Cooper, M.D.[3]

Departments of Radiology[1] and Pediatrics[2], North Shore University Hospital, Cornell University Medical College, Manhasset, New York; Brookdale Hospital, Brooklyn, New York[3]

Ten patients with coarctation of the aorta were evaluated by magnetic resonance imaging gated to the electrocardiograph. Ages range from 2.5 to 18 years. Six patients underwent balloon angioplasty. One patient had surgical repair. Pre and post therapy studies were performed in three cases. The anatomy of coarctation was best shown in the sagittal and the 60 degree left anterior oblique imaging planes. Post-treatment MRI revealed improvement in the site of coarctation in all cases. In three patients, there was dilatation of the aorta at the site of the angioplasty. Magnetic resonance imaging provides a useful noninvasive method for detection and follow up of coarctation of the aorta in children.

(Oral Presentation)

MEASUREMENT OF CARDIAC DIMENSIONS BY NUCLEAR MAGNETIC RESONANCE IMAGING: A COMPARISON TO ECHOCARDIOGRAPHY IN PATIENTS WITH HEART DISEASE

Cam F. Campbell, Val Dunn, James C. Ehrhardt, Steve M. Collins, David J. Skorton

Departments of Internal Medicine, Radiology, and Electrical and Computer Engineering, University of Iowa, Iowa City, Iowa

Nuclear magnetic resonance imaging is a promising method of noninvasively defining cardiac morphology. To determine the accuracy and reproducibility of magnetic resonance cardiac measurements in a clinical setting, magnetic resonance imaging and echocardiography were performed in 13 patients with ischemic, valvular, pericardial, or myopathic disorders. Gated, spin-echo magnetic resonance images were obtained using a 0.5 tesla superconducting system. Echocardiography was performed using a 2.25 MHz phased-array system. Measurements were made at end-diastole of the right ventricular cavity, ventricular septum, left ventricular cavity minor axis, and left ventricular posterior wall. Two independent observers measured the echocardiographic data from two-dimensional echocardiogram-derived M-mode tracings. Two other independent observers measured the cardiac dimensions from transaxial magnetic resonance images along the apparent cardiac minor axis, defined as perpendicular to the interventricular septum.

Results. Correlation coefficients between echocardiography and nuclear magnetic resonance imaging using measurements from individual cardiac structures and all cardiac structures for the two magnetic resonance observers are shown in the table below:

Structure	Correlations	
	Observer No. 1	Observer No. 2
Right Ventricular Cavity	.34	.50
Interventricular Septum	.60	.53
Left Ventricular Cavity	.83	.79
Left Ventricular Posterior Wall	.18	.63
All Cardiac Structures	.91	.92

Interobserver reproducibility was excellent for both nuclear magnetic resonance (r=.99) and echocardiography (r=.99).

Conclusions. We conclude that gated nuclear magnetic resonance imaging permits reproducible end-diastolic cardiac measurements in patients with a variety of cardiac disorders. Comparing nuclear magnetic resonance imaging and echocardiography: (1) right ventricular cavity correlation is relatively poor, (2) left ventricular cavity and interventricular septum correlations are relatively good, (3) the variable left ventricular posterior wall correlation is in part due to difficulty in appropriately defining the epicardial border.

MAGNETIC RESONANCE ASSESSMENT OF REGIONAL LEFT VENTRICULAR FUNCTION

SR Underwood, RSO Rees, PE Savage, RH Klipstein, DN Firmin, KM Fox, PA Poole-Wilson, DB Longmore

The National Heart and Chest Hospitals, London, UK

This study investigates magnetic resonance in the determination of regional left ventricular wall motion and thickness, and compares findings with X-ray ventriculography.

Coronal images were acquired through the aortic valve, and sagittal images in the plane of widest diameter of the left ventricle seen in the coronal image, both at end diastole and end systole. Comparison was made with antero-posterior and lateral X-ray contrast ventriculograms by two independant observers. The left ventricular wall was divided into three segments in each plane, and the motion of segments was classified as normal, hypokinetic, akinetic, or dyskinetic. Muscle thickness was measured in each segment and was considered abnormal either if in the systolic images it was less than 75% of that in neighbouring segments, or if it failed to increase by at least 25% between diastole and systole. 18 patients were studied: 9 with previous myocardial infarction, 4 with coronary artery disease without infarction, 1 with congestive cardiomyopathy, 1 with mitral stenosis, and 1 with an atrial septal defect, and 2 without detectable cardiac abnormality. The two methods agreed in 68 of 105 segments analysed, differed by 1 class in 32 segments, and by 2 classes in 5 segments. In three of these 5, magnetic resonance showed akinesis and thinning in patients with previous infarction, but ventriculography showed normal motion. In the fourth magnetic resonance showed paradoxical septal motion (confirmed by echocardiography) in a patient with atrial septal defect. In the fifth, ventriculography showed akinesis in a patient with coronary artery disease without infarction, but magnetic resonance was normal. These differences may be explained by the invasiveness of ventriculography and by the difference between a tomographic section and an X-ray projection. Magnetic resonance showed 25 segments to have abnormal wall thickness, all in patients with previous infarction. Only 1 subject with infarction (3 months previously) did not have an area of wall thinning, and no patient without infarction had an area of thinning.

Magnetic resonance allows an accurate non-invasive assessment of left ventricular wall motion and thickness, and is of value in determining regional left ventricular function.

MAGNETIC RESONANCE QUANTIFICATION OF ATRIAL SHUNTING AND VALVULAR REGURGITATION

SR Underwood, RH Klipstein, DN Firmin, KM Fox, PA Poole-Wilson, RSO Rees, DB Longmore

The National Heart and Chest Hospitals, London, UK

We have previously shown that both left and right ventricular volumes can be measured accurately by magnetic resonance. The purpose of this study is to quantify valvular regurgitation and left to right shunting through an atrial septal defect, by comparing left and right ventricular stroke volumes, which should be identical over the period of imaging, in the absence of regurgitation or shunting.

27 patients were studied by magnetic resonance, first pass and equilibrium radionuclide angiocardiography, and cardiac catheterisation. Multiple transverse magnetic resonance images were acquired at end diastole and end systole, using a Picker International machine operating at 0.24 tesla, and using a spin echo sequence with an echo time of 24ms. Ventricular volumes were calculated by summing their areas in the contiguous 1cm sections. In 20 normal subjects the mean left to right ventricular stroke volume ratio was 1.01 (SD 0.067), thus establishing a normal range of 0.88-1.14, and suggesting that the accuracy of individual volume measurements was approximately 2%. In 5 patients with atrial septal defect, the stroke volume ratio was abnormal and the correlation coefficient between magnetic resonance and oximetric determination of pulmonary to systemic flow ratio was 0.91. In 8 patients with mitral regurgitation and 12 with aortic regurgitation, the stroke volume ratio was also abnormal, and the degree of abnormality was similar to semi-quantitative assessment by X-ray angiocardiography (Figure 1). The correlation coefficients between magnetic resonance and radionuclide values of left ventricular ejection fraction, right ventricular ejection fraction, and stroke volume ratio were 0.88, 0.88, and 0.82 respectively. The radionuclide measurements underestimated right ventricular stroke volume however, especially in the patients with atrial septal defect and a dilated right heart, because of overlap of right atrium and ventricle in the left anterior oblique projection (Figure 2).

Magnetic resonance provides a noninvasive method to quantify valvular regurgitation and atrial shunting, and may improve the assessment of such patients.

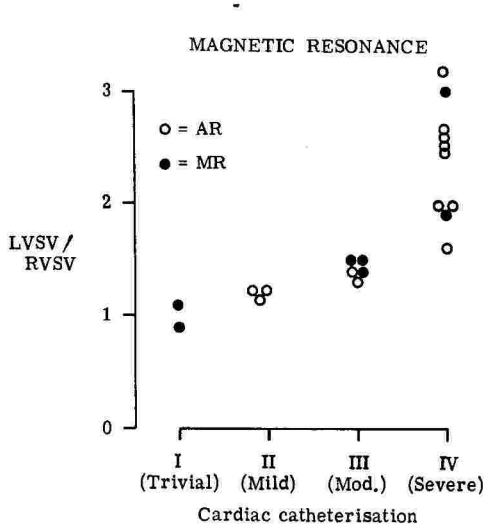

FIGURE 1

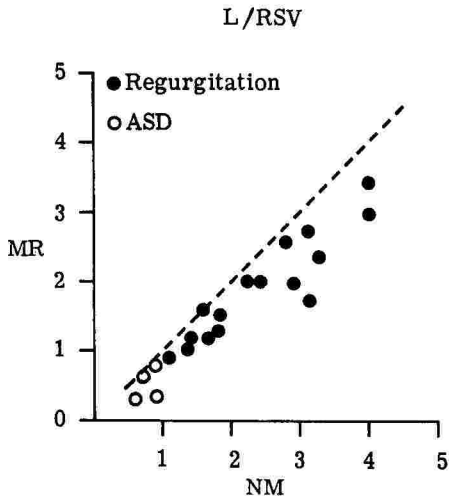

FIGURE 2

RAPID MEASUREMENT OF LEFT VENTRICULAR VOLUME FROM SINGLE OBLIQUE MAGNETIC RESONANCE IMAGES

SR Underwood, DN Firmin, RH Klipstein, KM Fox, PA Poole-Wilson, RSO Rees, DB Longmore

The National Heart and Chest Hospitals, London, UK

We have previously demonstrated that magnetic resonance allows the measurement of left ventricular volume with an accuracy of approximately 2%, from the sum of the areas of the ventricle in multiple contiguous sections. Data acquisition may however require up to 40 minutes, and a more rapid method is needed for routine use. The purpose of this study is to compare volumes calculated from multiple sections with those calculated from a single section containing the long axis of the ventricle.

25 normal subjects were studied using a Picker International machine operating at 0.24 tesla, and using a spin echo sequence with an echo time of 24ms. Contiguous 1cm sections were acquired at end diastole and end systole, parallel to the long axis of the ventricle, and each cutting it from septum to lateral wall. Left ventricular volume was calculated from the sum of the areas in each section (x), and from the area and length of the section containing the long axis, assuming the ventricle to be an ellipsoid of revolution (y). Regression of y on x gave $y = 1.00x - 2$, $r = 0.99$, for diastolic and systolic volumes together, and neither alone had a regression line significantly different from the line of identity (Figure 1). There was better correlation at end systole ($r = 0.96$) than at end diastole ($r = 0.88$). Mean end diastolic volumes were 128ml (SD 15.2) and 128ml (SD 17.6), mean end systolic volumes 48ml (SD 14.4) and 51ml (SD 12.6), and mean ejection fractions 0.62 (SD 0.081) and 0.60 (0.055) for methods x and y respectively. The correlation coefficient between the two methods for calculating left ventricular ejection fraction was 0.86 (Figure 2). A series of patients with previous myocardial infarction was also studied and the area-length method was found to be less accurate at end systole, when ventricular shape was further from an ellipsoid of revolution. Oblique sections were important in these patients for a proper description of ventricular wall motion and thickness.

It is concluded that left ventricular volume and ejection fraction may be determined from single oblique images at end diastole and end systole, and that imaging time may be shortened to a total of approximately 15 minutes. More accurate results are obtained in patients with previous infarction using a multislice technique.

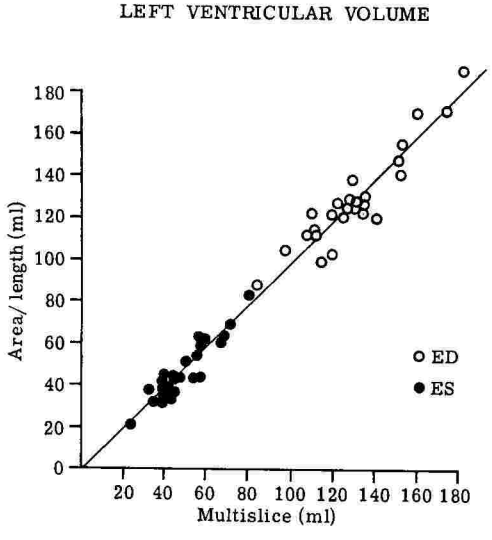

FIGURE 1

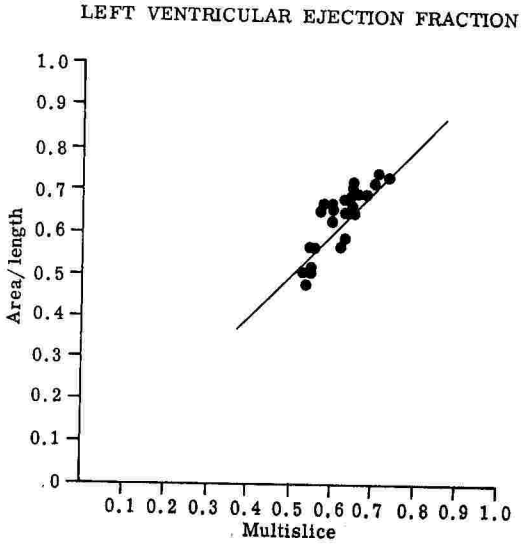

FIGURE 2

THE INVESTIGATION OF RECENT MYOCARDIAL INFARCTION USING ECG GATED T1 IMAGES

M A Smith, M Been, J P Ridgway, D M Kean, R H B Douglas, A L Muir and J J K Best

NMR Imaging Unit, University of Edinburgh, Royal Infirmary, Edinburgh.

A commercial 0.08T vertical field resistive MRI system (manufactured by M&D Technology) has been modified to produce ECG gated T1 images. The system produces a calculated T1 image using an interleaved saturation recovery and inversion recovery sequence. In the latter a non slice-selective adiabatic fast passage (AFP) inverting pulse is used which enables the inversion recovery sequence to be synchronised with the cardiac cycle as well as the saturation recovery sequence. Conventional ECG electrodes are attached to the right shoulder and right hip of the patient and the ECG is transmitted via an optical fibre. This configuration minimises gradient and RF interference on the ECG signal and also the introduction of noise into the system. The minimum delay from the R wave and the time in the cardiac cycle to be imaged is 230ms.

Images are generally acquired at end systole using 16mm sections and an acquisition time of between 4 and 6 minutes, depending on the patients heart rate. The MRI system is triggered on every heart beat unless the heart rate is greater than 70 beats per minute in which case every other beat is used. With the pulse sequence used the T1 values obtained are not significantly influenced by the R-R interval.

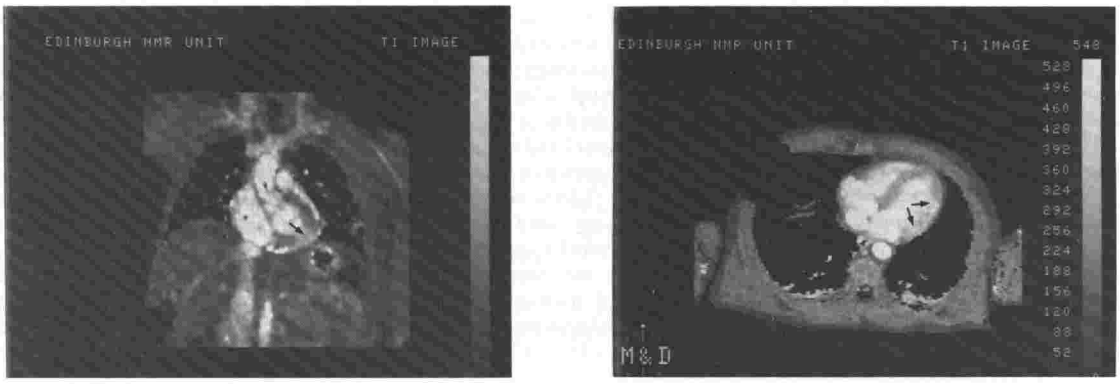

Gated T1 images from two patients with region of MI indicated.

The results of the first 13 patients studied at 2-12 days post MI demonstrated a significant increase in patients following recent MI compared with normals (Been, Smith et al, Lancet ii, 348-350, 1985). The mean T1 in normal myocardium was found to be 305ms ± 25ms compared with a mean maximum T1 in patients with MI of 426ms ± 70ms.

A subsequent study of 22 patients with a first MI, with stable cardiac rhythms and free from symptomatic pulmonary oedema confirmed the preliminary findings. These patients were imaged at the following times after MI: 16 between 1 and 3 days, 3 between 4 and 7 days and 3 between 8 and 14 days. The mean maximum T1 of these patients was 428ms ± 29ms.

The region of maximum T1 corresponded well with the site of infarction. In the group of 22 patients there were 13 anterior and 9 posterior infarcts; the anterior infarcts were visualised better in the transverse section and the posterior infarcts in the coronal section.

EVALUATION OF INTRATHORACIC NEOPLASMS BY MAGNETIC RESONANCE IMAGING

Batra, Poonam; Brown, Kathleen; Ovenfors, Carl
UCLA
Dept. of Radiological Sciences, Center for Health Sciences, Los Angeles, CA. 90024

Fifty-seven intrathoracic neoplasms were studied on MR imaging of the thorax of 92 subjects. The neoplasms included bronchogenic carcinoma (32), lymphoma (10), thymoma (2), chondrosarcoma of a rib (1), neurilemoma (1), metastases to lung, hila, mediastinum, pleura or chest wall (10) and mesothelioma (1). All patients had histologically proven neoplasms except for 3 with metastases. All images were obtained by a 0.3 Tesla permanent magnet system (Fonar Beta 3000) by spin echo technique (SE 500/28). T_2-weighted images were obtained in 36 cases. All images were obtained in axial plane in addition to 21 in sagittal and 25 in coronal. MR images were compared with previously obtained CT scans in 44 cases. On MRI

the mediastinal and lung masses were easily distinguished from vessels and central bronchi. MRI provided diagnostic information equivalent to CT for most mediastinal lesions but was superior for demonstrating hilar abnormality (2). CT was found superior for evaluating calcified lesions (4), small anterior mediastinal masses (2) and lymph nodes (2). MR aided further in anatomical evaluation by performing direct sagittal and coronal imaging. The advantages and limitations of MR versus CT for intrathoracic neoplasms are presented.

FOR ORAL PRESENTATION

MR IMAGES OF OAT CELL CARCINOMA OF LUNG

A 74 year old asymptomatic female demonstrated a mediastinal mass secondary to oat cell carcinoma of lung. The intermediate signal intensity mass (m) is easily distinguished from the bright signal intensity of fat. The displacement and compression of superior vena cava (straignt arrow) and flattening of right antero-lateral aspect of trachea (curved arrow) by the tumor are well demonstrated.

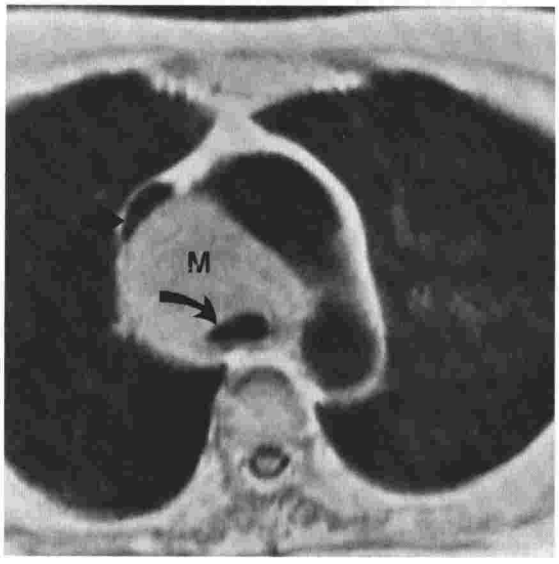

A. Axial SE 500/28 Scan

B. Coronal SE 500/28 Scan

LEFT VENTRICULAR EJECTION FRACTION AND TUMOR VOLUME MEASUREMENT WITH MAGNETIC RESONANCE IMAGING AT 0.5T

James R. LePage, M.D.; William S. Yamanashi, Ph.D.; Jimmie L. Valentine, Ph.D.; Cynthia H. Hood, B.S.N.; Deborah L. Hill, B.S. and Patrick D. Lester, M.D.

Department of Radiology, Pharmacology and Cardiology, City of Faith Medical and Research Center, Oral Roberts University School of Medicine, 8181 South Lewis Avenue, Tulsa, Oklahoma 74137-1270

Left ventricular ejection fraction (EF) and tumor volume were measured with proton magnetic resonance (MR) imaging at 0.5T.

The EF measurement was performed using cardiac gated MR and compared with EF values determined by established techniques such as 30 degree RAO left ventricular angio-cardiograms (CCV), right atrial digital subtraction angiograms of the left ventricle (RADSA) and nuclear medicine multiple contraction gated acquisi-angiograms (MUGA) in 20 degree RAO and standard 45 degree and 60 degree LAO views. The comparison between the mean EF (%) obtained by transaxial MR and by 30 degree RAO CCV resulted in SD of ± 2.62 with p less than 0.01 while comparisons in the saggital orientation are within SD of 15 with p less than 0.001.

The tumor volume measurement was evaluated in rats and guinea pigs with spontaneous tumors using a specially constructed receiving coil to improve the signal to noise ratio (S/N) of the MR images of tumor in these small animals. The sum of contiguous slices using the multiple slice and the area measure software and the elipsoid approximation were compared with the volume measured at the surgical resection.

Both of these measurements were done using a Picker MR VISTA 2055 imager operated at 0.49T (21.255 MHz) with a MR 4/TABF software which included 2DFT reconstruction and multiple slicing. The slice thickness was ca 10 mm, pixel matrix 9256 x 256), viewer matrix 9512 x 512). For the EF measurement, ECG gating was used, in which a radiofrequency transmitter was fiber-optically coupled to the MR transceiver. Leads were placed on wrists and right ankle. Images were obtained in end-diastole at the peak R-wave and at end-systole, at the end of T-wave. TE=40 ms with TR equal to patient's R-R interval was used. For the tumor volume measurement TE=40 ms with TR=1000 ms was used with a previously described surface coil.*

Reference

J.L. Westcott, C.S. Henschke, Y. Berkman, Proc. 3rd Ann. Meet. Soc. Mag. Res. in Med., p. 754 (1983).

*W.S. Yamanashi, et al., Magnetic Resonance Imaging, 3, 200 (1985).

MAGNETIC RESONANCE IMAGING OF THE CHEST IN AXIAL, CORONAL AND SAGITTAL PLANE

Poonam Batra, M.D., Carl Ovenfors, M.D., Kathleen Brown, M.D.

UCLA, Center for Health Sciences, Dept. of Radiological Sciences, Los Angeles, CA. 90024

MRI was performed in 6 normal volunteers and 67 patients with benign and malignant diseases involving the mediastinum and/or hila (41), pulmonary parenchyma (16), pleura (8), and chest wall (2) for abnormalities detected on chest radiographs (58 cases) and/or computed tomograms (52 cases). In all cases, images were obtained on a Fonar 0.3 Tesla permanent magnet imaging system using T1 weighted spin echo technique (TR500, TE28). T2 weighted (TR1500 - 2000, TE56) images were obtained in 24 patients. Cardiac gating was used in 6 patients and respiratory gating was attempted unsuccessfully in one. All images were obtained in the axial plane, 34 in coronal, 25 in sagittal, and 1 in oblique.

MRI was comparable to CT in 45 cases for detecting the presence of disease. In 3 cases MR defined the extent of disease better than CT. In all cases vascular displacement or invasion, hilar and mediastinal nodes, and masses could be differentiated from vasculature on MRI without contrast medium. Calcifications seen on CT in 6 cases were difficult to visualize on MRI due to lack of signal. In 3 cases pulmonary parenchymal nodules (1 cm or less in size) were not imaged or were poorly imaged on MRI due to long image acquisition time, which resulted in tissue averaging from respiratory and cardiac motion. Our study indicates that MRI is at least equivalent to CT with intravenous contrast medium for evaluating mediastinal and hilar lesions; while CT is superior for small parenchymal nodules and calcified lesions. The examples of normal anatomy and pathology in axial, coronal and sagittal plane shall be presented.

NON-ANGIOGRAPHIC IMAGING OF THE PULMONARY ARTERIES: CT AND MR IMAGING.

Conces DJ, Tarver RD, Augustyn GT

Indiana University Medical Center, Indianapolis, Indiana

The central pulmonary arteries may be involved by a variety of disease processes. Plain film radiography provides limited information on the involvement of the central pulmonary arteries by disease. Traditionally pulmonary angiography was used to evaluate both intrinsic and extrinsic disease processes involving these vessels. Computed tomography (CT) and magnetic resonance (MR) imaging provide additional methods of studying the central pulmonary arteries without resorting to angiography. A series of 21 patients with pathologic conditions involving the pulmonary arteries were studied with both CT and MR imaging. CT and MR imaging demonstrated the pathology involving the vessels in all cases. MR imaging better demonstrated the pathology or identified additional findings in 9 patients. Coronal MR images, which were done on all patients, provided unique information not seen on either CT or transverse MR images in 3 patients. Both CT and MR imaging are useful modalities with which to evaluate the central pulmonary arteries. MR imaging was better able to delineate the extent of disease involving the pulmonary arteries than was CT.

INITIAL RESULTS WITH MRI CAROTID ANGIOGRAPHY

JT Ruszkowski*, R Damadian**, A Giambalvo**, A Gomes***, W Hanafee***, D Hertz**, R Lufkin***, SD Smith**, D Wortham***

*State University of New York, Downstate Medical Center, **Fonar Corporation, Melville, NY, ***UCLA School of Medicine

A new technique to image the carotid artery has been developed that allows direct imaging in a single plane without reconstruction of several images. Imaging along an oblique angle has enabled us to directly examine the artery from the common carotid through the bifurcation into the internal and external carotids. Blood flow within the carotid is seen throughout the entire length of the vessel. The clinical applications of this method will be demonstrated in terms of the visualization of the anatomy of the carotid artery as well as the dynamics of blood flow. Applications of this technique to other structures will also be discussed.

A METHOD FOR IMAGING BLOOD VESSELS BY PHASE COMPENSATED/UNCOMPENSATED DIFFERENCE IMAGES

Leon Axel, Ph.D., M.D. and Daniel Morton, M.S.E.E.

Department of Radiology, Hospital of the University of Pennsylvania, Philadelphia, PA 19104

Images of blood vessels in tissues can be made that isolate the moving blood by utilizing either the time-of-flight effects of saturated or excited spins moving into or out of the imaging region or by the phase shifts acquired by excited spins moving along the magnetic field gradients used in imaging. These phase shifts can be seen either directly, with phase sensitive image reconstruction techniques, or indirectly, as a decrease in signal due to partial cancellation of the signal from spins with different phases (corresponding to different velocities) within a given picture element. Subtraction of conventional (magnitude) gated images made during cardiac systole and diastole has been proposed as a means of utilizing this indirect effect of motion-induced phase shifts.

We here report an alternative method of utilizing this phase shift produced intensity variation, that does not require gating. A conventional imaging pulse sequence is modified by adding additional magnetic field gradient pulses that cancel out the affects of constant velocity on phase, thus increasing the signal from moving blood. When a conventional image, made with a pulse sequence that is otherwise identical but lacks the compensating gradient pulses, its subtracted from the motion-compensated image, the stationary structures will be subtracted away, leaving the moving blood. This technique has been implemented for projection imaging. The signal data for the compensated and uncompensated images are acquired in a interleaved manner so as to avoid registration errors in the subtraction step.

Images of phantoms with flow through tubes have been successfully obtained with this technique and preliminary clinical studies are underway.

THE USE OF FLOW RELATED COLOR OVERLAYS IN THE EVALUATION OF VENOUS THROMBOSIS BY MAGNETIC RESONANCE IMAGING

William A. Erdman, M.D., Pat McNamee, M.S., Jeffrey C. Weinreb, M.D., Ronald M. Peshock, M.D.

University of Texas Health Science Center, Southwestern Medical School, Dallas, Texas

A post acquisition image processing algorithm was developed which generates a color overlay based on flow related phenomena in magnetic resonance images. T1 weighted and T2 weighted images, as well as phase images were recorded at .35 Tesla using multislice multiecho spin echo technique without EKG or respiratory gating. The post acquisition image processing assigned a color value to those pixels in which even echo rephasing phenomena occurred. In the final product, the magnitude image appeared in the usual grey scale; however, flowing blood appeared as red. This was helpful in clinical evaluation for possible venous thrombosis. In our previous clinical experience in 13 patients with known venous thrombosis, flow related artifacts within, around, or behind the clot were present in every instance. In addition, flow related signal sometimes mimicked the appearance of venous thrombus in normal vessels. The flow artifact varied from high signal to no signal and in certain instances, it was difficult if not impossible to distinguish from the thrombosis itself.

We performed magnetic resonance imaging on five animal external jugular veins in which thrombosis had been electrostatically induced in the laboratory. Evaluation of MRI studies in comparison with venograms and histologic section showed similar flow related artifacts to those seen in humans. Serial examinations revealed that flow changes were indicative of recanalization of thrombus. This was the only finding which seemed to change with the age of the clot.

The flow related color overlays were helpful in distinguishing between signal from flowing blood and the clot itself. In addition, changes within the clot due to recanalization may be better appreciated by the use of this algorithm.

MR ANGIOGRAPHY

C. L. Dumoulin and H. R. Hart Jr.

General Electric Corporate Research and Development Center, PO Box 8, Schenectady, New York 12301

Magnetic Resonance is a multi-faceted phenomenon which can be used to solve a variety of problems in clinical imaging. One such application is the use of certain characteristics of nuclear spins to obtain "angiographic" projections of blood vessels. With an appropriate experiment images of only those spins which have macroscopic motion can be obtained. In theory, spins which have not experienced macroscopic motion can be suppressed, although in practice total suppression is difficult due to the overwhelming abundance of stationary spins.

A pulse sequence which generates images of only moving spins will be presented. This experiment overcomes several limitations of other flow methods. Data are presented in a projection format similar to that of Digital Subtraction Angiography. In addition, arteries and veins can be visualized without the use of contrast agents. Suppression of non-moving spins is complete enough to allow a large dynamic range in the intensity of the imaged vessels.

Applications of this experiment include visualization of the vessel structure within any region of anatomy. Images of the neck and head will be presented. In these images the carotid arteries, jugular veins, straight sinus, sagittal sinus and other structures are easily visible.

VELOCITY AND ACCELERATION DESENSITIZATION IN 2DFT MR IMAGING

P. M. Pattany, M.Sc., R. Marino, B.S.C.S., J. M. McNally, Ph.D.

Picker International, Cleveland, Ohio

In the past, many different methods have been employed for slow flow velocity quantification using MR imaging. Material flowing through a field gradient experiences a phase shift linearly dependent on its flow velocity. At high flow velocities, there is severe loss of signal and artifacting due to turbulence, accelerative flow, and view to view variation in flow rate. As a result, erroneous phase maps are obtained.

In the conventional spin echo sequence, the echoes are formed for both frequency encoding and slice selection, flowing material in any of these directions will be phase shifted. If the flow is constant, then a constant phase term is introduced in the phase encoding, but if there is turbulence, accelerative flow and view to view variation in the flow rates, then this random phase change is seen as random noise in the phase encoding direction of 2DFT acquisition. These random phase shifts may be refocused with a second echo by even echo rephasing, but the echo times are particularly long and the RF deposition into a patient is high.

The technique described overcomes these difficulties. A gradient echo sequence has been designed using a computer simulation, where the term X(t) has been expanded into its power series

$$\phi = \int G(t)\, x(t)\, dt$$

$$\text{where } x(t) = x_o + \frac{\dot{x}\cdot t}{1!} + \frac{\ddot{x}\cdot t^2}{2!} + \ldots\text{etc.}$$

and each integral of the power series, up to the second order, has been brought to zero for a given frequency encode and slice selection gradient. Velocity or acceleration phase encoding is then achieved by amplitude scaling suitable sections of the gradient profiles; again this profile is obtained by making either the first or second order term in the above power series nonzero to sensitize velocity or acceleration phase encoding respectively. The residual phase shifts remaining in the images, attributed by imperfect flow rephasing, RF inhomogeneities and main field inhomogeneity, are removed constructing phase difference maps with and without velocity or acceleration modification, leaving phase shifts due entirely to motion in the selected direction.

The above effect has been presented both in vivo and in vitro. These studies include sequence calibration, phantom studies to determine technique accuracy and a variety of in vivo blood flow measurements including aortic and pulmonary flow imaging. Comparisons are presented among images obtained with conventional sequences and those obtained with the new technique.

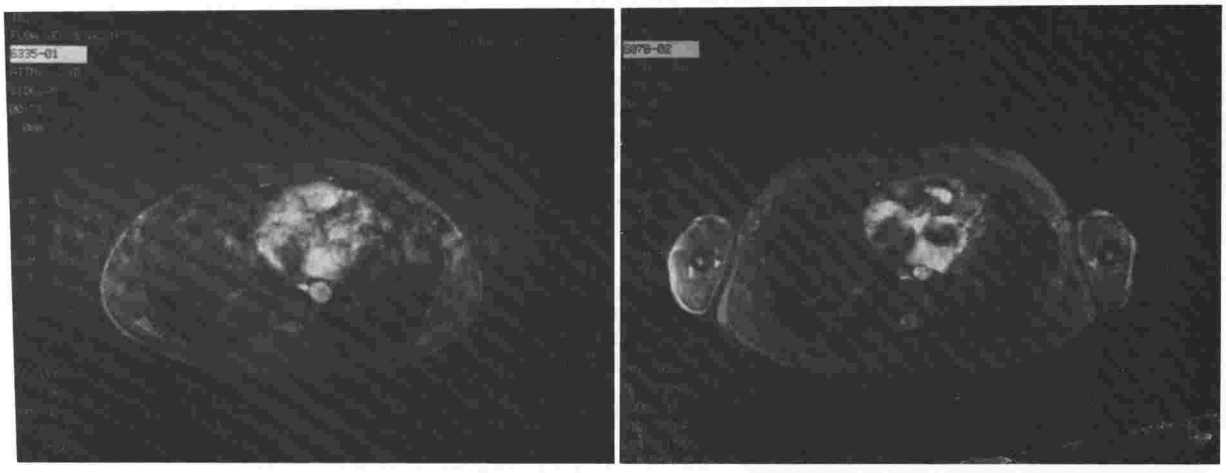

DESENSITIZED / UNGATED

COPE / CARDIAC GATED

REFERENCES

1. P.R. Moran, "A Flow Velocity Interlace for NMR Imaging In Humans," Mag. Res. Vol. 1, Pgs. 197-203 (1982).
2. D.J. Bryant, J.A. Payne, D.N. Firmin, and D. B. Longmore, "Measurement of Flow with NMR Imaging Using a Gradient Pulse and Phase Difference Technique", J.CAT Vol. 8, No. 4, Pgs. 588-593 (1984).
3. T.W. Redpath, D.G. Norris, R.A. Jones, and J.S. Hutchson, "A New Method of NMR Flow Imaging", Phys. Med. Biol. Vol. 24, No. 7, Pgs. 891-898 (1984).
4. K.J. Packer, "The Study of Slow Coherent Molecular Motion by Pulsed Nuclear Magnetic Resonance", Molecular Phys., Vol. 17, No. 4, Pgs. 355-368 (1969).
5. V. Waluch and W.G. Bradley, "NMR Even Echo Rephasing In Slow Laminar Flow", J. CAT, Vol. 8, No. 4, Pgs. 594-598 (1984).

A:137.
(12/09/85)

MULTISLICE MRI ANGIOGRAPHY

Graham L. Nayler[+] and David N Firmin*

[+]Advanced Development Group
Picker International Ltd
P O Box 2, East Lane, Wembley
Middx. HA9 7PR, U.K.

*Magnetic Resonance Unit
National Heart and Chest Hospitals
30 Britten Street
Chelsea, London SW3 6NN, UK.

NMR Imaging may be used as a completely non-invasive angiography technique. As opposed to conventional X-ray angiography, no external contrast media are required; consequently MRI angiograms may be obtained with the minimum of patient discomfort and preparation.

Contrast is developed by exploiting the phase shift on the NMR signal developed when protons move through a field gradient echo, which results in phase cancellation and low signal intensity from flowing blood. Gradient profiles have been developed which enable imaging of flowing blood without this accompanying phase shift. Consequently, images obtained with these profiles show flowing blood as regions of high signal intensity. Subtraction of conventional images from those taken with these profiles yields angiograms of patient blood vessels alone.

Conventional slice-selection offers the advantage of localising the NMR angiogram within a user-defined slice. Single broad slices are used to obtain angiograms of selected regions of interest. Alternatively, higher resolution in the slice-select direction may be obtained by using multislice techniques to acquire several thin-slice angiograms simultaneously. Images may then be processed further to construct thick-slice angiograms over different regions of interest, with no further acquisition required.

Acceptable multislice angiograms of relatively immobile vessels may be obtained without the use of cardiac gating. Multislice angiograms of the neck region are readily obtainable by this method in less than 8 minutes scanning. Cardiac gating is required to freeze the motion of more mobile vessels, and is used to study the coronary circulation.

The images below are from a 8 x 7mm multislice sequence acquired on a standard 0.5T Picker imager.

Flow refocussed image

7mm Angiogram

56mm Angiogram constructed from all 8 slices

CINE MAGNETIC RESONANCE BLOOD FLOW IMAGING IN CLINICAL USE

DB Longmore, DN Firmin, GL Naylor, SR Underwood, RH Klipstein

The National Heart and Chest Hospitals, and Picker International, London, UK

Magnetic resonance blood flow imaging techniques have not previously been sufficiently fast or reliable for routine clinical use. We describe the application of a technique that provides information of clinical value in a wide range of blood vessels and cardiac chambers.

A field echo sequence with even echo rephasing was used to produce images of flow velocity in each of the three perpendicular directions with respect to the imaging plane. The images were acquired in cine mode with a temporal resolution of 50 milliseconds, and a total acquisition time of approximately 10 minutes. The sensitivity of the technique was altered to show flow in veins, arteries, or cardiac chambers within the range 0 to 130 cm/sec. Comparison was made with range gated doppler ultrasound flow imaging in surface vessels, including the internal carotid and femoral arteries, and the two techniques showed the same timing of peak forward and reverse flow rates, and the same mean flow rates (Figure 1). Some differences were seen however because of the different conditions under which the measurements were made. Flow measurements of left and right ventricular output were also made on the ascending aorta and pulmonary artery, and were similar to measurements made from left and right ventricular volumes at end diastole and end systole (Figure 2). Backflow in the ascending aorta was seen in diastole allowing an indirect measurement of coronary artery flow. Within the cardiac chambers, flow patterns were seen corresponding to filling and emptying, and initial observations on patients with mitral and aortic regurgitation are encouraging.

Magnetic resonance flow measurements are reliable, fast, and accurate and will be of value in patients with a wide range of disorders of the cardiovascular system.

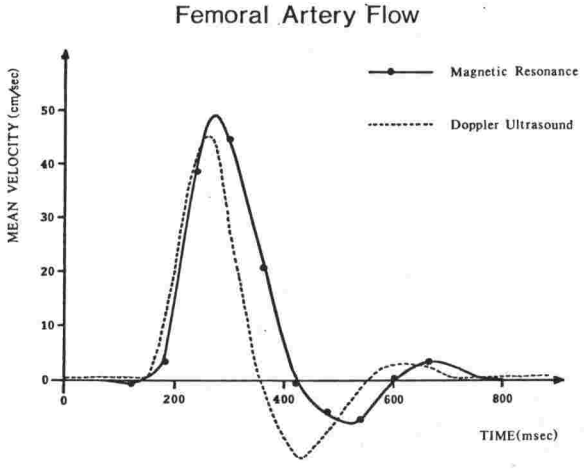

Fig.(1)

Mean velocity versus time for flow in the Femoral Artery as measured by Magnetic Resonance and Doppler Ultrasound.

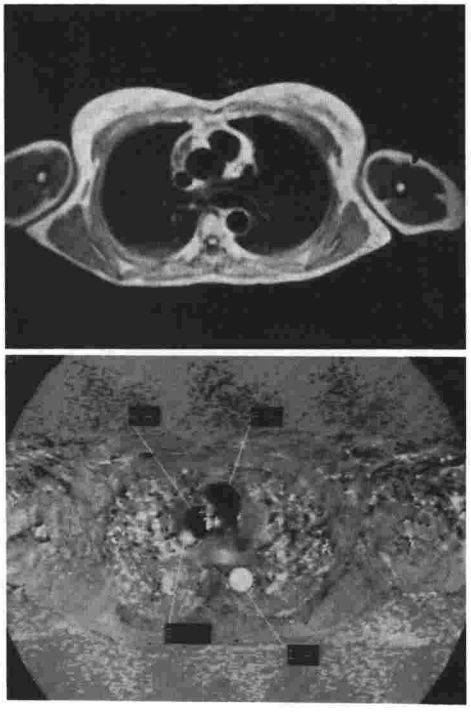

Fig.(2)

(a) Transverse section through the Ascending Aorta (AA) and Pulmonary Artery (PA) and (b) Phase Map of the same section with flow encoded at right angles to it. Flow up the body in the AA and PA is black and flow down in the DA and SVC is white.

INITIAL STUDIES OF PORTAL VEIN FLOW USING THE SELECTIVE SATURATION RECOVERY SPIN ECHO (SSRSE) METHOD IN COMBINATION WITH CARDIAC GATING

P. Schmalbrock, W. Hunter, A. Masaryk, F. Cornhill, S. Stiving, E. Herderick. The Ohio State University, Columbus, Ohio. F. Wehrli, A. Shimakawa, The General Electric Company, Milwaukee, Wisconsin

Knowledge of flow in the portal vein could significantly contribute to the assessment of patients with hepatic disease. Yet, this "hidden" vascular compartment remains inaccessible to all but the most invasive techniques of modern medicine. Although the venous flow is less pulsatile than arterial flow, significant velocity variation occurs during the cardiac cycle. Despite the trend of many investigators to assume steady state flow in the venous system cardiac gating would seem to be indicated for portal vein flow measurements. While standard multi-spin-echo pulse sequences provide qualitative information about the flow, the selective saturation recovery spin-echo method (SSRSE) enables quantification of velocity.[1,2] This method, which utilizes time of flight washout effects, consists of two selective 90° pulses followed by a selective 180° rephasing pulse. Protons flowing through the imaging slice are initially excited by the first 90° pulse. During the interpulse time (TI) between the 90° pulses these tagged protons are partially replaced by unexcited protons depending on velocity (v) and slice thickness (d). Since, in whole body imaging systems, spin-echoes rather than free induction decays are acquired, the two 90° pulses are followed at TE/2 by the selective 180° pulse. The resultant signal intensity (I) is a composite of the magnetization of tagged and untagged protons. For plug flow perpendicular to the imaging plane the relative intensity can be calculated from:

$$I = \begin{cases} [(V/d)TI + (1 - (V/d)TI\ (1 - \exp(-TI/T1)]\ (1 - (V/d)/(TE/2))\ \exp(-TE/T2) & \text{for } 0 \leq V \leq d/TI \\ [1 - (V/d)\ (TE/2)]\exp(TE/T2) & \text{for } d/TI \leq V \leq d/(TE/2) \end{cases}$$

Therefore, the velocity can be calculated from images perpendicular to the flow direction obtained at different interpulse times.

Sagittal images were acquired with a 500 msec delay following the QRS trigger signal. These images of 1cm slice thickness were obtained with five different TI. Figure 1 shows the relative pixel intensities at the center of the portal vein as a function of the interpulse time. From this curve a preliminary value for TI = 78 ± 25 msec at the turn over point can be obtained. This results in a velocity V = 13 ± 4 cm/sec at the center of the portal vein.

A more detailed analysis of the data including the calculation of velocity profile curves is in progress.

1.) F. W. Wehrli, J.R. MacFall, L. Axel, D. Shutts, G.H. Glover, R.J. Hertkins. Noninvasive Medical Imaging (1984) 127.
2.) F.W. Wehrli, A. Shimakawa, J.R. MacFall, L. Axel, W. Perman. Journal of Computer Assisted Tomography 9 (1985) 537.

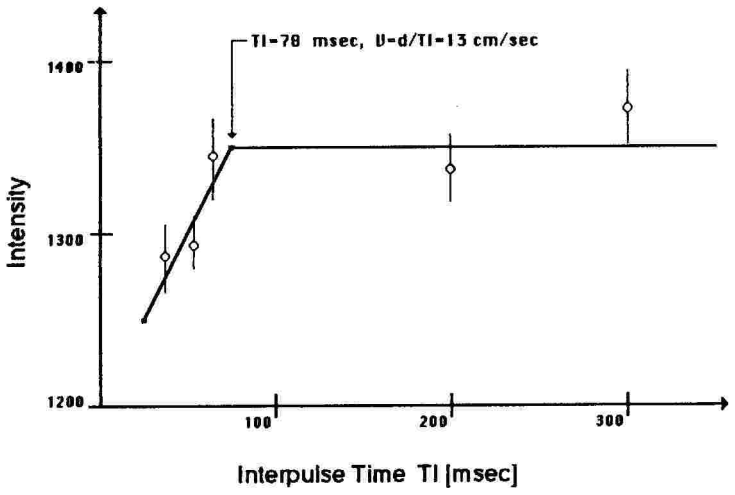

Figure 1: Relative Intensity for the center pixel in the portal vein as a function of the SSRSE interpulse time

MRI OF THE VASCULAR STRUCTURES ABOUT THE BRAINSTEM AND CEREBELLUM

Donald W Chakeres MD, Vicky Marcs MD, Kenneth Weiss MD, James Mosure MD

Ohio State Univerity College of Medicine ,Columbus, Ohio

High resolution MRI can visualize many small blood vessels about the brainstem and cerebellum with much greater frequency than CT. Using a General Electric Signa MRI scanner we were able to routinely identify most of the small vascular structures commonly seen on standard clinical cerebral angiography. All of the images were made with a General Electric 1.5 tesla Signa system. We review the MRI appearance of the following vessels as seen on varying pulse sequence images (spin echo and partial saturation techniques utilizing TR's ranging form 200-2500 msec,TE's 25-160) and section planes (axial,sagittal,coronal): basilar, vertebral, superior cerebellar, posterior cerebral, posterior communicating, and chorodial arteries; and the precentral cerebellar, lateral mesencephalic, basal veins of Rosenthal, cerebellar vermian veins. Direct comparison to standard angiograms on the same patients was avaiable in a large number of cases. We discuss the variable signal intensities visible on images of the same vessel related to flow dynamics. The clinical significance of understanding the normal anatomy of these venous structures includes: mass localization, arteriovenous malformations (AVM) evaluation, occlusive vascular disease, and separtion of venous from arterial structures. One major limitation is the absence of a vascular blush as is seen in standard agiography. IF MRI can accurately visualize the small vessels of the posterior fossa, then it is conceivable that MRI can have a major impact on angiography.

HIGH RESOLUTION MAGNETIC RESONANCE IMAGING OF THE LIMBIC SYSTEM

Donald Chakeres MD, Eric Flynn MD, and Kenneth Weiss MD

Ohio State University College of Medicine , Columbus , Ohio

The limbic system is composed of a ring of multiple gray and white matter structures that encircle the brainstem. The limbic system is felt to be important in disorders of smell, memory, behavior, emotion, and movement. MRI can visualize many of the individual structures forming the limbic system with much greater accuracy than CT. We describe the normal and pathologic anatomy of the hippocampus, dentate gyrus, columns of the fornix, mammillary bodies, stria terminalis, amygdala, uncus, cingulate gyrus , cingulum , and anterior commissure. It is believed that the limbic system acts as an interface between primitive homeostatic functions of the brainstem - hypothalamus and the cerebral cortex. CT has limited ability to identify abnormalities of the limbic system. Many of the structures simply cannot be consisitently visualized. The limbic system is one anatomic area where MRI has the potential to significantly expand the understanding of pathology involving this complex group of structures. Comparison of high resolution MRI images of normal and pathologic patients , and fixed cadaver brains to anatomic sections of normal brains sectioned in the same planes were made. All of the images were made with a General Electric Signa 1.5 Tesla imager. Multiple axial, sagittal, and coronal thin section (3-5mm) high resolution (8-20 cm field of view 256x256 pixel matrix) images using multiple spin echo techniques were made. The appearance and intensities of the components of the limbic system on multiple section planes and pulse sequences are reviewed. Examples of pathologic distortion of the limbic system are shown, including: mass lesions, congenital abnormalities, brain atrophy, and hydrocephalus.

MAGNETIC RESONANCE IMAGING IN CYSTICERCOSIS OF THE CENTRAL NERVOUS SYSTEM

H. Pribram, H. Fritts, D. Katz, R. Friedenberg

University of California, Irvine

Cysticercosis of the brain may be parenchymal, intraventricular, or cisternal. Spinal cysticercosis is relatively rare. We have had the opportunity to examine several patients with both CT and MR. CT findings in intraventricular cysticercosis have frequently required confirmation by metrizamide ventricululography whereas MR detects the cyst within the ventricle. In addition, we have noted that the scolex is frequently visualized within a cyst on MR. We feel that MR is superior to CT in detecting edema in active cysticercosis and that MR may help monitor the effect of praziquantel therapy.

MRI OF THE HEAD IN PATIENTS WITH TUBEROUS SCLEROSIS

H. Fritts, D. Katz, H. Pribram, R. Friedenberg

University of California, Irvine

Tuberous sclerosis is the most common of the neurocutaneous syndromes seen by pediatric neuroradiologists. In the brain the disease is characterized by hemartomatous glial deposits in the cortex and subependymal areas. Those in the latter eventually calcify and it is the calcification of the subependymal nodules that make up the characteristic CT picture. Because most of the nodules are small, projecting into the ventricles an average of 5 mm or less, they are hard to see on conventional CT when not calcified. Therefore, a negative CT examination, especially in an infant, does not rule out the diagnosis. Areas of focal demyelination in the brain have also been reported, which are not always appreciated with conventional CT.

The inherent advantages of MR imaging have been established with its lack of ionizing radiation which is of special interest in imaging infants and children. Superior spatial and contrast resolution, as well as the ability to image directly in three planes, makes MR imaging potentially ideal for visualization of non-calcified subependymal nodules and areas of demyelination which may not be appreciated with conventional CT.

To our knowledge there have been no reports of MR imaging of patients with tuberous sclerosis. MR imaging of the head will be reported in at least ten patients with either documented tuberous sclerosis or familial history of tuberous sclerosis. Most of these patients have had conventional CT examinations. Those with positive CT exams will be compared with the MRI findings. In these patients, as well as those with negative CT examinations, the MRI studies will be evaluated for any findings which may lead to an earlier diagnosis of CNS involvement.

MAGNETIC RESONANCE IMAGING OF THE POST-THERAPY BRAIN: DIFFERENTIATING RADIATION FIBROSIS OR SURGICAL CHANGES FROM RECURRENT INTRACRANIAL TUMOR

Shelly P. Baumann, M.D.; Brian P. Cornnell, M.D.; F. Reed Murtagh, M.D.

University of South Florida College of Medicine

Twenty four patients who had various forms of cerebral neoplasms and one with a malignant lacrymal gland tumor underwent radiation therapy either with or without surgery, and had followup ranging from 6 months to 9 years. Magnetic resonance images of the brain in these persons were obtained in an attempt to find some parameters to answer the age-old question of how to distinguish tumor recurrence from surgical changes from radiation necrosis. In addition to MRI tissue parameters, traditional factors such as evolution over time and presence of mass effect must be factored in. At the present stage of development of MRI knowledge, it appears as if the differential diagnosis is still difficult but MRI holds promise, especially with use of paramagnetic contrast agents.

MR IMAGING OF THE BRAIN: A CLINICAL COMPARISON OF HYBRID™ FAST-SCAN IMAGING WITH STANDARD 2DFT DATA ACQUISITION

Paul E. Coleman, M.D., Picker International, Cleveland, Ohio
Errol M. Bellon, M.D., Case Western Reserve University, Cleveland, Ohio

Clinical evaluation of the Hybrid™ fast scan techniques[1,2] has been carried out for MR imaging of a variety of clinical indications in the brain. Spatial and contrast resolution using this method is compared with standard 2DFT data acquisition techniques.

Because of the long scan times associated with MR imaging, a great deal of interest in fast scan techniques has been generated[1,2,3]. It has been shown that T2 weighted images are superior to T1 weighted images in providing lesion to normal tissue contrast in many cases[4]. Many fast scan techniques provide rapid acquisition by shortening the repetition time (TR) which reduced T2 weighting. There is a need for a fast data acquisition technique which provides T2 weighting while maintaining good spatial resolution. Hybrid™ fast scanning has been demonstrated to have these capabilities[1,2]. Clinical evaluation of this technique is currently underway and preliminary results are presented here.

Studies were performed on a Picker Vista ™ MR superconductive scanner operating at .5T using a standard 30cm head receiver coil. Patients referred for MR imaging of the brain presenting a variety of clinical indications were included in this preliminary clinical evaluation of Hybrid™ imaging. Patients were imaged using a standard 2DFT spin echo(TR2000 TE80)pulse sequence in the transverse, sagittal, or coronal plane followed by a comparable Hybrid™ sequence with TR2000, TE80. Additional standard sequences were performed as indicated by the patients' clinical condition.

The 2DFT images were acquired using two excitations and a 256 x 256 matrix for a total scan time of 17 minutes. Hybrid™ image acquisition for a two excitation, 128 x 256 data matrix was 4.3 minutes. Future hardware upgrade will allow acquisition of T2 weighted images with a 256 x 256 data matrix in one-fourth the time of standard techniques.

Images of the same lesion obtained using Hybrid™ fast scan and standard 2DFT techniques are shown in Figure 1. Hybrid™ technique shows a substantial increase in tissue T2 contrast when compared with standard technique. This increase in contrast can be used to further decrease imaging time through use of shorter TR values or it can increase clinical sensitivity with unchanged repetition times. The S/N obtained with Hybrid ™ imaging is somewhat decreased from normal, however, Hybrid™ imaging tends to distribute noise more evenly over the image and is less sensitive to motion.

In summary, preliminary clinical results indicate that Hybrid™ imaging provides for fast data acquisition while maintaining the high T2 tissue contrast required for lesion detection in MR imaging of the brain.

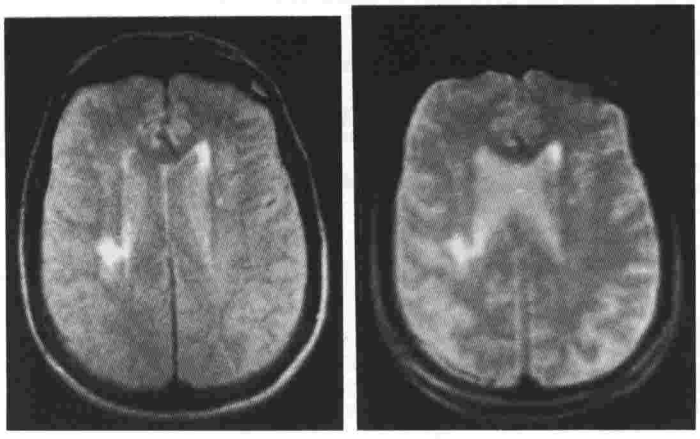

a b

FIGURE 1.

Demyelinating disease in the right periventricular region imaged with a) 2DFT TR2000 TE80 and b) Hybrid™ fast scan technique TR2000 TE80.

REFERENCES:

1) Haacke EM, Clayton JR, Linga NR, Bearden FH. Reduction of MR Imaging Time by Hybrid Fast-Scan Technique, accepted for publication in Radiology.

2) Haacke EM, Clayton JR, Linga NR, Bearden FH. Demonstration of a Flexible Fast-scan Technique. Radiology 1984; 153(P):244.

3) Haase A, Frahm J, Matthaei D, et al. Proc. SMRM Meeting, P. 980, London (1985).

4) Smith AS, Weinstein MA, Modic MT, et al. Magnetic Resonance with Marked T2-weighted Images: Improved Demonstration of Brain Lesions, Tumor and Edema. AJR 1985; 145:949-955.

POSTER AND PRESENTATION

THE ROLE OF MRI IN THE MANAGEMENT OF INTRACRANIAL ANEURYSMS

M.H. Johnson, M.D., G.J. DeFilipp, M.D., R.H. Rosenwasser, M.D., T.H. Liu, M.D., C.G. Drake, M.D., A.J. Macones, Jr., M.D., W.A. Buchheit,M.D., and J.A. Kenning, M.D.

Temple University Hospital

The Role of MRI in the Management of Intracranial Anerysms

The definitive imaging modality for the evaluation and follow-up of intracranial aneurysms and vascular malformations has remained arteriography despite the advent of newer modalities for intracranial imaging. CT scanning has been adjunctive in management as it is capable of demonstrating aneurysms plus associated hemorrhage and intramural calcifications. We have found MRI with its capacity to demonstrate differences between flowing blood and thrombus as signal intensity differences to be useful in the evaluation and follow-up of certain vascular lesions. Imaging on all cases was performed on a Fonar 0.3 Tesla Mobile MRI unit.

An illustrative case is presented in Figures 1 and 2. The patient was a thirty-eight year old man with ataxia. A CT scan demonstrated a giant basilar trunk aneurysm confirmed by angiography. MRI (Figure 1) with a spin echo sequence of TE 56, TR 2000 demonstrated the aneurysm with a thick wall and central flow. Surgical exploration was performed and a Drake tourniquet placed on the proximal basilar artery creating an angiographically confirmed 90% basilar artery stenosis. Repeat MRI (Figure 2) the same spine echo sequence demonstrates almost complete thrombosis of the lesion with only a small residual lumen.

The capacity of MRI to demonstrate thrombosis is particularly useful in the giant aneurysm situation where an attempt to induce thrombosis rather than clipping is the therapy of choice. Similar results have been identified in a case where arteriographic balloon occlusion of the carotid was utilized for the promotion of thrombosis in a non-clippable carotid cavernous aneurysm.

In patients with associated AVM's and aneurysms which have hemorrhaged, MRI is useful in the evaluation of thrombosis within the aneurysmal component, the usual site of bleeding. In the more usual saccular aneurysms, MRI may demonstrate both the aneurysm and the presence of complete or incomplete thrombosis post hemorrhage. We are currently prospectively evaluating our patient population with documented subarachnoid hemorrhage and negative arteriography to evaluate our capacity for demonstrate thrombosed aneurysms which thrombosed after hemorrhage.

THE ROLE OF MRI IN THE MANAGEMENT OF INTRACRANIAL ANEURYSMS

M.H. JOHNSON, M.D.,et al

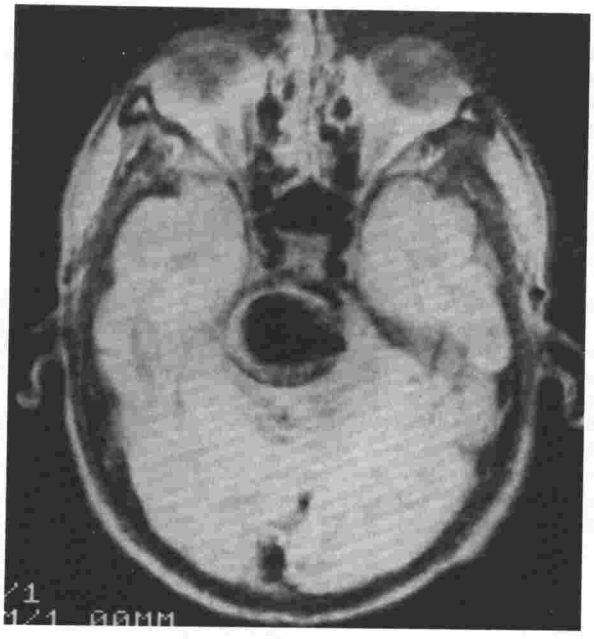

Figure I

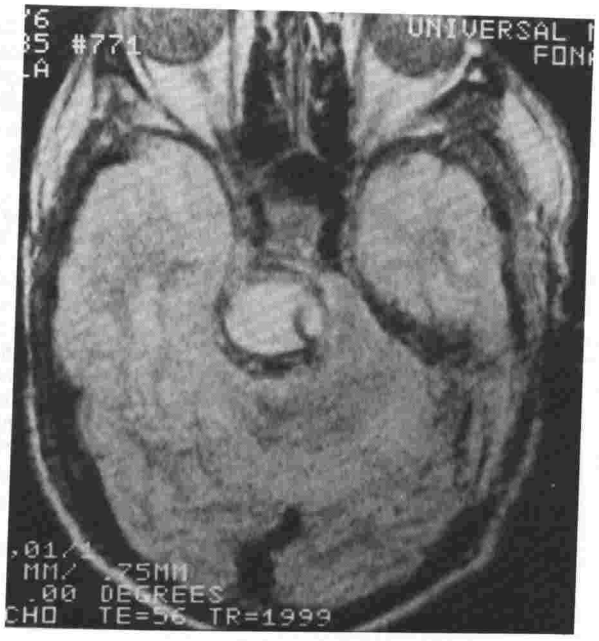

Figure 2

MAGNETIC RESONANCE IMAGING OF THE EXTRATEMPORAL FACIAL NERVE: ANATOMIC CORRELATION

Kolin E, Teresi L, Lufkin R, Wortham D, Ward P, Hanafee W

Mount Sinai School of Medicine(EK), UCLA School of Medicine(LT,RL,DW,PW,WH)

Cryosection specimens of fresh human cadavers were compared with MR images from normal volunteers. The seventh nerve was followed from the stylomastoid foramen through the parotid bed. Five normal volunteers and 15 patients with pathology involving the parotid gland and extratemporal facial nerve were studied with a 0.3 Tesla permanent magnet MR system. Images were obtained with surface coils using various 2D-FT spin echo pulse sequences. 5mm thick sections with 0.5 mm pixels on a 512 x 512 acquisition matrix were used whenever possible.

Visualizing the main trunks of the facial nerve required special scanning planes, using scout images for optimal localization. 30-35 degree obliques from the axial plane were best for defining the main facial nerve trunks for most parotid gland pathology. The nerve appeared as a low signal structure surrounded by high signal fat and parotid gland parenchyma. It is important not to mistake low signal vessels which course medial to the retromandibular vein or truncation errors for the facial nerve. MRI produces excellent images of the extratemporal facial nerve, allowing visualization of the main trunks of the facial nerve in the parotid bed not possible with any other imaging technique.

THE MRI APPEARANCES OF CYSTICERCOSIS AT 0.6 T.

F.W. Smith, H. Fritts, H. Pribham, R. Friedenberg.

Department of Radiological Sciences, University of California, Irvine.

The larval form of the pork tapeworm (Taenia Solium) affects man as its intermediate host, when the larvae lodge in the central nervous system they may cause a variety of presenting signs and symptoms. They may be found in the subarachnoid space where they present as meningitis, in the ventricular system where they may cause obstructive hydrocephalus or in the cerebral parenchyma where they may cause seizures or mental deterioration.

The X-Ray CT appearances of these larval cysts are well recognised and depending on their stage of development appear as either iso dense with C.S.F., or hypo dense cystic lesions in the ventricular system or parenchyma. They have irregular margins which enhance with intravenous contrast injection. When the larvae die, calcification occurs and they are recognised as central calcification, that represents the scolex, surrounded by a curvilinear calcified band.

The MRI appearances have not been described. Using Spin-echo sequences, intra ventricular cysts are iso intense as C.S.F. when both short and long TR values are used. The cyst wall is best seen using a TR = 2000, TE = 45 double echo sequences where the wall and any surrounding oedema is adjacent parenchyma is best demonstrated with the second echo. The scolex is visualised with all sequences but best with the first echo. Parenchymal cysts display a similar appearance, but because of their situation within the brain, the cyst wall is more clearly seen with the first echo and any surrounding oedema with the second. The scolex is best seen with the first echo and with short TR = 500, TE = 35 sequences.

DYNAMIC RANGE COMPRESSION IN SURFACE COIL MRI

Sharples T, Lufkin R, Flannigan B, Hanafee W

FONAR Corporation(TS), UCLA School of Medicine(RL,BF,WH)

The large dynamic range in signal intensity present in MR surface coil images makes proper windowing and photography difficult. By removing the low spatial frequency information due to variations in surface coil field intensity from the high spatial frequency information containing the image data a considerable compression of this dynamic range of signal intensity is possible.

A technique to accomplish this was implemented on a digital computer for use with MR surface coil image data. The compression was done as a post processing option after the patient scan had been completed and therefore did not alter actual scan times. Although the image signal to noise was not altered, the image quality and ease of photography for most images was improved. Thus, digital dynamic range compression is a practical technique to aid in surface coil MRI studies.

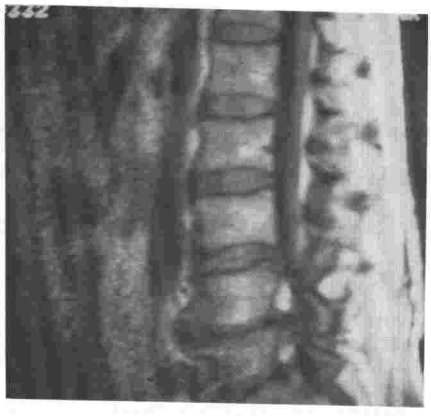

Fig. 1. Sagittal scan through the normal lumbar spine using a planar spine surface coil.

A) Windowed to demonstrate the spinal canal. (Window level=750 Window width=1800) This region is optimally seen at the expense of deeper and more superficial tissues.

B) Same scan as A following image intensity dynamic range compression (same windowing). Now all depths of tissue are fairly well seen and may be evaluated on one image.

SOLENOID SURFACE COILS IN MR IMAGING

Votruba J, Lufkin R, Reicher M, Bassett L, Smith S, Hanafee W

FONAR Corporation(JV,SS) and UCLA School of Medicine(RL,MR,LB,,WH)

A nonplanar solenoidal surface RF coil is used as a receiver with a conventional transmitter coil in a magnetic resonance imaging system. The improved signal to noise ratio, compared with conventional fixed saddle or solenoid receiver coils permits higher resolution imaging and thinner image sections. In addition, the problem of signal dropoff that occurs in deep structures with planar and other noncircumferential surface coils is eliminated. Solenoid surface coils are particularly useful in imaging deep structures in anatomic regions that do not fit standard head and body coils such as the neck, knees, and other smaller body parts.

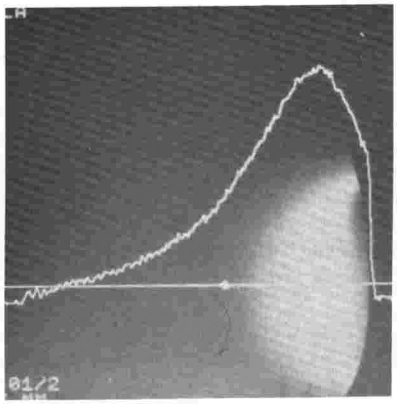

fig Comparison of signal detection of planar and solenoidal surface coils applied to a uniform 2.5 mM NiCl solution phantom. The curves are plots of signal intensity through the midportion of the phantom.

A) The 14 cm planar surface coil shows low noise and high superficial signal detection but rapid signal dropoff with increasing distance from the coil surface.

B) The 14.5 cm solenoid surface coil shows improved deep signal detection.

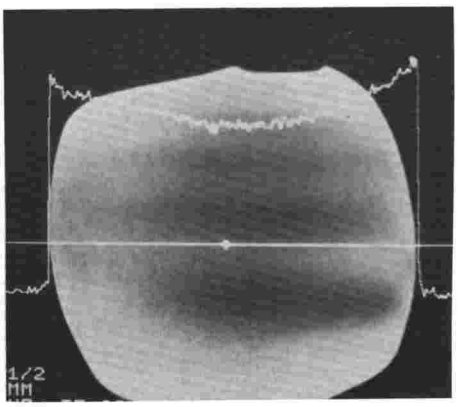

RF COIL DECOUPLING SYSTEMS FOR NMR SURFACE COIL IMAGING

George J. Misic, Dr. Gregory C. Hurst, Janice E. Hahn, Dr. John L. Patrick, and Dr. Charles Citrin*

Picker International, Cleveland, Ohio *Magnetic Imaging of Washington, Chevy Chase, Maryland

NMR systems using crossed coil probes generally depend upon orthogonal placement of two linearly polarized coil systems to provide the needed isolation between the transmit and receive coils. This is a workable technique for coil systems of a fixed geometry, such as body or head coil system. The problem of maintaining sufficient probe isolation is greatly complicated when the coil placement is not accurately controlled by the structure of the scanner. Such is the case with surface coils. In addition, the desired region of sensitivity and patient comfort constraints are restrictive of surface coil geometry, thus making the arbitrary selection of the coil polarization impractical in some situations.

The problem was addressed by creating an electronic means of eliminating the effects of coupling between the transmit coil system, in this case the whole body coil, and any other receive probe used within the scanner, irrespective of the orientation of the receive probe. During the sampling of the NMR signal, the transmit coil is electrically disconnected from the resonating capacitance; and the two halves of the saddle coil are electrically disconnected from each other. Thus, the coupling effects of the transmit body coil are eliminated, allowing the best possible sensitivity of the receive probe, and eliminating the problem of field distortion of the receive probe by the idler tank effect of a second coupled resonant circuit.

During the transmit portion of the NMR sequence, the receiver probe is decoupled by electronically destroying the resonance of the coil. Protection is also provided to the RF front end of the preamplifier to prevent damage caused by induced power reaching the preamp from the probe. Sufficient protection and decoupling exists to allow the receive probe to be oriented fully in line with the transmit field without adverse effects.

The hardware was evaluated under both phantom and human imaging conditions using a variety of surface coil types. Experiments were conducted to evaluate the interaction of the coil systems both from the standpoint of signal sensitivity and field shape. In all cases, the interaction of the coil systems was reduced to an undetectable level irrespective of receiver probe orientation.

SURFACE COIL IMAGING : OPTIMIZATION OF THE TECHNIQUES AND ITS CLINICAL APPLICATIONS

M.V. Kulkarni, S.D. Mehta, J.A. Patton, R.R. Price

University of Texas Health Science Center at Houston and Vanderbilt University Medical Center, Nashville, TN

Magnetic resonance imaging has been widely used in clinical practice. Recent development in surface coil (SC) technology has significantly improved the signal to noise (S/N) ratio which can be utilized to decrease the slice thickness and pixel size which ultimately leads to diminished partial volume averaging and improvement in the spatial resolution. Since multiple types of SC have been developed we need a method to determine the best type of SC to be used in an individual clinical setting and try to optimize spatial resolution by magnification techniques while keeping the imaging time to a minimum.

A flat phantom filled with a solution of propylene glycol was used to measure S/N ratios for each SC as well as for routinely used radiofrequency (RF) coils for head and body. Imaging parameters were constant and S/N ratios were plotted for each of the coils. Similarly S/N ratios were plotted for different pixel sizes and compared to S/N ratios obtained using routine pixel size. S/N Ratio was also studied as a function of scan averages and demonstrated improvement in S/N ratio with increasing number of averages. Using these graphs an objective method was developed to perform SC images in 150 patients. We will demonstrate the improvement in image quality after optimizing the imaging parameters using this technique when compared to conventional MR imaging. Magnification techniques to determine pixel size were developed according to the area of the body and the type of SC used.

We conclude that this technique, by using objective parameters, is extremely useful in selecting not only the appropriate degree of magnification, but also in choosing the SC. Imaging protocols can be developed using this method according to the organ system examined. Imaging time is also kept to a minimum leading to diminished patient discomfort and adequate image quality.

PLOT of S/N versus distances for various coils.

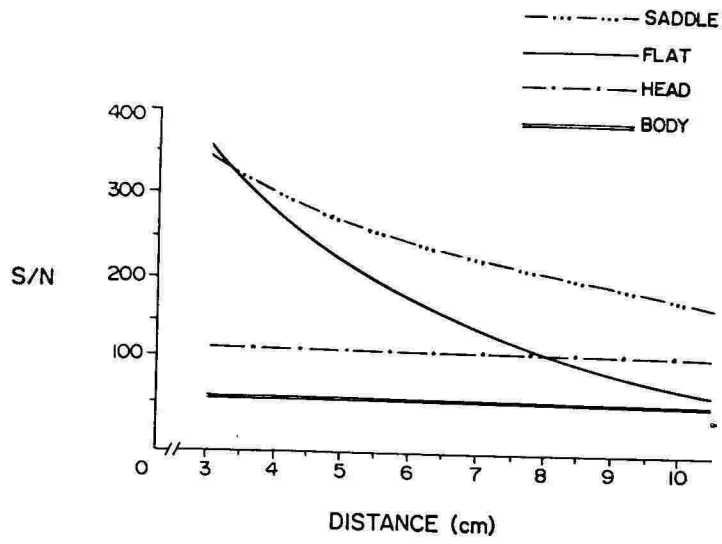

PLOT of S/N versus distance for varying degrees of magnification using surface coil (Saddle).

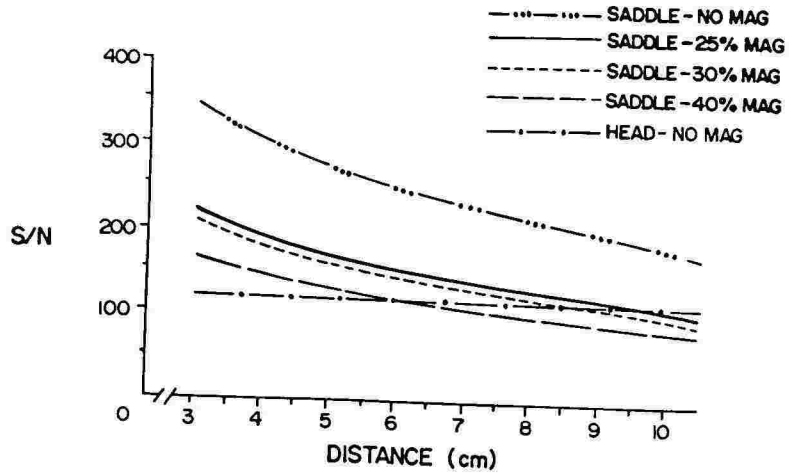

SPECIALISED RECEIVER COILS FOR A LOW FIELD NMR IMAGER

Thomas W. Redpath

Department of Bio-Medical Physics and Bio-Engineering, University of Aberdeen, Scotland.

INTRODUCTION

Small, closely fitting receiver coils have been developed to improve the signal-to-noise ratio, and hence image quality, for a number of regions of the body, such as the eyes, neck and limbs. The improved sensitivity is a result of the close coupling of the coil to the precessing magnetisation. The thermal noise at the coil terminals is the fundamental limit to image quality and has two components, one due to the coil itself, the other due to the patient. The noise due to the coil itself is independent of coil scale (1), but the noise introduced by the linkage of the coil to noisy eddy current loops in the patient is reduced as the coil is made smaller. For this reason it is important to design small specialised coils for low field imagers to have a high unloaded Q factor, as the coil itself will be the dominant noise source. The coils described here approximate a saddle configuration with the receive r.f. magnetic field horizontally across the patient. Images are presented from the Aberdeen 3.4 MHz proton imager.

COIL DESIGN

Initial trials with flat loops showed promise with tank phantoms, but their advantage was not realised in practice because they tend to stand off the curves of the body leaving a large gap. Since the depth response of a simple loop is poor, the gain in sensitivity was lost. The problem was overcome by taping wire coils on to close fitting thermoplastic formers which are made from plaster moulds using techniques developed in radiotherapy departments. Figures 1 and 2 show eye and knee coils as examples. The coils consist of two 3-turn sections of 2.6 mm diameter wire connected in series. The eye coil has an inductance of 3.3 μH with an unloaded Q factor of 370 at 3.4 MHz, dropping to 260 with a patient in position. The inductance of the knee coil is 6.0 μH with a natural Q of 460, dropping to about 320 on loading.

RESULTS

Figures 3 and 4 show 128 x 128 single slice saturation recovery images obtained in 128s with TR = 1s over a 180 x 180 mm field of view with a slice width of 8 mm. The eye image demonstrates sub-retinal haemorrhage causing retinal detachment. The knee image is normal. The coils are used in a crossed configuration with the solenoidal body coil which produces an r.f. transmit field along the patient. The static field is vertical. The coils would be suitable for conventional systems where the transmit and static field directions are interchanged.

ACKNOWLEDGEMENT

I thank Mr. J. McKirdy of the Radiotherapy Department, Aberdeen Royal Infirmary, for making the plastic formers.

REFERENCE

T.W. Redpath and J.M.S. Hutchison, 1982, Design of a radiofrequency coil suitable for NMR imaging of heads, Phys. Med. Biol., 27, p.443-447.

Fig. 1.

Fig. 2.

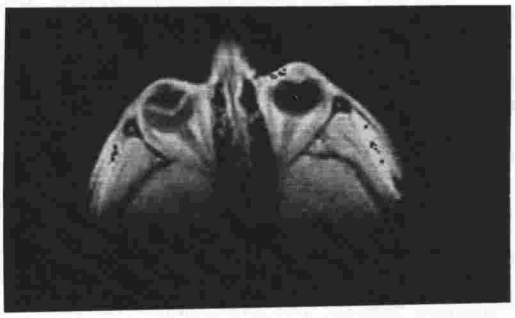

Fig. 3.

Fig. 4.

MULTIPLE FREQUENCY NMR PROBE DESIGN BASED ON FOSTER NETWORK PRINCIPLES

Wade Holcomb, John C. Gore and H. Dirk Sostman

Department of Diagnostic Radiology, Yale University School of Medicine, New Haven, CT 06510

We have reviewed the design requirements for coils for successful multi-nuclear in vivo NMR spectroscopy. The lack of true multinuclear probes constrains the range of applications of modern broadband spectrometers with digital control of radio frequency transmitters and receivers. Coil systems designed for simultaneous operation at several frequencies have previously been developed. Our chosen model follows the teaching of Ronald Foster [R.M. Foster-A Reactance Theorem. Bell System Technical Journal, 3:259-267 (1924)] for design of one port networks with multiple zeros and anti-resonant poles. Foster, in effect, stated that the input impedance of any one-port lossless network is completely specified by its internal poles and zeroes, and a scale factor, and proved the theorem showing that the poles and zeroes alternate along the frequency axis which is sometimes called the separation property. We will demonstrate that the zeroes can be set to several desired Larmor frequencies for relatively simple networks. Unfortunately the choice of component inductances are not all at the designers discretion.

For example, the probe inductance is largely pre-determined for the designer by its size and shape, but Foster's analysis shows how such constraints may be accommodated. Examples of the application of this will be presented including the construction of small animal and test tube probes for use in a 2.0 T spectrometer. A probe simultaneously tuned to protons, phosphorus and sodium has proven of particular interest for cells in culture.

THE RF-COIL AS A SENSITIVE MOTION DETECTOR FOR MRI STUDIED UP TO 2 TESLA

D. Buikman, T. Helzel, P. Röschmann

Philips GmbH Forschungslaboratorium Hamburg,
Vogt-Koelln-Str. 30, D-2000 Hamburg 54, FRG

Patient motion is still a major problem in magnetic resonance imaging leading to substantial loss of diagnostic image quality. Gating and triggering techniques have proven successful in reducing artifacts from respiratory and cardiac motion, although respiratory gating has the disadvantage of a longer measuring time. Recently, methods have been introduced in which the data acquisition mode is determined by patient motion, such as respiratory ordered phase encoding (ROPE) (1). These techniques do not increase the scan time and seem promising. In order to apply such methods a sensor is required to monitor the instantaneous position of the patient. For example a thoracic belt device with optical sensor has been successfully tested by us (2).

In this talk we show that the coil used for rf-transmission and detection is itself a sensitive motion sensor. Patient movement inside the rf-coil causes changes in the rf-impedance match: these can be measured as variations in the reflected rf-power. This method turns out to be very sensitive and even allows for the discrimination of signals from respiratory and cardiac movements: these two signals are obtained simultaneously by applying appropriate electronic filtering techniques. An additional feature is that both the period and the amplitude of the respiratory motion is determinable, thus enabling triggering or gating at an arbitrary state in the respiratory cycle, or applying a ROPE-like acquisition method.

An important advantage using this principle is that no sensors have to be connected to the patient. Furthermore, the sensor also detects non-periodic movements (such as swallowing), which can thus be excluded from the scan.

Fig. 1 compares a respiratory gated scan with an ungated scan of the liver of a volunteer, measured at 85 MHz (2 Tesla) using a ring-resonator body-coil (3). The applicability as a motion sensor has also been established for saddle coils in the range 20-65 MHz (0.5-1.5 Tesla). Fig. 2 shows a gated scan of a patient's liver at 2 Tesla.

Cardiac triggered images with this rf-sensor are not yet available because of the additional hardware effort required (time sharing between rf-transmission, rf-detection and continuous motion monitoring), but successful application for cardiac triggering has been presented from an optical belt-sensor (2), which has a similar response to patient motion as the rf-coil.

In conclusion, the use of the rf-coil as a motion detector results in an elegant and sensitive approach to reduce artifacts from patient motion in MRI.

(1) D.R. Bailes et al., Society of Magnetic Resonance in Medicine, Fourth Annual Meeting, London 1985, Book of Abstracts, p. 939.
(2) G. Martens, T. Helzel, J. Kordts, SPIE Symposium of Fiber Optic Sensors, Cannes, November 1985.
(3) P. Röschmann, SMRM Third Annual Meeting, New York 1984, Book of Abstracts, p. 634.

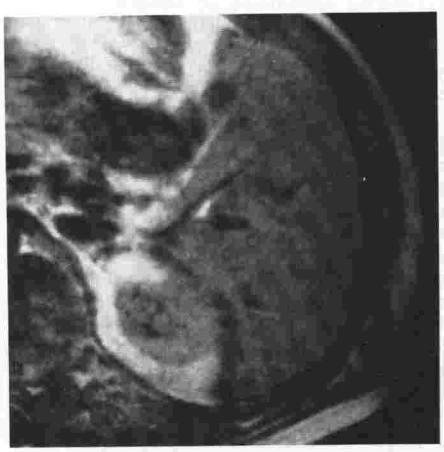

a)

b)

Fig. 1. a) Respiratory gated scan (SE, T_E = 30 ms, T_R = 800 ms, 1 average) of the liver at 2 Tesla, using the low-pass filtered reflected rf-signal for motion monitoring.
b) Ungated scan of the same slice (2 averages), approximately the same scan time as in a).

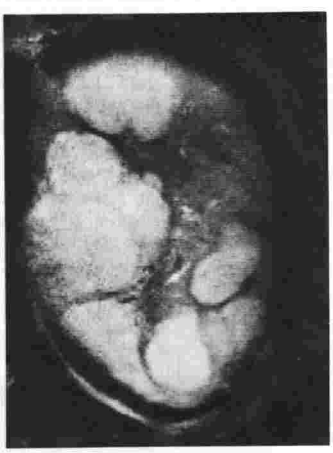

Fig. 2. Respiratory gated scan of a patient's liver at 2 Tesla. The image is a weighted sum of the first four echo images of an SE sequence (T_E = 30-60-90-120 ms, T_R = 800 ms).

SADDLE COIL DESIGN FOR SHORT ECHO TIME 23NA MRI

Peter M. Joseph and Ronald M. Summers

Pendergrass Diagnostic Radiology Research Laboratory, University of Pennsylvania School of Medicine, Philadelphia, Pennsylvania 19104

Abstract

Sodium-23 magnetic resonance imaging (MRI) has recently been presented in the literature(1). It has shown the potential to be useful when the extracellular fluid is increased, as in the edema surrounding a tumor or infarction(1). The cerebrospinal fluid and organs containing a large quantity of blood, including the heart, liver and spleen are easily visualized.

Unfortunately, it is difficult to generate sodium images of soft tissue such as muscle or fat which do not contain a large quantity of extracellular or intravascular sodium. There are several reasons for this. Intracellular sodium is much less concentrated than extracellular sodium (140 vs 12 millimolar). In addition, the T2 of intracellular sodium is very short, typically from 3 to 30 ms. Complicating this is the fact that, due to quadrupolar relaxation, 60% of the intracellular sodium signal decays with a T2 of approximately 1.5 ms, while the remaining 40% decays with a T2 of 15 ms(for muscle)(2).

In order to obtain the rapidly decaying signal from intracellular sodium, one needs to use very short pulse lengths. We have designed a saddle coil for use in our 1.4 Tesla imaging system which meets this need. It is a modification of a previously presented design(3). It produces a highly homogeneous RF field and, by increasing the number of turns, has a high inductance so that smaller valued capacitors with a high voltage rating may be used. This latter fact is important if one wants short pulse lengths.

We have constructed 2 sodium coils using this design. When measured inside our 6 inch diameter imaging bore, both our 3-inch diameter "rat-sized" coil and our 4-inch "cat-sized" coil have a Q of about 310 (unloaded). Using a gradient echo pulse sequence with a 90 degree pulse width of 125 microseconds at an RF power level of 100 watts and a TE of 4 ms, we have been able to see a background tissue "flush" corresponding to the short T2 component. We are also better able to obtain a high signal-to-noise ratio for the extracellular sodium. In addition, we are able to obtain proton images of any specimen without moving it, using the larger RF proton coil which surrounds the smaller sodium coil.

Conclusion

A high Q, highly homogeneous RF coil has been designed and constructed for sodium-23 MRI. It may be used with high RF driving power and thus short pulse lengths for imaging the very short T2 component of intracellular sodium.

References

1. S.K. Hilal, A.A. Maudsley, J.B. Ra, et al, J Comput Assist Tomogr **9**(1), 1 (1985).
2. D.C. Chang and D.E. Woessner, J Magn Res **30**, 185 (1978).
3. P.M. Joseph and J.E. Fishman, Med Phys, **12**(6), 679 (1985).

MRI OF LUMBAR SPINE: SURFACE COIL DESIGNS WITH MORE UNIFORM FIELD FOR SAGITTAL AND CORONAL PLANES

Clarke LP, Schnitzlein HN, Jones JD, Philips C, Silbiger M

University of South Florida, College of Medicine, Tampa, Florida 33612

Magnetic Resonance Imaging (MRI) of the lumbar or cervical spine for the detection of intervertebral disc disease, ideally requires high resolution (sub-millimeter) imaging in the sagittal, coronal, and paraxial planes using 5 mm. or less slice thickness. Surface coils are required to obtain good spatial resolution, signal to noise, and realistic imaging times. One limitation, however, is their limited sensitive area and fall off in sensitivity in all imaging phases. Hence a compromise between optimum coil design for signal/noise, and a more uniform field in the sagittal and coronal planes is required. Three coil types were therefore designed for a Siemens 1.0 Tesla magnetom imaging system at 15 MHZ: (1) circular two turn coil of 18 cm diameter, (b) elliptical coil with long axis equal to the length of the RF transmitter coil, and (c) opposed elliptical coils in series of similar dimensions.

The loaded and unloaded Q values were as follows: (a) 150 (80), (b) 150 (100), and (c) 130 (85). In addition the coils were also modified to include more than one turn, with the center turn taped in the form of an impedence matching transformer and appropriately grounded to reduce loading effects. Varactors were also used to allow convenient remote tuning of coils for lumbar spine. Comparable image quality was obtained for the large elliptical coils (spatial resolution 0.5 - 0.7 mm.) using contiguous multislice imaging at 5 mm. or 10 mm. slice thickness, with the added advantage of a more uniform field as illustrated in clinical images in Figures 1 and 2. The opposed elliptical coil design had the most uniform field, permitting easier clinical interpretation of images in sagittal and coronal planes through the spinal column. Field uniformity measurements were performed using both phantoms and cadavers to demonstrate the practical clinical advantages of each coil design.

Figure 1 - Representative sagittal view of the lumbar spine using two turn circular surface coil.

Figure 2 - Representative sagittal view of the lumbar spine using the single turn elliptical surface coil.

DESIGN, CONSTRUCTION AND EVALUATION OF MULTI-PURPOSE RECEIVING COILS, AN OPEN-SIDED SADDLE (OSS) COIL AND RECTANGULAR LOOP (RL) COIL FOR MR IMAGING FOR THE BRAIN STEM, BREAST, ORBIT, C-, T- AND L-SPINE, SACRUM, FEMUR, KNEE, ANKLES AND FOOT

William S. Yamanashi, Ph.D., John W. Ross-Duggan, M.D., Patrick D. Lester, M.D. and Gregory S. Thomas, B.S.

City of Faith Medical and Research Center, Oral Roberts University School of Medicine, Department of Radiology 8181 South Lewis Avenue, Tulsa, Oklahoma 74137-1270

Two multi-purpose receiving coils were designed for gaining more signal to noise ratio (S/N) in imaging specific areas of interest. The OSS coil was designed to image the orbit, TMJ, breast, knee and ankles; the RL coil was intended to cover longer ROI's in one setting. For example, the RL coil was able to image the area equivalent to 12 vertebrae. The OSS coil has loop diameter of 5" and interloop distance of 6½", fabricated of 1/8" OD copper tubing, whereas the RL coil has rectangular dimensions of 3 9/16" x 14" and constructed of 1/4" copper tubing. The output of both coils are fed into the preamplifier via 100 ohm twin axial cable. The quality factor Q of these coils were ca 130 without the load and ca 90 with dielectrically lossy load (tissue phantoms): a Hewlett-Packard 3585A spectrum analyzer and 4193A vector impedance meter were used in coil parameter measurements, Picker MR VISTA 2055 imager at 0.497T (21.255 MHz) with MR4/TABF software were used in conjunction with these coils. Majority of images were obtained using the head coil protocol in the MR4/TABF and Hahn spin echo sequence with TE=40 ms and TR=850 ms. The advantage of OSS coil is that S/N of ROI's such as in the neck, knee and ankle where it can sandwich the region is significantly improved over that of the head coil. Whereas the advantage of the RL coil is that it has greater coverage along the spinal cord from the brain stem to the sacrum when compared to a spherical loop coil or a head coil, also better S/N ratio and less artifacts at the loop boundaries than a spherical loop coil. An example of the comparison is shown in Figures 1a and 1b.

References

L. Axel, Magn. Reson. in Med. 1, 84-5 (1984).
T.W. Redpath, Magn. Reson. in Med. 1, 232-4 (1984)
W.S. Yamanashi, et al, Proc. Soc. Magn. Reson. Imaging 3rd Ann. Meeting, March 22-26, San Diego, California, p. 57 (1985).

Figure 1a
Rectangular Loop Coil

Figure 1b
Spherical Loop Coil

ABDOMEN

THE MRI APPEARANCE OF THE RUPTURED SPLEEN

Anthony R. Lupetin, M.D.; Richard H. Daffner, M.D.; Nilima Dash, M.D.; Rolf L. Schapiro, M.D.;

Allegheny General Hospital, Pittsburgh, Pennsylvania

PURPSOSE: To demonstrate the usefulness of MRI in the detection of intrasplenic and perisplenic hematoma secondary to disruption of the splenic capsule (splenic rupture).

METHODS: Fifteen patients with surgically-proven splenic rupture were evaluated preoperatively with MRI. Etiologies of rupture included: trauma (10 cases), idiopathic (3 cases), idiopathic thrombocytopenic purpura (1 case), splenic metastases (1 case). All studies were performed on a 0.5 T cryogenic magnet (Siemens Magnetom) which operated at 0.352 T (5 cases) and 0.494 T (10 cases). T1 and T2-weighted spin echo pulse sequences (TR = 0.5, 2.1 sec; TE = 35, 70 msec) were obtained in each case utilizing axial and coronal planes.

RESULTS: Intrasplenic and perisplenic hematoma demonstrated a similar high signal intensity on T1 and T2-weighted studies. The signal intensity difference between hematoma and normal spleen was greatest on T1-weighted studies (TR = 0.5 sec; TE = 35 msec). In general, MRI provided greater contrast between hematoma and normal spleen than CT. MRI was useful in the clinically-stable trauma patient as a screening procedure for significant splenic trauma. There was no characteristic signal intensity of a specific hematoma to allow identification of its etiology.

CONCLUSION: MRI is a useful procedure to detect the presence of splenic rupture and the attendent perivisceral and intravisceral hematoma.

MAGNETIC RESONANCE IMAGING AND COMPUTED TOMOGRAPHY OF PEDIATRIC LIVERS

Jeffrey C. Weinreb, M.D., Jesse M. Cohen, M.D., Edward Armstrong, M.D., William A. Erdman, M.D.

University of Texas Health Science Center, Southwestern Medical School; and Children's Medical Center, Dallas, Texas

The livers of 30 subjects, age 2 weeks to 16 years, were examined with magnetic resonance imaging (MRI). Fourteen patients had normal livers, 7 had focal liver disease, 6 had diffuse liver disease, and 3 had a combination of focal and diffuse liver disease. MRI was performed at 0.35 Tesla using multislice, multi-echo spin echo technique without EKG or respiratory gating. These studies were retrospectively reviewed in order to ascertain the useful information available in comparison to CT. Image quality of 83% of the MR studies was rated as excellent, 17% as adequate, and none as poor. Image quality of 96% of the CT scans was rated as excellent. Normal intrahepatic venous anatomy (main portal vein, lobar and segmental portal vein branches, and hepatic veins) was visualized more frequently with MRI regardless of presence of disease, type of disease, or age. Focal hepatic lesions were either iso- or hypointense on T1 weighted images and were hyperintense on T2 weighted images. There were three cases in which lesions seen with MRI were not appreciated with CT. There were two other cases in which the CT scans were interpreted as abnormal but were normal on MRI. Adenopathy, varices, and splenomegaly were depicted similarly with MRI and CT. MRI was superior to CT for evaluation of inferior vena cava patency. It is concluded that MRI has the potential to replace CT as the second imaging modality of the pediatric liver (after ultrasound) in many cases, especially for infants and young children.

RAPID MR IMAGING OF THE LIVER

Shmuel Albert, D.Sc. and Pradip Pattany, M.Sc.

Clinical Science Center, Picker International, Cleveland, Ohio

Several problems that are encountered when imaging the liver with conventional spin echo (SE) and inversion recovery (IR) sequences are:[1-3]

1. Respiratory motion artifacts.
2. Possible artifacts due to the presence of abdominal wall and intra-abdominal fat.
3. Insensitivity to fatty infiltration of the liver.
4. Relatively long imaging time when using conventional IR sequences such as IR 1500/400/30.

In order to overcome these problems, we have been using various pulse sequences with relatively short TR (repetition times), short TI (inversion times) and short TE (echo times). The following single and multislice pulse sequences have been developed:

a. Spin Echo (SE) sequences with TE=26ms and TR=200-300ms.
b. Partial saturation (PS) sequences with field echo data collection and TR times of 200-300ms.
c. Inversion Recovery (IR) sequences with short TI (50-200ms) and TR (300-700ms) times.

Comparative studies between images obtained with these sequences and those obtained using conventional methods have been made on volunteers and on patients with hepatic metastases. The experiments have been carried out with a Picker International VISTA 2055 imager operating at a field strength of 0.5T (frequency of 21.31 MHz) using 2DFT techniques. Good four slice images (two repetitions, 256 views, and slice thickness of 10mm) of the liver have been obtained with a TR time of 300ms. The imaging time was 2.6 minutes. Under these conditions the TE26 and IR images are quite similar: the abdominal fat is visualized on both of them, but visualized only partially on the PS images. Using a somewhat longer TR time and appropriate TI values with these IR sequences, we obtained liver images without the fat component as well as separate images of the fat component. The water/fat separation is based on the short spin-lattice relaxation time (T_1) of the lipid compared to other liver tissues, and enables us to study fatty infiltration of the liver. It is possible to remove or separate any specific component within the image by selecting an appropriate TI value. Our studies indicate that the IR images provide good correlation with results obtained by other modalities.

Images have also been obtained by combining these methods with respiratory gating. The imaging time was increased to 6-8 minutes, including the extra time required for the gating; however, the image quality was excellent.

REFERENCES:

1) Middleton, M.S., Stark, D., Grief, L., Saini, S., Rosen, B., Brady, T.J. Abstracts, SMRI, First Annual Meeting, P. 197, Feb. 14-18, 1983, Colorado Springs, 1983.
2) Lupetin, A. R., Dash, N., Schapiro, R.L., Deeb, Z. L., Daffner, R. H., and Sefczek, R. Abstracts, SMRI, Third Annual Meeting, P. 54, March 22-26, 1985.
3) Heiken, Jay P., Lee, Joseph, K.T. Lee, Glazer, Harvey S., and Linig, David, Radiology, 156, 423-427, 1985.

MRI OF INTRA-ABDOMINAL HEMATOMA

Peter F. Hahn, M.D., Ph.D., Sanjay Saini, M.D., David D. Stark, M.D., Joseph T. Ferrucci, Jr., M.D.

Massachusetts General Hospital, Harvard Medical School, Boston, MA

Intra-abdominal hematomas present a distinct MRI appearance and undergo a well-defined temporal evolution. We studied ten intra-abdominal hematomas with serial MRI (0.6 Tesla). In addition, a canine model of splenic hematoma was developed to allow more frequent scanning and to correlate MR image appearance of early hematoma with MR spectroscopic and biochemical parameters.

During the first 48 hours, hematomas are homogeneous and have relaxation times similar to normal spleen. In the period between 12 and 48 hours, the hematoma undergoes a reduction in T1. The T1 reduction gradually becomes localized to the periphery, so that after two to three weeks the hematoma has a "ringed" appearance. There may be an additional outer rim, corresponding to the pseudocapsule, with very low signal on all sequences.

In the canine model, fresh hematomas (<12 hours) have undetectable or low methemoglobin levels, T1 similar to normal spleen, and T2 much longer than spleen (200 vs 70 msec). Between 12 and 48 hours increased methemoglobin levels are associated with dramatic reductions in T1 while T2 is relatively unchanged. Maximal T1 shortening occurs at 4 days. During the next 4 weeks hematoma size nearly doubles and both T1 and T2 increase. A central "clot," seen in older hematomas, can have very short T1 and T2 relaxation times. At autopsy "clot" was a darkly pigmented fibrinous mass. The "ring" surrounding the central clot was a fluid with a relatively short T1 and long T2.

The study suggests that the concentration and chemical distribution of iron within the hematoma are the principal determinants of the magnetic resonance presentation of the lesion. Furthermore, the concentric ring appearance of subacute and chronic hematoma may be a tissue specific feature, allowing differentiation of this lesion from necrotic tumors, abscesses, and other nonhemorrhagic fluid collections.

MAGNETIC RESONANCE IMAGING OF DILATED BILE DUCTS

Susan Stafford, M.D., David D. Stark, M.D., Peter F. Hahn, M.D., Ph.D., Peter Mueller, M.D., Rodney J. Butch, M.D., Sanjay Saini, M.D., Joseph F. Simeone, M.D., Jack Wittenberg, M.D., Joseph T. Ferrucci, Jr., M.D.

Massachusetts General Hospital, Harvard Medical School, Boston, MA

We studied the MRI appearance of the normal and pathologic biliary system in 88 patients with known normal biliary anatomy and 20 patients with biliary pathology defined by ultrasound, CT, cholangiography and/or surgery. Extrahepatic biliary obstruction was secondary to pancreatic carcinoma in 9 patients, malignant periportal adenopathy in 4 cases, choledocholithiasis in 2, and chronic pancreatitis in one patient. Four patients with pneumobilia were also imaged. A 0.6 Tesla Technicare system was used to obtain T1 weighted spin echo (SE 260/18) and inversion recovery (IR 1500/450/18) sequences as well as a T2 weighted multiecho sequence (SE 2350/60,120,180).

Normal intrahepatic bile ducts were not identified by any pulse sequence technique. The normal cystic duct was visualized in 2 cases and the distal common bile duct was seen in 11. Anatomic resolution of these structures was best using the SE 260/18 sequence. T2 weighted images were inferior for delineating extrahepatic anatomy due to reduced signal-to-noise levels, reduced contrast with retroperitoneal fatty tissue planes, and susceptibility to motion induced artifacts. However, the T2 weighted SE sequence was useful for distinguishing intrahepatic biliary structures from blood vessels.

Pancreatic cancer was best seen on the SE 260/18 sequence. Choledocholithiasis was diagnosed in one patient with a 2 cm stone. 2-5 mm size stones were missed in another patient. Dilated intrahepatic bile ducts had a grey appearance on T1 weighted images and were distinguish from black "signal void" portal and hepatic veins. Duct-vein contrast increased dramatically on the T2 weighted spin echo images. Pneumobilia was also detected on T2 weighted images by visualizing a gas-fluid level in dilated central ducts. Overall, the T2 weighted images were more sensitive for detecting intrahepatic biliary dilatation while the T1 weighted SE images were best for delineating extrahepatic bile ducts and pancreatic pathology.

Our experience suggests that T2 weighted SE images best separate patients with intrahepatic biliary dilatation from normals. T1 weighted SE images offer improved anatomic resolution and are complimentary for delineating the extrahepatic pathology causing biliary obstruction.

GADOLINIUM-DTPA ENHANCED MRI OF THE LIVER CANCER USING RAPID SCANNING TECHNIQUES.

Sanjay Saini, M.D., Joseph T. Ferrucci, Jr., M.D., David D. Stark, M.D., Jean-Claude Bousquet, M.D., Jack Wittenberg, M.D.

Massachusetts General Hospital and Harvard Medical School, Boston, MA

Early published results suggest only a limited role for gadolinium-DTPA (Gd-DTPA) in contrast enhanced MRI of liver metastases. Carr et al noted a decrease in the tumor-liver signal difference following a bolus infusion of 0.1 mmoles/kg of Gd-DTPA (1,2). This negative effect has been attributed to the extracellular distribution of Gd-DTPA whose physiologic behavior is identical to the iodinated contrast medial used in excretory urography and computed tomography. Unfortunately, the long scan times available to Carr et al were not well suited to the rapidity with which the pharmacokinetic distribution of Gd-DTPA occurs. Similarly, their minimal TE of 44 msec does not optimally portray the T1 shortening effects of Gd-DTPA (3).

METHODS: We performed **in vivo** magnetic resonance imaging experiments in a rat model of liver cancer. Surgical implantation of mammary adenocarcinoma was used to produce solitary intrahepatic tumor masses. MRI (1.4 Tesla) was performed using a rapid scanning technique with a short TE-spine echo (250/15/1) pulse sequence. With this technique, liver images can be produced in 36 seconds. Gd-DTPA was administered as a bolus infusion (0.2 mmoles/kg) via a tail vein.

RESULTS: Our studies show a marked enhancement in tumor-liver signal difference in the first minute image. At this time, Gd-DTPA is primarily in the vascular space and not in the extracellular compartment. Thus, little Gd-DTPA has leaked into tumor producing only a modest increase in tumor signal intensity (71%). However, the large vascular perfusion of liver results in a much greater increase in its signal intensity (112%) and a substantial improvement in SD/N between the two tissues results. The tumor size, however, appears slightly smaller because peripheral tumor perfusion is closer to that of hepatic tissue.

Over the course of the next 15 minutes as the Gd-DTPA becomes distributed in the extracellular space, hepatic signal intensity decreases while the signal intensity in tumor increases. As a result, in the 15 minute scan there is no measurable signal difference between the two tissues.

CONCLUSION: Currently Gd-DTPA is the only MR contrast agent available for human studies. Our results show significant potential for its use in MRI of liver cancer. Better suited pulse sequences (fast scan times; short TE) may demonstrate a marked increase in the signal difference between normal liver and tumor in the immediate post-bolus period. A loss in contrast occurs as the contrast agent becomes distributed in the extracellular compartment and a negative effect is seen in delayed images.

1. Carr DM, Brown J, Bydder GB, et al: Gadolinium-DTPA as a contrast agent in MRI: initial clinical experience in 20 patients. AJR 143:215-224, 1984.
2. Carr DM, Graif M, Bydder GB, et al: Gd-DTPA in assessment of liver tumors by MR imaging. Abstracts of RSNA, p 44, 1985.
3. Grief WL, Buxton RB, Lauffer RB, et al: Pulse sequence optimization of MR imaging using a paramagnetic hepatobiliary contrast agent. Radiology 157: 461-466, 1985.

MR IMAGING OF LIVER CANCER: T1 WEIGHTED PULSE SEQUENCES

David D. Stark, M.D., Jack Wittenberg, M.D., Robert R. Edelman, M.D., Michael Middleton, Ph.D., M.D.*, Sanjay Saini, M.D., Rodney J. Butch, M.D., Joseph T. Ferrucci, Jr., M.D.

Massachusetts General Hospital, Harvard Medical School, Boston, MA, and Mercy Hospital, San Diego, CA

Currently, T2 weighted spin echo images are considered optimal for the detection of focal liver lesions. T1 weighted spin echo images (SE 500/30) have not been favored because of poor lesion detectability. Inversion recovery sequences have been unavailable or suffered from restricted multislice capabilities. Recently, the minimal achievable repetition time (TR) and spin echo delay (TE_{min}) have been reduced, allowing increased T1 weighting and improved multislice capabilities.

We compared T1 and T2 weighted images in 30 patients with primary or metastatic liver cancer. To allow direct comparison of pulse sequence performance each patient was imaged with multiple sequences (mean 9± 1.7), using comparable scan time for each sequence. Signal averaging was used for all pulse sequences, however, the number of averages varied inversely with TR. For example, using the SE 260/18 pulse sequence 16 data acquisitions could be obtained and averaged with a total scan time of 8.9 minutes; the IR 1500/450/18 pulse sequence allowed 3 data acquisitions in 9.6 minutes; the SE 2000/90 pulse sequence allowed 2 data acquisitions in 8.5 minutes. As the entire protocol required nearly 90 minutes of imaging time, many patients were examined on consecutive days.

Signal intensity measurements were obtained from tumor, uninvolved liver, spleen, muscle, and background noise. Contrast (tumor-liver) to noise ratios (C/N) were calculated for each pulse sequence (3-5). Expressed as a fraction of the greatest C/N value (mean ±S.D.) for each patient (N=30), pulse sequence performance was as follows: SE 260/18 (0.83 ±.18); IR 1500/280/18 (0.64 ±.2); IR 1500/450/18 (0.63 ±.25); SE 2000/90 (0.62 ±.31); IR 1500/450/30 (0.53 ±.18); SE 2000/60 (0.5 ±.3); SE 260/30 (0.3 ±.15); SE 500/30 (0.23 ±.17); SE 2000/30 (0.19 ±.12).

These results show that T1 weighted SE or IR sequences outperform conventional T2 weighted sequences for distinguishing cancer from normal liver. Furthermore, the SE 260/18 sequence was fast, allowed increased signal averaging, had less noise, fewer respiratory artifacts, and as a result had the best anatomic resolution of all the sequences studied. Dramatic improvements in image quality and C/N result in increased lesion conspicuity. The SE 260/18 sequence (9 minutes) was equal or superior to CT for detecting focal liver lesions in all 30 patients. A prospective study is underway to confirm that MR has become the imaging modality of choice for the evaluation of liver cancer.

EVALUATION OF HEMOLYSIS BY MR: SPLENIC IRON OVERLOAD

David D. Stark, M.D., Bruce R. Bacon, Ph.D.*, Denise M. Tager,
Ralph C. Felder, M.D., Peter F. Hahn, M.D., Joseph T. Ferrucci, Jr., M.D.

Massachusetts General Hospital, Harvard Medical School, Boston, MA and Case Western Reserve University, Cleveland, Ohio

Chronic iron overload dramatically alters the MR image appearance of liver, bone marrow, pancreas, and kidneys. Recent **in vitro** studies have shown unusually large R2/R1 ratios, suggesting that tissue iron enhances proton relaxation by a unique paramagnetic interaction. It is not known whether the molecular form or cellular distribution of iron influences this selective T2 relaxation rate enhancement.

To determine the relaxation effects of tissue iron overload in an additional clinically relevant pathologic condition, we developed a model of subacute hemolysis in the laboratory rat. Heat treated erythrocytes were administered by intraperitoneal injection for 6-9 weeks and the liver and spleen were analyzed **in vitro** for MR relaxation times, biochemical iron content, and histological iron distribution.

Splenic iron levels increased from 0.1 mg/gm to 3 mg/gm while hepatic iron levels increased from 0.1 mg/gm to 0.8 mg/gm. Liver and spleen showed R2/R1 ratios similar to those previously reported (16/1) for chronic dietary iron overload in the liver.

Our data indicate that iron overload alters proton relaxation by a characteristic mechanism that is relatively independent of the underlying pathologic process or tissue distribution of iron. Ferritin and hemosiderin are the common denominator in a variety of pathologic processes and are likely to be the molecular species responsibe for paramagnetic relaxation effects.

COMPARISON BETWEEN BOLUS AND BOLUS-DRIP INFUSION TECHNIQUES FOR GADOLINIUM-DTPA ENHANCED MRI OF LIVER CANCER

Sanjay Saini, M.D., Jean-Claude Bousquet, M.D., Joseph T. Ferrucci, Jr., M.D.,
David D. Stark, M.D., Jack Wittenberg, M.D.

Massachusetts General Hospital and Harvard Medical School, Boston, MA

The application of gadolinium-DTPA (Gd-DTPA) in imaging liver metastases has not been very successful. Published results show a decrease in tumor-liver signal difference following a bolus infusion of the contrast agent (1,2). This negative effect has been attributed to the extracellular distribution of Gd-DTPA and to the rapidity with which this occurs. This physiologic action is identical to that of the iodinated contrast media used in computed tomography. Contrast enhanced CT imaging techniques, however, demand dynamic scanning after a bolus infusion because these contrast agents get distributed in the interstitial space within a few minutes. Alternatively, the imaging period may be prolonged by a combined bolus-drip infusion technique. Furthermore, once the contrast agent is distributed in the extracellular compartment, imaging is much inferior to the unenhanced CT scans. Unfortunately, currently available MR scan times are much longer than those available for CT and rapid scanning following a bolus infusion is not possible. We therefore evaluated the effect of a bolus-drip infusion technique for Gd-DTPA enhanced MR imaging of liver-cancer.

METHODS: MRI was performed at 1.4 Tesla using a fast scan time (36 seconds; Spin Echo 250/15/1). A rat model of liver cancer was utilized. In this model surgical implantation of adenocarcinoma is used to produce solitary intrahepatic tumor masses. A total of 10 animals were imaged. A dose of .2 mmoles/kg Gd-DTPA was used. It was administered as a bolus (5 animals); or, as a bolus-drip (5 animals) in which half the dose was given as a bolus and the remainer electronically infused over 10 minutes. Signal intensity (SI) was measured for tumor, liver, and background and signal difference to noise ratio (SD/N) calculated.
(SD/N = [SI tumor - SI liver]/SI background).

RESULTS: Bolus infusion of Gd-DTPA produces a marked improvement in the tumor-liver in the first minute scan. This signal difference gradually decreases such that by the 15 minutes the two tissues become isointense. Bolus-drip infusion, however, delays the rate at which the two tissues become isointense. Using this technique, significant tumor-liver SD/N exists even at the 10 minute scan when compared with the image obtained with a bolus technique. However, at 20 minutes the two tissues have similar SI.

CONCLUSION: Gd-DTPA is the only contrast agent available for human investigation. However, its use in imaging liver cancer has not been very promising. Based upon experience gained from contrast enhanced CT of liver metastases, our studies suggest that a bolus-drip infusion technique is better suited for Gd-DTPA enhanced MRI of liver cancer. By maintaining a gradient between the tumor and liver levels of Gd-DTPA this technique will allow discrimination between the two tissues even using imaging techniques with relatively long scan times (5-10 minutes).

1. Carr DM, Brown J, Bydder GB, et al: Gadolinium-DTPA as a contrast agent in MRI: initial clinical experience in 20 patients. AJR 143:215-224, 1984.
2. Carr DM, Graif M, Bydder GB, et al: Gd-DTPA in assessment of liver tumors by MR imaging. Abstracts of RSNA, p 44, 1985.

INTERVENTIONAL MR: SUCCESSFUL DESIGN AND USE OF A NON-FERROMAGNETIC NEEDLE FOR ASPIRATION/BIOPSY

Peter R. Mueller, M.D., David D. Stark, M.D., Joseph F. Simeone, M.D., Joseph T. Ferrucci, Jr., M.D., Paul Beaulieu, R.T., Rodney J. Butch, M.D.,

Massachusetts General Hospital, Harvard Medical School, Boston, MA

MR has proven to be a sensitive imaging modality for detecting hepatic, renal, pelvic, and musculoskeletal masses. Unfortunately, the tissue specificity of MR has been limited, requiring sonographic or CT guided percutaneous biopsy as a supplemental procedure. Standard stainless steel needles available for needle localization and biopsy have not been suitable for MR because of extensive ferromagnetic image artifacts.

We have analyzed standard biopsy needles to determine the relationship of needle size, tip geometry, annealing, and metal alloy (304, 316, and MP35N stainless steel) to the size of the artifact produced on multi-slice images at 0.6 Tesla. We also studied non-standard needles that contained different amounts of chromium, nickel, and other non-ferrous metals (titanium, brass). While the needle tip design did not appear to make a difference in terms of ferromagnetic artifact, the needle size and metal alloy did. With this information we have developed a 20 gauge needle with appropriate ferromagnetic qualities that makes a ferromagnetic defect 2 mm in size, at the needle tip only.

In vitro testing confirms that the artifact created by our needle allows visualization of the tip within small lesions without causing larger artifacts that would confuse localization. Using this newly designed needle, we have now performed three successful MR guided liver biopsies on humans.

PARTICULATE IRON-OXIDE (MAGNETITE) AS A POTENTIAL BOWEL CONTRAST AGENT FOR MRI

Sanjay Saini, M.D., Joseph Sullivan, B.S., Joseph T. Ferrucci, Jr., M.D., David D. Stark, M.D., Jack Wittenberg, M.D..

Department of Radiology, Massachusetts General Hospital, Boston, Massachusetts; and Harvard Medical School, Boston, Massachusetts 02114

INTRODUCTION: Early experience with MRI of the abdomen has demonstrated the need for a suitable bowel contrast agent. Experiments using Signal-Enhancing agents such as Mineral-Oil have not been very fruitful. Bowel distal to the ligament-of-Tritz usually is not identifiable due to dilutional effects. Magnetite is a superparamagnetic iron-oxide that has been investigated as a potential liver contrast agent. Superparamagnetic substances possess large magnetic moments even in weak external fields and produce large local magnetic field inhomogenaeties. This results in a rapid dephasing of protons and an extremely short T2 relaxation time. For reasons poorly understood, T1 remains relatively unaffected. We have investigated the potential of magnetite as a potential bowel contrast agent for use in abdominal MRI.

MATERIALS AND METHODS: A surgical gastrostomy was placed in rats. Contrast was instilled and the anesthetised animals imaged. CT scans were obtainrd with dilute gastrograffin (10%) and MRI (1.4 T) performed with both signal-enhancing mineral oil and signal-depleting magnetite. T1 and T2 weighted pulse sequences were used: SE250/15; SE500/50; SE2000/120. The results were evaluated against the non contrast images.

RESULTS: Opacification of the entire bowel is easily achieved by the experimental design as seen on the CT scans. Abdominal MRI with magnetite produces a signal-depletion from bowel permiting easy identification of extra luminal structures such as mesenteric fat. Mineral oil is a poor substitute because (1) enhancing bowel lumen makes separation from mesenteric fat difficult; and, (2) bowel motion causes misregistration of signal in the phase-encoding direction rendering a degredation in image quality.

CONCLUSION: Our studies suggest a significant potential for magnetite as a bowel contrast agent. By utilizing a signal depleting substance, motion artifacts in the phase encoding direction are avoided and extra luminal structures easily identified on all pulse-sequences. Magnetite is superior to mineral oil which has been proposed as a signal enhancing bowel contrast agent.

MRI DETECTION OF EARLY AVASCULAR NECROSIS

Javier Beltran, M.D., Leigh J. Herman, M.D., Jane M. Burk, M.D.

Department of Radiology, Ohio State University Hospitals

The usefulness of MRI in detecting avascular necrosis was studied. An experimental model of AVN was developed to assess the ability of MRI to detect early changes of ischemia. The femoral heads of immature swine were surgically devascularized, and sequential postsurgical images were obtained. In six of eight swine, changes consisting of decreased signal intensity in the experimental femoral epiphyses were seen within 24 hours of surgery. The changes were best seen on T2 weighted images.

Patients at high risk for developing AVN were studied with MRI, Tc-MDP skeletal scintigraphy, and Tc-sulfur colloid marrow scintigraphy. Thirty hips were studied. MRI sensitivity was 73%, specifity 100%, and accuracy 75%. Nuclear medicine sensitivity was 50%, specificity 43% and accuracy 60%. AVN was detected and pathologically confirmed in five asymptomatic hips.

MRI detects AVN with a sensitivity and specifity superior to skeletal and bone marrow scintigraphy. Experimental work suggests that MRI can detect changes of ischemia earlier than any other available imaging modality.

Fig. 1

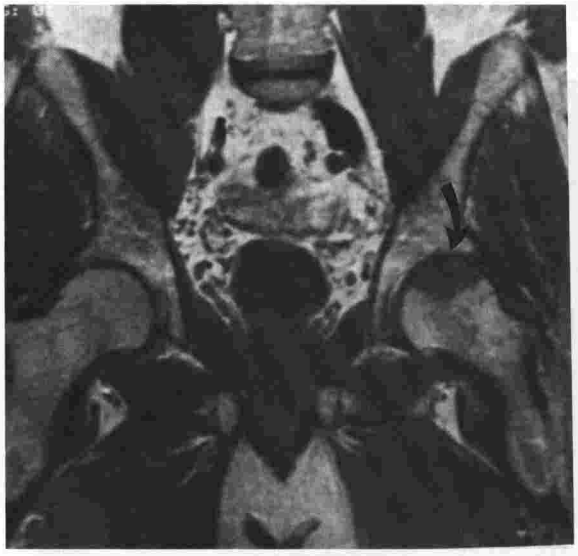

Fig 1 - 55 y. o. black male with avascular necrosis of left femoral head (curved arrow).

Fig 2

Fig 2 - Immature swine one hour post surgical devascularization of right femoral head. There is decreased intensity in the epiphysis (curved arrow).

SURFACE COIL, HIGH MAGNETIC FIELD (1.5 TESLA) MRI: THE ANKLE JOINT

Javier Beltran, M.D., James Mosure, M.D., Angela Noto, M.D., Kenneth Weiss, M.D.

Ohio State University Hospitals

Ankle and tarsal joint injuries are an exceedingly common health problem. This is particularly true in competitive athletes as well as the noncompetitive sport enthusiast. One of the major problems relates to the large percentage of soft tissue injuries without radiographic evidence of fracture. For most patients clinical correlation and routine plain film evaluation is all that is required. In selected patients however, a more complete examination might involve stress radiographs, radionuclide exams, and ankle arthrography or tenography. The advantages and disadvantages of each of these modalities is well documented.

The MRI has emerged as a noninvasive, nonionizing, multiplanar imaging modality capable of not only imaging the bony structure but also demonstrating articular cartilage, ligaments, tendons, and vessels. This has been clearly shown in published reports on the normal anatomy as well as ligamentous and cartilagenous injuries of the knee. We have successfully applied multiplanar, thin section, surface coil, high magnetic field (1.5 Tesla) magnetic resonance imaging to the ankle joint. Utilizing axial localization we first imaged normal volunteers with no history of ankle trauma in both coronal and sagittal planes. Fresh cadaver ankles were subsequently imaged on the MRI in coronal or sagittal plane, sectioned in each respective plane, and finally photographed. The normal anatomy of the MRI images was obtained by directly correlating the respective anatomic sections to the appropriate MRI images. Multiple pathological cases of the ankle, including post traumatic complications, inflammatory conditions, and cartilagenous injuries were then imaged. We conclude that MRI may be helpful in evaluating select ankle pathology, and by so doing afford optimal management decisions.

MAGNETIC RESONANCE IMAGING IN MARFAN'S SYNDROME

Marcia C. Fishman[1], M.D., Harry L. Stein[1], M.D., Robert A. Boxer[2], M.D., Michael A. LaCorte[2], M.D.

Departments of Radiology[1] and Pediatrics[2], North Shore University Hospital, Cornell University Medical College, Manhasset, New York

ECG gated magnetic resonance imaging studies were done on eight patients with Marfan's syndrome. Patients ranged in age between 10 to 27 years. On a 0.6 tesla superconducting magnet, 0.75-1.0 cm. thick sections were obtained. The aortic root, ascending aorta, aortic arch, and descending aorta were well delineated by MRI. In all patients with Marfan's syndrome, the aortic root and ascending aorta were dilated. The descending aorta was normal in each patient. The aortic isthmus, descending aorta, and collateral vessels were best seen on the sagittal view. The aortic root and arch were best identified on the left anterior oblique view. MRI gave excellent delineation of the thoracic aorta and provides a noninvasive technique for serial evaluation and follow up in Marfan's syndrome.

(Oral Presentation)

MRI IN EVALUATING LESIONS OF THE EXTREMITIES

Marcia C. Fishman, M.D., Donald Fagelman, M.D., Harry L. Stein, M.D.

Department of Radiology, North Shore University Hospital, Cornell University Medical College, Manhasset, New York

MRI of ten lesions of the extremities was performed on the 0.6 tesla superconducting magnet using two-dimensional spin-echo technique in three projections. Comparison to CT scan was made in four cases. MRI distinguished between soft tissue structures in the extremities providing not only morphologic but also diagnostic information. Two surgically proved schwannomas were diagnosed preoperatively by MRI not only because of their location. They were also characterized by intermediate signal intensities near that of skeletal muscle on T1 weighted scan, with extremely bright signals on T2 weighted scan. Other lesions included liposarcoma, metastatic breast carcinoma to the brachial plexus, aneurysmal bone cyst, and osteosarcoma. Two lesions were post-traumatic: fracture of the femoral head and tear of the posterior cruciate ligament of the knee. MRI was very sensitive in defining the extent of bone neoplasms within the medullary cavity. With its superior contrast resolution, MRI was better than CT scan in all four cases with comparison for delineating the exact location and extent of musculoskeletal lesions.

(Oral Presentation)

APPLYING MR IMAGING TO BIOMECHANICAL PROBLEMS: AN IN-VIVO INVESTIGATION OF MASTICATORY BIOMECHANICS AND CRANIOFACIAL MORPHOLOGY

E.K. KEELER
Clinical Science Center, Picker International, Cleveland, Ohio

M.D. RUSSELL and O.J. OYEN
School of Dentistry, Case Western Reserve University, Cleveland, Ohio

Biomechanical studies involve estimation of muscle force vectors acting on skeletal elements. In the past, these estimates could only be calculated from cadaver muscle cross-sections or dry weights. MRI's high tissue contrast and spatial resolution now make it possible to measure soft tissue variables necessary for the calculation of muscle force vectors in living subjects.

It has been hypothesized that skull shape is affected by masticatory (chewing) biomechanics. To test this, we use rigid frame models for the craniofacial skeleton in which the independent variables are bite force and masticatory muscle force vectors and the dependent variable is bone strain. Previous work on this problem has been on dry skulls, with the vectors estimated from crude osteological indicators of muscle size. However, a study is now underway in which the relevant force vectors are being calculated precisely, using MR images in combination with bioelectric muscle stimulation and radiography.

The subjects of this experimental study are growing vervet monkeys. The variable, masticatory muscle force, is manipulated by varying the consistency of the diet the monkeys are raised on. Biolectrically stimulated maximum bite forces are measured periodically for correlation with in-vivo muscle force vectors calculated from MR scan data and cephalographs. In-vivo strain gages are then implanted to test the accuracy of predictions made from the frame models and vector analysis.

The figures below show how MRI is used to obtain the soft tissue data required for analysis of muscle action on the skeleton, using the masseter as an example. The masseter's line of action is determined from muscle fiber direction, seen here in sagittal and coronal sections (Fig 1). Instant Oblique Reconstruction (Fig. 2) or Direct Oblique Imaging are used to obtain sequential muscle cross-section from origin to insertion. These areas are multiplied by slice thickness and summed to obtain muscle volume. MR soft tissue data is then correlated with radiographs to establish the muscle's point of application.

The results of this study will be useful in both orthodontia and reconstructive craniofacial surgery. Studies of dietary consistency and biomechanical factors affecting occlusion, palate shape, gum disease and general dental health are also being carried out. The MR techniques developed in this study for measuring muscle volume, lines of action and points of application are generally applicable to biomechanical research problems and to orthopaedics.

Research supported by NSF grant BNS 82-17034

Figure 1: MR images through the masseter muscle of a vervet monkey showing the long axis of the muscle fibers in the sagittal (a) and coronal (b) planes.

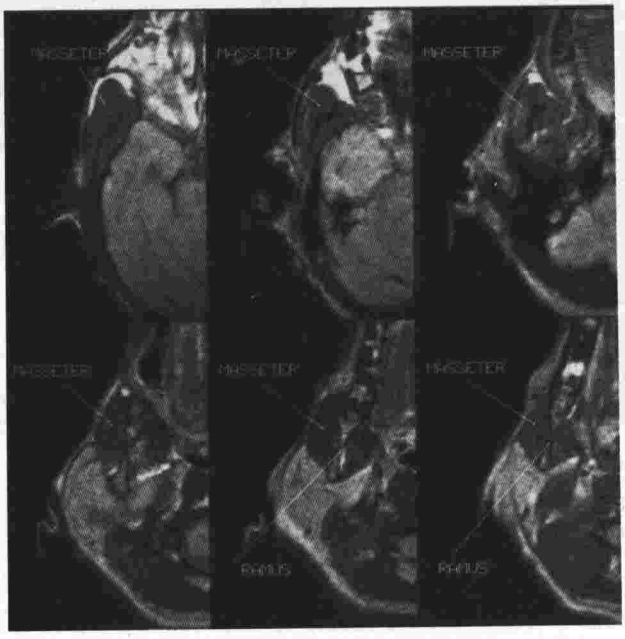

Figure 2: MR images showing sequential, contiguous slices through the masseter muscle. These oblique cross-sectional views were produced using instant oblique reconstruction (IOR).

MAGNETIC RESONANCE IMAGING IN THE DETECTION OF MENISCAL INJURIES.

Matthew Lotysch, M.D., Jerrold Mink, M.D., John V. Crues, M.D., and S. Andrew Schwartz, M.D.

Departments of Radiology and Orthopedic Surgery, Cedars-Sinai Medical Center, Los Angeles, California
Department of Medicine, UCLA Medical Center, Los Angeles, California.

88 knees in 83 patients were imaged by Magnetic Resonance (MR) for evaluation of suspected meniscal injuries. Subsequent surgical correlation with the MR findings was done in 23 patients. Coronal and sagittal imaging of the entire knee was performed in an average time of 25 minutes using a 5.5 inch flat surface coil at 1.5 Tesla field strength.

Normal menisci are homogeneously low intensity on MR imaging. Signal within the meniscus is thought to be abnormal, but many menisci containing signal are normal at arthroscopy. In an attempt to improve the specificity of MRI of the knee in predicting surgically significant lesions, we have developed the following grading system. Grade 1 represents a globular signal intensity within the meniscus which is not contiguous with an articular surface. Grade 2 is defined as a linear signal intensity within the meniscus that lacks extension to an articular surface. A grade 3 score includes any signal intensity within the meniscus contiguous with an articular surface.

Using this grading system, 7 of 8 grade 3 signals in the medial and 10 of 12 grade 3 signals in the lateral meniscus were confirmed as tears at surgery. 1 of 5 and 1 of 4 grade 2 signals in the medial and lateral menisci respectively were also confirmed as tears at surgery. All 9 grade 1 medial and all 3 grade 1 lateral meniscal signals were reported as normal at surgery. No meniscal tears were seen at surgery which were not associated with grade 2 or 3 signals. In conclusion, we believe that MRI is a rapid and accurate method of noninvasive evaluation of the knee for meniscal injuries and may compare favorably with arthrography.

HIGH RESOLUTION MRI OF THE KNEE IN HUMANS AND EXPERIMENTAL ANIMALS

Angela Noto, M.D., Javier Beltran, M.D., James Mosure, M.D.

Ohio State University Hospitals

MR imaging was performed using a 1.5 Tesla Magnet (General Electric, Signa) on eight immature swine knees with surgically produced vertical and horizontal meniscal tears, seven normal knees (five volunteers) and seven pathologic knees (seven patients). Surface coils were used on the seven normal knees, and seven patients while the head coil was used for imaging the swine knees. The sagittal images of the swine knees demonstrated the mid-meniscal tears best, while coronal views identified the anterior and posterior horn lesions to their greatest advantage. Of the seven patients studied seven medial meniscal tears, three anterior cruciate ligament tears, a posterior cruciate ligament avulsion, an old osteochondral fracture, femoral condylar chondromalacia, and a case of semimembranous tendon reinsertion were identified. These lesions correlated well with recent double contrast arthrography or surgery. All meniscal tears in the human knees were identified in both sagittal and coronal planes.

MRI advantages over the current diagnostic method of arthrography are as follows: noninvasive, uses no ionizing radiation, and provides excellent soft tissue contrast resolution. As small meniscal lesions and ligamentous injuries can be readily identified, surface coil MRI may eventually replace the more invasive arthrogram.

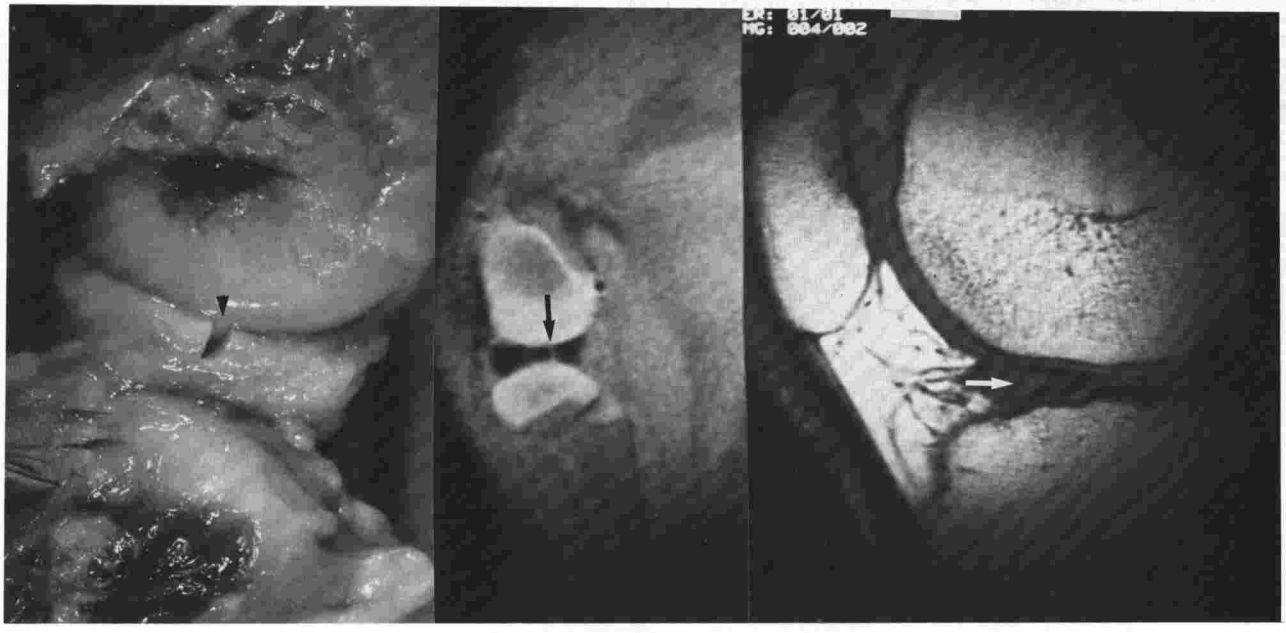

BONE MARROW PATTERNS BY MRI DURING PAINFUL CRISIS IN SICKLE CELL ANEMIA

Vijay M. Rao, Robert M. Steiner, Samir Ballas, Marcia Fishman, Leon Axel, Murray Dalinka, Warren Gefter, Herbert Kressel.

Department of Radiology, Hospital of the University of Pennsylvania, 3400 Spruce Street, Philadelphia, PA 19104.

Fifteen patients with sickle cell anemia (SCA) were studied during painful crisis. T1 (TR 600; TE 20-25 msec) and T2 (TR 2000-2500; TE 60-80 msec) weighted images at 1.5 Tesla were obtained. The symptomatic areas studied include 6 spines, 10 knees, 5 shoulders, 1 ankle, and 2 hips. Hemopoietic marrow hyperplasia was noted in all 4 spines and 8/10 (80%) knees. Fatty marrow was preserved at the epiphyseal margin of the knees. Ten of the 12 painful extremities (5/7 knees, 3 shoulders, 1 hip, 1 ankle) revealed single or multiple focal marrow infarcts on short TR/TE sequence. Long TR/TE sequence images were available in 7/10 painful extremities; all showed increased signal intensity indicating edema. In the asymptomatic extremities, the focal infarcts seen on short TR/TE sequence did not show hyper-intensity on long TR/TE sequence suggesting chronicity. In 2 cases, secondary hemosiderosis was detected. Our study indicates that MRI has the potential to differentiate acute versus chronic infarcts and that hyper-intensity on long TR/TE sequence accurately reflects the activity of the infarctive process.

Address Correspondence to: Vijay M. Rao, M.D.
Department of Radiology,
Thomas Jefferson University Hospital,
111 S.11th. Street,
Philadelphia, Pa 19107
215-928-7250

MAGNETIC RESONANCE IMAGING OF LUMBAR DISC DISEASE

John D. Reeder, M.D. and Samuel Andelman, M.D.

University of Maryland and Johns Hopkins Schools of Medicine

Magnetic resonance imaging (MRI) of the lumbar spine was performed on patients with disc herniation as demonstrated by high resolution computed tomography (CT) to assess the relative sensitivity and specificity of MRI. All of the MRI examinations were performed using a spine surface coil on a 1.0 Tesla magnet operating at 0.5 Tesla. Preliminary results indicate that MRI is more sensitive than CT in detecting disc degeneration and dessication. MRI and CT are equally sensitive in the identification of a bulging annulus. However, MRI manifests less specificity in terms of differentiating a bulging from a herniated disc. At the level of the lumbar neural foramen, difficulty exists with MRI, in distinguishing narrowing due to cortical osseous hypertrophy from narrowing due to the presence of a disc fragment positioned immediately adjacent to cortical bone. MRI proved to be of particular value in obese patients in whom scatter resulted in significant degradation of the CT image. MRI represents an extremely sensitive diagnostic modality in the evaluation of lumbar disc disease but more experience is required to improve specificity in differentiating the bulging from the herniated disc.

MAGNETIC RESONANCE IMAGING OF ROTATOR CUFF TEARS

John D. Reeder, M.D. and Samuel Andelman, M.D.

University of Maryland and Johns Hopkins Schools of Medicine

Magnetic Resonance Imaging of the shoulder was performed on patients identified as having sustained a rotator cuff tear, based on conventional shoulder arthrography. For comparison, a series of normal shoulders were also examined with all studies being performed on a 1.0 Tesla Magnet operating at 0.5 Tesla. The images demonstrated excellent anatomic detail in both the normal and injured shoulders. Preliminary results indicate that MRI of the shoulder provides the surgeon with additional information concerning the size and location of a rotator cuff tear. Additionally, MRI represents a non-invasive alternative for evaluation of the rotator cuff in patients unable or unwilling to undergo conventional contrast arthrography.

MRI OF THE SHOULDER: NORMAL ANATOMY AND PATHOLOGY

Leanne L. Seeger, MD, Lawrence W. Bassett, MD, Harvard Ellman, MD, Richard D. Kahmann, MD Stephen P. Kay, MD.

Departments of Radiology and Orthopedic Surgery, UCLA

To evaluate the role of Magnetic Resonance Imaging (MRI) in the evaluation of shoulder pathology, the normal anatomy was first defined by correlating multiplanar cadaver microcryosections with scans of normal volunteers. Cadavers were prepared by arterial (and in some, intra-articular) injection of dye, followed by fresh-freezing. Microcryosections 0.5 mm thick were then obtained. Development of appropriate scanning techniques and a surface coil allowed high resolution images to be acquired. Scans were obtained on a Fonar Beta-3000 0.3 Tesla permanent magnet, with a pixel size of 0.75 mm and matrix of 256 x 256. Slice thickness was 5 mm, at 7 mm intervals.

Following definition of normal anatomy, several patients with various forms of osseous and soft tissue abnormalities of the shoulder were scanned. All had either arthrographic, arthroscopic, surgical or radiographic confirmation. With a limited number of patients, MRI has thus far accurately depicted complete rotator cuff tear, osteonecrosis of the humeral head, intratendinous localization of soft tissue calcification, anterior labrum avulsion, complete union of greater tuberosity avulsion fracture, and acromial spur/impingement syndrome.

Due to the complex 3-dimensional anatomy of the shoulder, each scan must be tailored to the suspected pathology. Scan time can be minimized by use of a rapid acquisition axial scout scan to use as reference for subsequent imaging planes.

● *Calendar of Events*

February 2–7, 1986
Diagnostic Radiology Seminars, The Gant, Aspen, Colorado. Contact: Radiology Postgraduate Education, Registration Office, Room 569-U, University of California, San Francisco, CA 94143-0958 (415) 476-5808.

February 5–7, 1986
Computers for the Practicing Physician: Update 1986. Contemporary Resort at Walt Disney World, Lake Buena Vista, Florida. Contact: Dept. of Continuing Medical Education, Boston University School of Medicine, 80 E. Concord St., Boston, MA 02118, (617) 638-4605.

February 8–15, 1986
Second Annual Sun Valley Imaging Meeting, Sun Valley, Idaho. Contact: Sun Valley Imaging, 665-810 West Broadway, Vancouver, B.C. Canada, V5Z 4C9.

February 16–19, 1986
Magnetic Resonance Imaging Update. Sponsors: Boston University Medical Center and JFK Memorial Hospital, Lake Worth, Florida. Hyatt Palm Beaches, West Palm Beach, Florida. Contact: Dept. of CME, Boston University School of Medicine, 80 E. Concord St., Boston, MA 02118, (617) 638-4605.

February 17–21, 1986
Winter Imaging Seminar: An Appraisal of Developing and Mature Imaging Methods. Krystal Hotel, Cancun, Mexico. Contact: Ms. Janice Ford, CME Coordinator, Dept. of Radiology, Hospital of the University of Pennsylvania, 3400 Spruce St., Philadelphia, PA 19104, (215) 662-6904.

February 23–29, 1986
Diagnostic Imaging: Update 1986, Shadow Ridge, Park City, Utah. Contact: Radiology Postgraduate Education, Registration Office, Room 569-U, University of California, San Francisco, CA 94143-0958, (415) 476-5808.

February 28–March 28, 1986
International Continuing Medical Education Series. Barbados: Controversies in Medicine. Contact: Dept. of CME, Boston University School of Medicine, 80 E. Concord St., Boston, MA 02118, (617) 638-4605.

March 2–7, 1986
Ninth Annual Skeletal Symposium, Sun Valley, Idaho. Contact: Ms. Janice Ford, CME Coordinator, Dept. of Radiology, Hospital of the University of Pennsylvania, 3400 Spruce St., Philadelphia, PA 19104, (215) 662-6904.

March 10–14, 1986
Diagnostic Imaging 1986: CT, Ultrasound, MRI and Interventional Radiology, Waiohai Hotel, Kauai, Hawaii. Contact: Radiology Postgraduate Education, Registration Office, San Francisco, University of California, Room 569-U, CA 94143-0958, (415) 476-5808.

March 12–15, 1986
Joint Meeting of the World Health Organization and the European Workshop on Nuclear Magnetic Resonance in Medicine, Monte Carlo, Monaco. Contact: European Workshop on Nuclear Resonance in Medicine, c/o Dr. Robert N. Muller, Faculté de Medécine, Université de Lietat, B 7000 Mons, Belgium.

March 15–22, 1986
Seventh Annual Ultrasound at Vail. Write to Ultrasound at Vail, P.O. Box 6093, Cherry Creek Station, Denver, CO 80206.

March 24–28, 1986
Twenty-Ninth Annual Diagnostic Radiology Postgraduate Course, Fairmont Hotel, San Francisco, CA 94143. Contact: Radiology Postgraduate Education, Registration Office, Room 569-U, University of California, San Francisco, CA 94143-0958, (415) 476-5808.

March 24–28, 1986
Neuroradiology at Snowmass, The Snowmass Club, Snowmass, Colorado. Contact: Ms. Janice Ford, Dept. of Radiology, Hospital of the University of Pennsylvania, 3400 Spruce Street, Philadelphia, PA 19104, (215) 662-6904.

April 11–13, 1986
OB/GYN and Abdominal Sonography: Update 1986. Fairmont Hotel, San Francisco. Contact: Radiology Postgraduate Education, Registration Office, Room 569-U, University of California, San Francisco, CA 94143-0958, (415) 476-5808.

April 17–19, 1986
Thoracic Imaging Update: 1986, Hyatt Regency, Monterey. Contact: Radiology Postgraduate Education, Registration Office, Room 569-U, University of California, San Francisco, CA 94143-0958, (415) 476-5808.

April 30–May 15, 1986
International Continuing Medical Education Series. Paris/Versailles, France: Controversies in Medicine. Contact: Dept. of CME, Boston University School of Medicine, 80 E. Concord St., Boston, MA 02118, (617) 638-4605.